



*Flight Research – Aerospace Research*

## **Canadian Airspace Modeling**

LTR-FRL-2023-0055

16 June 2023

Author/Auteur: Teresa Krings<sup>1</sup>, Josh Chang<sup>1</sup>, Daniel Nelson<sup>1</sup>, Aman Basawanal<sup>1</sup>, Sam Kingma<sup>1</sup>, Brendan Ooi<sup>1</sup>, Iryna Borshchova<sup>2</sup>, and Jeremy Laliberte<sup>1</sup>

1 – Carleton University, 2 – National Research Council of Canada



National Research  
Council Canada

Conseil national de  
recherches Canada

**Canada**

FLIGHT RESEARCH LABORATORY

## ***Canadian Airspace Modeling***

Report No.: LTR-FRL-2023-0055

Date: 16 JUNE 2023

Authors/Auteurs: Teresa Krings, Josh Chang, Daniel Nelson, Aman Basawanal, Sam Kingma, Brendan Ooi, Iryna Borshchova, and Jeremy Laliberte

Classification:	Unclassified	Distribution:	Unlimited
<b>For:</b>			
<b>Reference:</b>			
Submitted by:	Iryna Borshchova, Research Officer		
Approved by:	Heather Wright Beatty, <b>Director R&amp;D FRL</b>		

Pages: 89	Copy No:
Fig.: 71	Diagrams:

1 – Carleton University, 2 – National Research Council of Canada

*This Report May Not Be Published Wholly Or In Part Without The Written Consent Of NRC Aerospace Portfolio*

## TABLE OF CONTENTS

<b>List of Figures.....</b>	<b>5</b>
<b>List of Tables.....</b>	<b>8</b>
<b>1.0 Executive Summary .....</b>	<b>10</b>
<b>2.0 Acknowledgements .....</b>	<b>11</b>
<b>3.0 Introduction and Project Overview.....</b>	<b>12</b>
3.1 Previous Work .....	15
3.2 Data Sources .....	155
<b>4.0 Data Pipeline.....</b>	<b>17</b>
4.1 Summary of Process .....	17
4.2 Export from .dmp to .csv (Steps 1-7) .....	18
4.3 Data Processing Pipeline (Steps 8 – 14) .....	19
<b>5.0 Data processing and scaling .....</b>	<b>21</b>
5.1 Processing Time Optimizations .....	21
5.2 Disk Space Optimizations .....	22
<b>6.0 Statistical Model Development .....</b>	<b>23</b>
6.1 Stage 1: Data Processing, Track Smoothing, and Variable Extraction.....	23
6.1.1 Data Processing.....	24
6.1.2 Track smoothing .....	27
6.1.3 Overview of Simulated Flights .....	33
6.1.4 Variable Extraction .....	33
6.1.5 Variable interpolation and data arrangement .....	36
6.2 Stage 2: Determination of Statistical Characteristics and Arrangement of the Dataset.....	37
6.2.1 Cut-Point Determination.....	42
6.2.1.1 Light Aircraft Model Results: .....	44
6.2.1.2 Medium Aircraft Model Results: .....	45
6.2.2 Data Discretization and Distributions Set Up .....	46
6.3 Stage 3: Determination of the Bayesian Network Structure and Generation of Frequency Tables .....	48
6.3.1 Data Count File Generation .....	51
<b>7.0 Conclusion .....</b>	<b>53</b>
<b>8.0 Future Work.....</b>	<b>54</b>
8.1 Data processing for the 2020 RDPS Dataset.....	54
8.2 Assessment of RDPS Dataset Suitability for Low-Level Altitude Statistical Airspace Models.	54
8.3 Traffic Density Modelling .....	54
8.4 Terminal and Enroute Statistical Airspace Model .....	55
8.5 Development of Statistical Models for RPAS Flight Data .....	55
<b>9.0 References.....</b>	<b>56</b>
<b>A Results of analysis of statistical characteristics by airports .....</b>	<b>58</b>
A.1 Billy Bishop Toronto City Airport (CYTZ).....	58
A.2 Lester B. Pearson International Airport (CYYZ).....	59
A.3 Ottawa Macdonald-Cartier International (CYOW) .....	60
A.4 Montréal-Trudeau International Airport (CYUL) .....	61
A.5 Montréal-Mirabel International Airport (CYMX).....	62
A.6 Timmins Victor M. Power Airport (CYTS).....	63
A.7 Victoria International Airport Model (CYYJ) .....	64
A.8 Vancouver International Airport (CYVR) .....	65
A.9 Winnipeg James Armstrong Richardson International Airport (CYWG).....	66

A.10	Canadian Forces Base Goose Bay (CYYR).....	67
A.11	Yellowknife Airport (CYZF) .....	68
A.12	Iqaluit International Airport (CYFB) .....	69
<b>B</b>	<b>Cut-Points and Bayesian Network Structure Determination .....</b>	<b>70</b>
B.1	Light aircraft below 10,000 ft ASL.....	70
B.2	Light aircraft between 10,000 and 25,000 ft ASL .....	72
B.3	Light aircraft above 25,000 ft ASL.....	74
B.4	Medium aircraft below 10,000 ft ASL.....	76
B.5	Medium aircraft between 10,000 and 25,000 ft ASL.....	78
B.6	Medium aircraft above 25,000 ft ASL .....	80
B.7	Heavy aircraft below 10,000 ft ASL.....	82
B.8	Heavy aircraft between 10,000 and 25,000 ft ASL.....	84
B.9	Heavy aircraft above 25,000 ft ASL .....	86
B.10	Helicopter aircraft below 10,000 ft ASL.....	88

## LIST OF FIGURES

Figure 1: Data import and processing summary .....	17
Figure 2: Data split procedure for query time optimization.....	21
Figure 3: Stacking procedure for disk space optimization.....	22
Figure 4: Stage 1 workflow (Steps 1-9).....	24
Figure 5: (a) Before and (b) after of UTM Standardization Step.....	24
Figure 6: Before (a) and after (b) of Repeated Row Check Step .....	25
Figure 7: (a) Before and (b) after of Time Check Step .....	26
Figure 8: Track of Boeing 737-400- Commercial aircraft commencing a descent.....	31
Figure 9: Track of Eurocopter EC120 Colibri- Helicopter in ascent .....	31
Figure 10: Track of Swearingen Merlin 3-Business Turboprop in ascent .....	32
Figure 11: Track of Vans Aircraft RV-6- Light aircraft performing turns .....	32
Figure 12: Data obtained and track smoothing process .....	33
Figure 13: Airspace Class determination Algorithm Visualization .....	34
Figure 14: Before (Above) and after (Below) of Variable extraction Process.....	36
Figure 15: Ottawa/Macdonald–Cartier International Airport Model (CYOW) 0-10,000 ft ASL (a) Mixed model distribution (b) Aircraft categories percentages (c) Variables distributions by aircraft category (d) Underlying distributions shape .....	38
Figure 16: Victoria International Airport Model (CYYJ) 0-10,000 ft ASL (a) Mixed model distribution (b) Aircraft categories percentages (c) Variables distributions by aircraft category (d) Underlying distributions shape .....	39
Figure 17: Montréal–Trudeau International Airport (CYUL) 0-10,000 ft ASL (a) Mixed model distribution (b) Aircraft categories percentages (c) Variables distributions by aircraft category (d) Underlying distributions shape .....	40
Figure 18: Canada Wide 2017 - All Altitudes (a) Mixed model distribution (b) Aircraft categories percentages (c) Variables distributions by aircraft category (d) Underlying distributions shape .....	41
Figure 19: Sample of cut-point selections results .....	43
Figure 20: Light aircraft model histograms below 10,000 ft ASL.....	44
Figure 21: Medium aircraft model histograms below 10,000 ft ASL .....	45
Figure 22: (a) Data Discretization Workflow and (b) results .....	46
Figure 23: Initial and transition distributions algorithm workflow .....	47
Figure 24: Initial (above) and transition (below) distributions file example .....	47
Figure 25: Initial Distributions for (a) Light aircraft model and (b) Medium aircraft model .....	49
Figure 26: Transition Distributions for (a) Light aircraft model and (b) Medium aircraft model .....	50
Figure 27: The Bayesian network structure is shown in (a), along with its corresponding distribution table in (b). Frequency tables for the first, second, and third variables of the network are presented in (c), (d), and (e), respectively.....	51
Figure 28: Generated tracks with identical initial conditions .....	52
Figure 29: Flight Path Visualization - 2D and 3D visualization with vertical section zoom.....	52
Figure 30: Billy Bishop Toronto City Airport (CYTZ) 0-10,000 ft ASL (a) Mixed model distribution (b) Aircraft categories percentages (c) Variables distributions by aircraft category (d) Underlying distributions shape .....	58
Figure 31: Lester B. Pearson International Airport (CYYZ) 0-10,000 ft ASL (a) Mixed model distribution (b) Aircraft categories percentages (c) Variables distributions by aircraft category (d) Underlying distributions shape .....	59
Figure 32: Ottawa Macdonald-Cartier International (CYOW) 0-10,000 ft ASL (a) Mixed model distribution (b) Aircraft categories percentages (c) Variables distributions by aircraft category (d) Underlying distributions shape .....	60

Figure 33: Montréal-Trudeau International Airport (CYUL) 0-10,000 ft ASL (a) Mixed model distribution (b) Aircraft categories percentages (c) Variables distributions by aircraft category (d) Underlying distributions shape .....	61
Figure 34: Montréal-Mirabel International Airport (CYMX) 0-10,000 ft ASL (a) Mixed model distribution (b) Aircraft categories percentages (c) Variables distributions by aircraft category (d) Underlying distributions shape .....	62
Figure 35: Timmins Victor M. Power Airport (CYTS) 0-10,000 ft ASL (a) Mixed model distribution (b) Aircraft categories percentages (c) Variables distributions by aircraft category (d) Underlying distributions shape .....	63
Figure 36: Victoria International Airport Model (CYYJ) 0-10,000 ft ASL (a) Mixed model distribution (b) Aircraft categories percentages (c) Variables distributions by aircraft category (d) Underlying distributions shape .....	64
Figure 37: Vancouver International Airport (CYVR) 0-10,000 ft ASL (a) Mixed model distribution (b) Aircraft categories percentages (c) Variables distributions by aircraft category (d) Underlying distributions shape .....	65
Figure 38: Winnipeg James Armstrong Richardson International Airport (CYWG) 0-10,000 ft ASL (a) Mixed model distribution (b) Aircraft categories percentages (c) Variables distributions by aircraft category (d) Underlying distributions shape .....	66
Figure 39: Canadian Forces Base Goose Bay (CYYR) 0-10,000 ft ASL (a) Mixed model distribution (b) Aircraft categories percentages (c) Variables distributions by aircraft category (d) Underlying distributions shape .....	67
Figure 40: Yellowknife Airport (CYZF) 0-10,000 ft ASL (a) Mixed model distribution (b) Aircraft categories percentages (c) Variables distributions by aircraft category (d) Underlying distributions shape .....	68
Figure 41: Iqaluit International Airport (CYFB) 0-10,000 ft ASL (a) Mixed model distribution (b) Aircraft categories percentages (c) Variables distributions by aircraft category (d) Underlying distributions shape .....	69
Figure 42: Light aircraft model histograms below 10,000 ft .....	70
Figure 43: Initial Distributions for Light aircraft model below 10,000 ft.....	71
Figure 44: Transition Distributions for Light aircraft model below 10,000 ft.....	71
Figure 45: Light aircraft model histograms between 10,000-25,000 ft ASL .....	72
Figure 46: Initial Distributions for Light aircraft model between 10,000-25,000 ft ASL .....	73
Figure 47: Transition Distributions for Light aircraft model between 10,000-25,000 ft ASL.....	73
Figure 48: Light aircraft model histograms above 25,000 ft ASL .....	74
Figure 49: Initial Distributions for Light aircraft model above 25,000 ft ASL .....	75
Figure 50: Transition Distributions for Light aircraft model above 25,000 ft ASL.....	75
Figure 51: Medium aircraft model histograms below 10,000 ft ASL.....	76
Figure 52: Initial Distributions for Medium aircraft model below 10,000 ft ASL .....	77
Figure 53: Transition Distributions for Medium aircraft model below 10,000 ft ASL .....	77
Figure 54: Medium aircraft model histograms between 10,000-25,000 ft ASL.....	78
Figure 55: Initial Distributions for Medium aircraft model between 10,000-25,000 ft ASL.....	79
Figure 56: Transition Distributions for Medium aircraft model between 10,000-25,000 ft ASL.....	79
Figure 57: Medium aircraft model histograms above 25,000 ft ASL .....	80
Figure 58: Initial Distributions for Medium aircraft model above 25,000 ft ASL.....	81
Figure 59: Transition Distributions for Medium aircraft model above 25,000 ft ASL.....	81
Figure 60: Heavy aircraft model histograms below 10,000 ft ASL.....	82
Figure 61: Initial Distributions for Heavy aircraft model below 10,000 ft ASL .....	83
Figure 62: Transition Distributions for Heavy aircraft model below 10,000 ft ASL.....	83
Figure 63: Heavy aircraft model histograms between 10,000-25,000 ft ASL .....	84
Figure 64: Initial Distributions for Heavy aircraft model between 10,000-25,000 ft ASL.....	85
Figure 65: Transition Distributions for Heavy aircraft model between 10,000-25,000 ft ASL.....	85

Figure 66: Heavy aircraft model histograms above 25,000 ft ASL .....	86
Figure 67: Initial Distributions for Heavy aircraft model above 25,000 ft ASL.....	87
Figure 68: Transition Distributions for Heavy aircraft model above 25,000 ft ASL.....	87
Figure 69: Helicopter aircraft model histograms below 10,000 ft ASL.....	88
Figure 70: Initial Distributions for Helicopter aircraft model below 10,000 ft ASL .....	89
Figure 71: Transition Distributions for Helicopter aircraft model below 10,000 ft ASL .....	89

## LIST OF TABLES

Table 1: Summary of Relevant Raw Data Columns .....	18
Table 2: Summary of Interpolated Data Columns After Processing.....	20
Table 3: Summary of Subtrack Rejection Reasons at Data Processing .....	26
Table 4: Radar Performance Characteristics ICAO (2007) .....	30
Table 5: IMM Calculated Error .....	30
Table 6: Data classification according to aircraft characteristics.....	35
Table 7: Descriptive Statistics of Variable Distributions for CYOW (0-10,000 ft ASL): Mean, Mode, and Standard Deviation.....	38
Table 8: Descriptive Statistics of Variable Distributions for CYYJ (0-10,000 ft ASL): Mean, Mode, and Standard Deviation.....	39
Table 9: Descriptive Statistics of Variable Distributions for CYUL (0-10,000 ft ASL): Mean, Mode, and Standard Deviation.....	40
Table 10: Descriptive Statistics of Variable Distributions for Canada (All altitudes): Mean, Mode, and Standard Deviation.....	41
Table 11: Light aircraft model cut point for tracks below 10,000 ft ASL .....	44
Table 12: Medium aircraft model cut point for tracks between 10,000 and 25,000 ft ASL .....	45
Table 13: Descriptive Statistics of Variable Distributions for CYTZ (0-10,000 ft ASL): Mean, Mode, and Standard Deviation.....	58
Table 14: Descriptive Statistics of Variable Distributions for CYYZ (0-10,000 ft ASL): Mean, Mode, and Standard Deviation.....	59
Table 15: Descriptive Statistics of Variable Distributions for CYYZ (0-10,000 ft ASL): Mean, Mode, and Standard Deviation.....	60
Table 16: Descriptive Statistics of Variable Distributions for CYUL (0-10,000 ft ASL): Mean, Mode, and Standard Deviation.....	61
Table 17: Descriptive Statistics of Variable Distributions for CYMX (0-10,000 ft ASL): Mean, Mode, and Standard Deviation.....	62
Table 18: Descriptive Statistics of Variable Distributions for CYTS (0-10,000 ft): Mean, Mode, and Standard Deviation.....	63
Table 19: Descriptive Statistics of Variable Distributions for CYYJ (0-10,000 ft ASL): Mean, Mode, and Standard Deviation.....	64
Table 20: Descriptive Statistics of Variable Distributions for CYVR (0-10,000 ft ASL): Mean, Mode, and Standard Deviation.....	65
Table 21: Descriptive Statistics of Variable Distributions for CYWG (0-10,000 ft ASL): Mean, Mode, and Standard Deviation.....	66
Table 22: Descriptive Statistics of Variable Distributions for CYYR (0-10,000 ft ASL): Mean, Mode, and Standard Deviation.....	67
Table 23: Descriptive Statistics of Variable Distributions for CYZF (0-10,000 ft): Mean, Mode, and Standard Deviation.....	68
Table 24: Descriptive Statistics of Variable Distributions for CYFB (0-10,000 ft ASL): Mean, Mode, and Standard Deviation.....	69
Table 25: Light aircraft model cut point for tracks below 10,000 ft.....	70
Table 26: Light aircraft model cut point for tracks between 10,000-25,000 ft ASL .....	72
Table 27: Light aircraft model cut point for tracks above 25,000 ft ASL.....	74
Table 28: Medium aircraft model cut point for tracks below 10,000 ft ASL .....	76
Table 29: Medium aircraft model cut point for tracks between 10,000-25,000 ft ASL.....	78
Table 30: Medium aircraft model cut point for tracks above 25,000 ft ASL.....	80
Table 31: Heavy aircraft model cut point for tracks below 10,000 ft ASL.....	82
Table 32: Heavy aircraft model cut point for tracks between 10,000-25,000 ft ASL.....	84
Table 33: Heavy aircraft model cut point for tracks above 25,000 ft ASL.....	86

Table 34: Helicopter aircraft model cut point for tracks below 10,000 ft ASL ..... 88

## Nomenclature

ADS-B	Automatic Dependant Surveillance-Broadcast
AGL	Above Ground Level
ASL	Above Sea Level
BIC	Bayesian Information Criterion
BVLOS	Beyond Visual Line of Sight
CA	Constant Acceleration
CAM	Canadian Airspace Modelling
CAR	Canadian Aviation Regulations
CREATE	Collaborative Research and Training Experience
CT	Constant Turn
CV	Constant Velocity
DAA	Detect and Avoid
GNSS	Global Navigation Satellite Systems
IAM	Integrated Aerial Mobility
ICAO	International Civil Aviation Organization
IFR	Instrument Flight Rules
IMM	Interacting Multiple Model
JARUS	Joint Authority on Rulemaking for Unmanned Systems
MIT-LL	Massachusetts Institute of Technology Lincoln Laboratory
MLE	Maximum Likelihood Estimation
NRC	National Research Council of Canada
PSR	Primary Surveillance Radar
RDPS	Radar Data Processing
RPAS	Remotely Piloted Aircraft System
SPEA	Strength Pareto Evolutionary Algorithm
SORA	Specific Operations Risk Assessment
SSR	Secondary Surveillance Radar
TC	Transport Canada
TDOA	Time Difference of Arrival
UTM	Universal Transverse Mercator
VFR	Visual Flight Rules
VLOS	Visual Line of Sight
VNC	Virtual Network Computing
WTC	Wake Turbulence Category

## 1.0 EXECUTIVE SUMMARY

The Canadian Airspace Modelling project was a multi-year, multi-disciplinary project that was spearheaded by the National Research Council of Canada and Carleton University, in partnership with Transport Canada and NAV CANADA. The main goal of this project was to make use of historical aircraft track data provided by NAV CANADA to develop statistical models of the airspaces in Canada. The methodology employed to develop Canadian models was influenced by the renowned MIT LL (Massachusetts Institute of Technology Lincoln Laboratory). However, it was acknowledged that their models, which were primarily based on US data, might not be directly applicable to Canadian airspaces. Ultimately, the objective of this project was to provide valuable insights and findings that would contribute to the development of Transport Canada's regulations regarding Remotely Piloted Aircraft Systems (RPAS) in Canada.

The project lasted for over two years, and was mostly funded by Transport Canada, as well as, the Natural Sciences and Engineering Research Council of Canada (NSERC) Collaborative Research and Training Experience (CREATE) Uninhabited Aircraft Systems Training, Innovation, and Leadership Initiative (UTILI) Program. The project comprised of three separate phases, with the completion of the project slated for the end of the 2023 fiscal year. National Research Council of Canada partnered with NAV CANADA, who supplied historical aircraft track data for model development. Phase 1 of the project focused on selecting the specific airspace suitable for analysis. Phase 2 of this project focused on developing algorithms to filter the aircraft track data and to develop the statistical model of that selected airspace. With the learnings of both Phase 1 and Phase 2 of this project, the research team focused on developing a streamlined methodology to standardize the Canadian airspace model generation process. Phase 3 of the Airspace Modeling project was dedicated to the large-scale processing and development of mixed statistical model of Canada, as well as, models for 12 selected regions that highlight the unique nature of Canadian airspace. This project report documents the final workflow for handling the track data received from NAV CANADA, as well as, the generation and analysis of the model outputs. Detailed descriptions of the tools and methodologies developed to create the statistical airspace models are presented in this report. Finally, concluding remarks on the project are given, as well as, future work to further the development of the tools and methodologies highlighted in this report.

## 2.0 ACKNOWLEDGEMENTS

The research team would like to thank both Transport Canada (TC) and the Natural Sciences and Engineering Research Council of Canada (NSERC) Collaborative Research and Training Experience (CREATE) Uninhabited Aircraft Systems Training, Innovation, and Leadership Initiative (UTILI) Program for the financial contributions made to enable the completion of this project. Special thanks to Carleton University for enabling several undergraduate students to participate in the research carried out over the three-year period through the Internship - Carleton University Research Experience for Undergraduate Students (I-CUREUS) Program. We express our gratitude to the National Research Council of Canada's (the NRC's) Integrated Aerial Mobility (IAM) Program for the financial support and in-kind contributions.

Additionally, we thank Carlos Ruella, Tom Hastie, and Owen Peterson from the TC Remotely Piloted Aircraft System (RPAS) Task Force, for shaping this research and for providing their valuable inputs. We thank Kris Ellis and Charles Vidal from the NRC for their support and advocacy for the importance of this project to support TC's data-driven approach to RPAS regulations development.

The research team would also like to recognize and thank NAV CANADA for the in-kind support that helped to enable the successful completion of this project. NAV CANADA provided access to the underlying dataset that was crucial for the development of the airspace statistical models presented in this report. Special thanks to Alexandra Officer, Janelle Denton, Alan Chapman, and Ken Lange from the NAV CANADA team for the support in transferring and accessing the dataset.

Finally, the research team would like to recognize the contributions of previous project team members: Jonathan Planger, Yichen Zhang, and Samuel Nadler.

### **3.0 INTRODUCTION AND PROJECT OVERVIEW**

In recent years, the Canadian airspace has seen a large influx of Remotely Piloted Aircraft Systems (RPAS) being deployed by various industries for a wide range of applications, including remote sensing and package delivery. In 2019, Transport Canada released Part IX of the Canadian Aviation Regulations (CAR), which provides a uniform set of regulations that relate to the use of RPAS for Visual Line of Sight (VLOS) operations. While the current regulations have enabled greater commercial application of RPAS technology, there are some limitations that are currently imposed by the VLOS requirements that prevent industry from fully harnessing the potential benefits of RPAS technology. To address this issue, TC has begun working with numerous organizations to allow for the use of RPAS for Beyond Visual Line of Sight (BVLOS) operations in a limited scope. TC has drafted a modified version of the Specific Operations Risk Assessment (SORA) process that was developed by the Joint Authority on Rulemaking for Unmanned Systems (JARUS, [1], [2]) to provide Canadian operators with a structured process to assess the risks associated with RPAS operations, with a specific focus on BVLOS operations in the Canadian region. Part of this risk assessment includes a detailed evaluation of the operational airspace, which considers numerous factors including the class of airspace and the rate of encounters with manned aircraft.

The Canadian airspace is classified into seven classes: Class A, B, C, D, E, F (controlled), and G (uncontrolled), all differing in their altitude ranges and their primary uses. RPAS operators must understand the airspace classes they will be operating in, and the potential hazards associated with each class, which is essential to conduct a comprehensive risk assessment and ensuring safe operations. More detailed information on airspace classes and their requirements can be found in [3].

Towards this end, the Canadian Airspace Modelling (CAM) project was undertaken as a collaboration between the National Research Council of Canada (NRC) and Carleton University (CU), in partnership with TC and NAV CANADA. The CAM project was initially proposed by the NRC as a tool to aid TC in the process of reviewing BVLOS RPAS operations in Canada. By developing a model of the Canadian airspace, it would become possible to determine the risks associated with operations of a RPAS with traditional aviation in a specific operational volume of non-segregated airspace. By utilizing real, historical flight data obtained from NAV CANADA, alongside publicly available aircraft movement data from Statistics Canada, this project aimed to develop airspace models that would allow for the simulation of RPAS encounters with intruder aircraft that are typical for the operational airspace. The developed Canadian airspace model aimed to facilitate the development of operational standards for RPAS operations and support the derivation of requirements to Detect and Avoid (DAA) systems for various airspaces, which are of interest to TC, NAV CANADA, and NRC. As shown by Ellis and Borshchova [4], airspace models are essential for the determination of the Risk Ratio of a candidate DAA system.

The CAM project was a multi-year project comprising of the following three major phases:

Phase 1 – November 2020 – March 2021: Selection of the specific airspace and its aircraft tracking sensor coverage analysis

- The selected airspace for initial assessment of the project scope and data suitability was centered around Winnipeg James Armstrong Richardson International Airport (CYWG) due to the variety of available sensors (primary and secondary radars etc.). Initial methods for processing sample datasets provided by NAV CANADA were developed, including data management and flight track visualization routines.

Phase 2 – April 2021 – March 2022: Development and Validation of Canadian Statistical Airspace Models in Region selected in Phase 1

- Phase 2 of the project continued with a focus on CYWG. A month worth of data for the airspace in 2020 was provided by NAV CANADA, allowing for the tuning of the filter developed for data pre-processing, to enable accurate recreation of the flight track data. The methodology for creation of the airspace statistical models was developed using flight data provided for CYWG and then validated compared to data from Statistics Canada [5].

Phase 3 April 2022 – March 2023: Development of Canada-wide Statistical Airspace Models

- Phase 3 of the project served as an application of the methodologies developed in Phases 1 and 2, along with the implementation of a large-scale data processing pipeline, to ensure that an advanced procedure was developed to enable the creation of statistical models (both the mixed model of Canada, as well as, models of 12 selected regions).

This project report details the work that has been completed in fulfillment of all 3 Phases, and consists of three major tasks:

#### Task 1: Development of Data Processing Pipeline

- Methodologies to enable large-scale data processing, allowing for the development of statistical airspace models.

#### Task 2: Development of methodology for Filtering of Canada-Wide Aircraft Track Data

- Large-scale data filtering and interpolation
- Creation of statistical models for the Canadian Airspaces based on the following variables:
  - Geographic location
  - Airspace Class
  - Altitude Layer
  - Speed
  - Acceleration
  - Turn Rate
  - Vertical Rate
- Application of Bayesian Networks to generate synthetic aircraft trajectory:
  - Initial distribution – Bayesian network that shows the initial distribution of the model variables.
  - Transition distribution – Bayesian network that shows how the model variables evolve over time.

#### Task 3: Canada-wide Data Analysis and Creation of the Models of 12 Selected Regions

- To demonstrate the capabilities of the methodologies developed over the duration of this project, the statistical models for the Canada-wide dataset was created, as well as, for 12 selected airports in Canada that cover a wide range of sizes and geographical characteristics:
  - CYTZ: Billy Bishop Toronto City Airport
  - CYYZ: Toronto Pearson International Airport
  - CYOW: Ottawa Macdonald-Cartier International Airport
  - CYUL: Montréal-Pierre Elliott Trudeau International Airport
  - CYMX: Montréal-Mirabel International Airport
  - CYTS: Timmins Victor M. Power Airport
  - CYYJ: Victoria International Airport
  - CYVR: Vancouver International Airport

- CYWG: Winnipeg James Armstrong Richardson International Airport
- CYYR: Goose Bay Airport
- CYZF: Yellowknife Airport
- CYFB: Iqaluit Airport

### 3.1 Previous Work

Kochenderfer et al. [6] [7] at the Massachusetts Institute of Technology-Lincoln Laboratory conducted research leading to the creation of two models for analyzing the risk of mid-air collisions between aircraft. The first model, the Uncorrelated Encounter Model, does not consider the role of air traffic control in aircraft trajectory, while the second model, the Correlated Encounter Model, accounts for cooperation between aircraft and air traffic control. Weinert [8] and Underhill [9] later updated and improved this work. The resultant models were based on aircraft tracks collected from 120 aircraft tracking sensors in the United States where aircraft were operating under Visual Flight Rules (VFR) between 500 feet Above Ground Level (AGL) and 18,000 feet Above Sea Level (ASL). The model was derived by analyzing variables such as geographic location, airspace class, altitude layer, airspeed, vertical ascend/descend rate, turn rate, and acceleration which were extracted for a posterior smoothing and quantization working with predetermined cut points that best described the data according to histograms to finally determine the Bayesian structure for the initial and transition distributions, and perform sampling and track simulation.

The MIT-LL has since developed additional models for specific types of aircraft and geographic locations[10] [11] [12]; however, these models may not be suitable for other countries, such as Canada, due to differences in geographic, environmental, regulatory, and economic factors that could affect air traffic density, aircraft types, transponder equipage, and behavior. Additionally, the MIT-LL's public Github repository [13] lacks the ability to process different data sets and create Bayesian networks for customized models.

To address these limitations, this work presents a methodology to build on the MIT-LL models to calculate and analyze mid-air collision risks in Canada using real information about the behavior and distributions of different categories and types of manned aircraft in various classes of Canadian airspace. Unlike previous models, this methodology considers both Visual and Instrument Flight Rules (VFR and IFR) and takes into account the aircraft's Wake Turbulence Category (WTC) as an additional variable influencing its behavior. It also offers flexible methods for generating customized datasets to meet the user's needs.

### 3.2 Data Sources

The dataset used for the development of the statistical models presented in this report was provided by NAV CANADA and is known as the “RDPS” (Radar Data Processing System) dataset. The flight track data for the entirety of Canada was provided in two separate databases, for the years of 2017 and 2020 respectively. Phase 1 and 2 of the project were completed on sample data extracted from the 2020 RDPS dataset. However, due to the unique nature of the 2020 dataset as a result of the COVID-19 pandemic, the research team opted to focus efforts on the large-scale data processing and statistical model development on the 2017 RDPS dataset. Both datasets contain the same structure of data, with the 2020 dataset including additional information on the contributing sensor(s) for the recorded aircraft track. The methodologies developed and presented in this report can also be extended to the 2020 RDPS dataset, which is planned for future work. This will allow for an investigation into how the pandemic has influenced air traffic densities in Canada. NAV CANADA’s RDPS system leverages multiple surveillance technologies to gather data, which is then analyzed, associated, and amalgamated to produce a track. The sensors implicated in this process include Primary Surveillance Radar (PSR), Secondary Surveillance Radar (SSR), and Automatic Dependent Surveillance-Broadcast (ADS-B), Multilateration, and Space-Based ADS-B.

PSR emits a signal that reflects back to the radar when it encounters an object such as an aircraft, terrain, obstacles, or migrating birds. Based on the elapsed time and the antenna's azimuth during the interaction, the aircraft's position can be calculated. However, PSRs do not furnish information on altitude or the aircraft's identity.

In contrast, SSR sends an interrogation signal to transponder-equipped aircraft and receives an encoded response that often contains information about the aircraft's identity and altimeter reading. Similar to PSR, the arrival time of the transponder response is used to estimate range/position.

ADS-B does not require active signals from ground-based equipment and instead relies on aircraft equipped with ADS-B to automatically transmit their position and velocity information derived from Global Navigation Satellite Systems (GNSS). Space-based ADS-B operates in a similar manner, but utilizes ADS-B receivers located on satellites as opposed to ground stations.

Multilateration is a technology that has been in use for several decades in aviation. It is based on a methodology known as Time Difference of Arrival (TDOA) that allows the position of an aircraft to be determined from several receivers on the ground and an aircraft transponder.

RDPS data received from NAV CANADA contained fields, such as: Flight ID, Aircraft ID, Aircraft Registration, carrier information, route information, departure and destination airport ID, aircraft position, altitude, time stamp, speed, heading, type of flight rules (IFR or VFR), maximum take-off weight and others. Due to non-disclosure agreement with NAV CANADA, further details on the dataset are not provided.

## 4.0 DATA PIPELINE

### 4.1 Summary of Process

The raw data was initially provided in a proprietary file format of Oracle Database dump files (*.dmp*). This raw data was unsuitable for the project to work with due to licensing restrictions and limited availability of Oracle licenses. Furthermore, variable extraction was required to create airspace models, therefore requiring all data to be ran through the airspace variable extraction process.

Consequently, a decision was made to export this data into an open-source relational. Given the scale of the data, the methodology was developed that required multiple data conversions using two relational database software (Oracle 11g and PostgreSQL), and two programming languages (python and MATLAB). This process is summarized in Figure 1 and described in the following subsections for Steps 1-7 and Steps 8-14.

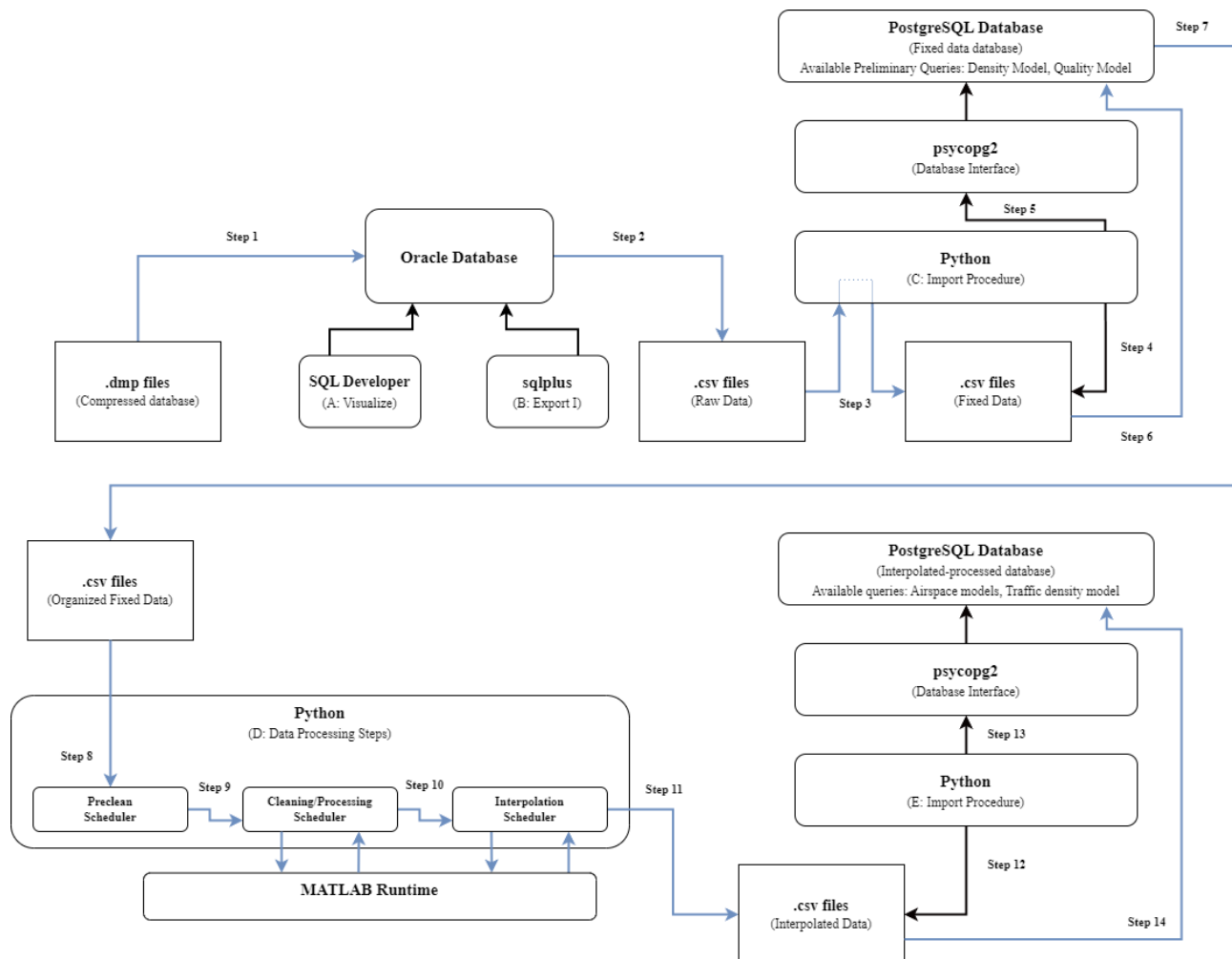


Figure 1: Data import and processing summary

## 4.2 Export from .dmp to .csv (Steps 1-7)

The 2017 dataset consisted of approximately 250 GB of compressed dump file data which, when expanded into the database, was approximately 790 GB. To provide a file format *postgres* is capable of importing, an export to comma-separated values (.csv) was necessary. The columns that were extracted and identified as necessary are summarized in Table 1.

**Table 1: Summary of Relevant Raw Data Columns**

Name	Type	Explanation
<b>NATIONAL_FLIGHT_ID</b>	Integer	A unique identifier for each individual track in our dataset
<b>FLIGHT_EVENT_DATE</b>	Date	Date at which observation occurs
<b>FIR_AIRSPACE_CODE</b>	String	Believed to state the data source of the observation
<b>COAST_STATE_ID</b>	Integer	Believed to indicate interpolation/ alternate data collection methods
<b>COAST_TYPE_ID</b>	Integer	Believed to indicate interpolation/ alternate data collection methods
<b>DESTINATION_AERO_ID</b>	Integer	Numerical identifier for the destination airport
<b>DEPARTURE_AERO_ID</b>	Integer	Numerical identifier for the departing airport
<b>AC_TYPE_DSGNTR_CODE</b>	String	ICAO aircraft type identifier if known
<b>FLIGHT_FIX_LATITUDE_DEG</b>	Float	Latitude position, with 7 decimal places
<b>FLIGHT_FIX_LONGITUDE_DEG</b>	Float	Longitude position, with 7 decimal places
<b>FLIGHT_FIX_SPEED_KN</b>	Integer	Speed in knots, rounded to whole number
<b>FLIGHT_FIX_ALTITUDE_ESTAB_FT</b>	Integer	Altitude in feet, rounded to whole number
<b>FLIGHT_FIX_HEADING_DEG</b>	Integer	Heading, rounded to nearest 10 degrees

Both importing and exporting was done using the *impdp* (import data pump) tool and SPOOL command remotely in *sqlplus*. The authors are aware of other formal export methods using *sqldeveloper* but found them not suitable for this application, given: 1) the instability of the network connection, 2) the quantity of data which required export, and 3) the significantly slower export speeds. In our empirical testing, a *sqldeveloper* export occurred at a 2 GB/hour rate (requiring 395 hours) in contrast to spooling at 29 GB/hour (requiring 27 hours). *Sqldeveloper* was used purely as a visualization tool and a way to quantify the existing size of the dataset.

The .csv exported 2017 data was adjusted for minor errors in *Python* followed by an import into *postgres* using *psycopg2*. Once the process was completed, preliminary traffic density queries could be run. A second export step separated the .csv files into manageable sections and ensured full track information was available for the data processing steps. Prior to data processing, the fixed data was read and manipulated (Steps 4 through 6) by *Python* and *postgres* to extract information of the full trajectory in Step 7 for the data processing steps.

### **4.3 Data Processing Pipeline (Steps 8 – 14)**

Data processing pipeline consisted of three steps: 1) a preclean procedure in *Python*, 2) a combined cleaning and processing methodology in MATLAB, and 3) an interpolation procedure in MATLAB. In Step 8, *preclean* removed duplicate points and assigned a category to each trajectory. Categories were primarily based on the ICAO’s wake turbulence category (WTC) with additional categories for unconventional aircraft such as military aircraft, gyrocopters and ultralights or trajectories which we have no information on. WTC is derived from the maximum takeoff weight field in RDPS data. Step 9 involved the cleaning and processing, which comprise of steps to modify the raw data file followed by an extraction of the airspace variables, UTM zone, and airspace class at every timestamp. Lastly, the interpolation process in Steps 10 and 11 standardized all trajectories to one second intervals. Finally, the data was re-imported into *postgres* database in Steps 12 through 14 with Table 2 summarizing the columns of the computed, interpolated dataset.

The processing of the data necessitated the handling of a substantial volume of information, which in turn required extensive automation, parallelization, and the utilization of an external server. All code was run on a Debian Linux system with 48 CPU threads and 128 GB of RAM. MATLAB code was pre-compiled on an alternate Debian Linux system using MATLAB on Linux over Virtual Network Computing (VNC). These codes were executed as part of a pipeline and were managed using three “schedulers” responsible for each step of the process. Each scheduler was parallelized using the multiprocessing library in *Python* with MATLAB code ran using the MATLAB Runtime. Time estimates of each process vary but approximations of each step include 1 days for the preclean process, 5 days for the cleaning/processing steps, and 2 days for interpolation.

**Table 2: Summary of Interpolated Data Columns After Processing**

Name	Type	Explanation
<b>flightid</b>	Integer	A unique identifier for each individual track in our dataset
<b>flightdate</b>	Date	Date at which observation occurs
<b>fir_airspace</b>	String	Believed to state the data source of the observation
<b>coastid</b>	Integer	Believed to indicate interpolation/ alternate data collection methods
<b>coasttype</b>	Integer	Believed to indicate interpolation/ alternate data collection methods
<b>actype</b>	String	ICAO aircraft type identifier
<b>subtracknum</b>	Small-Int	Unique identifier for each subtrack in a track to identify where tracks are split
<b>airclass</b>	Small-int	Airspace class of area (Class A = 1, Class B = 2 ... Class G = 7)
<b>acgroup</b>	Small-Int	Aircraft Type: 0 = Amphibious, 1 = Gyrocopter, 3 = Helicopter, 4 = LandPlane, 5 = SeaPlane, 6 = Tiltrotor
<b>engtype</b>	Small-Int	Type of Engines: 0 = Electric, 1 = Jet, 2 = Piston, 4 = Rocket, 5 = Turboprop/Turboshaft
<b>engnum</b>	Small-Int	Number of engines on aircraft
<b>utmzone</b>	String	UTM zone
<b>latitude</b>	Float	Latitude position, with 5 decimal places
<b>longitude</b>	Float	Longitude position, with 5 decimal places
<b>speed</b>	Float	Speed in kts, with 5 decimal places
<b>altitude</b>	Integer	Altitude in feet, to nearest whole number
<b>heading</b>	Integer	Heading, to the nearest degree, or $^{\circ}$
<b>accel</b>	Integer	Acceleration in hundredths, or kt/s
<b>trate</b>	Integer	Turn rate in hundredths, or $deg/100s$
<b>vrate</b>	Integer	Vertical rate in feet per second, or $ft/s$

## 5.0 DATA PROCESSING AND SCALING

To run airspace models at the scale of data previously described, certain optimizations were designed and tested to ensure sufficient querying speeds. High level descriptions of these optimizations are described followed by their implementation for the creation of airspace models. These optimizations are broadly categorized into two forms: processing time optimizations (to improve querying speeds) and disk space optimizations.

### 5.1 Processing Time Optimizations

Processing time optimizations are currently done using indexes and the data split procedure. Both forms of processing optimization limit the range of data which must be searched by the *postgres* database. Indexes provide an ordering to the data allowing for *postgres* to identify chunks of data that do not require analysis. Out of the index types available in *postgres*, the default B-tree indexes were the only ones found to be effective. The creation of B-tree multidimensional indexes across longitude, latitude, and altitude accelerates queries with geographic constraints which improves the speed to generate airspace models across a wide variety of geographic areas. Additional one-dimensional indexes were also created on each of the columns of airspace variables.

In contrast to this approach, data split physically separates the data into unique tables allowing *Python* to identify the relevant tables for a particular query. This data split procedure acts as a form of horizontal sharding and has been used to separate observations by latitude, longitude, and altitude bands as shown in

Figure 2.

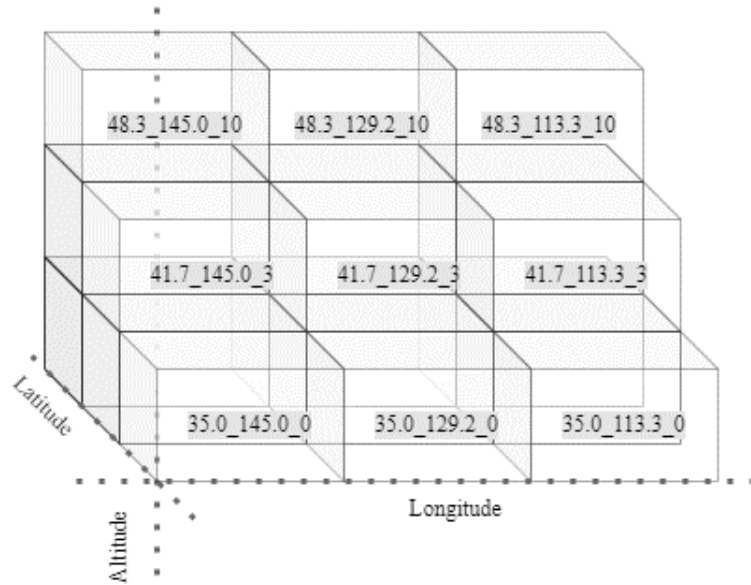


**Figure 2: Data split procedure for query time optimization**

The data split methodology could be extended in the future to be hosted on separate disks or servers unlike indexing methods. Data split methods require greater coding and are not amenable to changes in the data structure or new data but provide greater query reduction speeds relative to indexing. The usage of one of these two methodologies is required to run queries at any form of acceptable speed. Our experiments show

that certain queries may take over 15 times longer when ran without indexes; query time reductions of 95% to 98% have been observed and measured on raw and processed data with other queries.

## 5.2 Disk Space Optimizations

The volume of disk space used by the database presents a storage and querying speed issue. Increased quantities of data increase the number of read/write steps or input/output (I/O) required to perform requested actions. Furthermore, as all processing time optimizations require some form of increased disk space, reductions in disk space provide a greater range of options for disk space optimization.

Only one method has been considered for disk space optimization and is referred to as ‘stacking’. Stacking merges 5 rows of data into one by storing the relevant variables as columns, as shown in Figure 3.

flightid	fligthdate	var	flightid	fligthdate	var	varp1	varp2	varp3
000000001	0:00:01	1	000000001	0:00:01	1	2	3	4
000000001	0:00:02	2	000000001	0:00:05	5	6	-10000	-10000
000000001	0:00:03	3	000000002	0:00:04	2	...	...	...
000000001	0:00:04	4						
000000001	0:00:05	5						
000000001	0:00:06	6						
000000002	0:00:04	2						

Figure 3: Stacking procedure for disk space optimization

Stacking reduces disk space in two ways: 1) it reduces the duplication of certain parameters that never change (such as *flightid*, *acid*, or *actype*) or change in a predetermined way (such as *fligthdate*), 2) it reduces the total row count to display the same information of which has a fixed cost. Experimental testing on the 2017 dataset indicate stacking reduces disk space requirements by approximately 65%.

While reducing disk space, stacking maintains the resolution of airspace models while sacrificing the query resolution. As the query itself is filtered at 5 second intervals, airspace variables which occur up to 4 seconds later may be counted; therefore, queries which analyze a short temporal period encounter increased errors. However, for even a temporally short one-day airspace model this error would be under 0.01% and was determined to be an acceptable error.

## 6.0 STATISTICAL MODEL DEVELOPMENT

The development of an airspace model for a Canada-wide perspective was carried out while ensuring compatibility with the server's requirements for storing and managing large datasets. The development process comprised of three main stages, namely:

- Processing, track smoothing, and variable extraction;
- Determination of statistical characteristics and arrangement of the dataset; and
- Determination of the Bayesian network structure and generation of frequency table files.

Each of these stages plays a crucial role in the creation of the model and serves to streamline the process for obtaining information necessary for analyzing the statistical characteristics of aircraft operating in Canadian airspace. The files generated because of this process contain valuable information and can be used for further applications such as the generation of realistic tracks and collision probability analysis.

The first stage of the process involves processing the RDPS data to guarantee the quality of the tracks. The second stage comprises an analysis of the statistical characteristics of the data, enabling the identification of cut-points essential for further discretization. This is a crucial step for the final stage, which involves determining the Bayesian network structure and generating frequency tables.

The following sub-sections will provide a detailed discussion and explanation of the steps and algorithms implemented for each of the three stages.

### 6.1 Stage 1: Data Processing, Track Smoothing, and Variable Extraction

All algorithms associated with this stage were developed in MATLAB. Figure 4 provides an overview of the various steps undertaken during this stage. Firstly, data reliability and quality were evaluated via a series of preprocessing steps designed to ensure track consistency (represented by the first 5 steps in Figure 4). The next step involved track smoothing to minimize noise interference from sensors and additional calculations such as speed and acceleration (represented by Step 6 in the Figure 4). Subsequently, relevant variables were extracted (represented by Step 7 in Figure 4), and the frequency of observations was increased to conduct a statistical analysis of the data (represented by Step 8 in Figure 4). Finally, the resultant data was rearranged in a manner conducive for storage in the server (represented by Step 9 in Figure 4).

Prior to Step 1, the data underwent pre-processing, during which the latitude and longitude observations were transformed to the Universal Transverse Mercator (UTM) coordinate system and the Unix timestamp was computed and added as extra columns. The data was provided as a .csv file containing several pieces of information that are not necessary for the analysis; therefore, only the following information was extracted to start with the processing steps:

- UTM-X coordinates
- UTM-Y coordinates
- Altitude
- Time
- UTM Zone (saved in a separate variable)

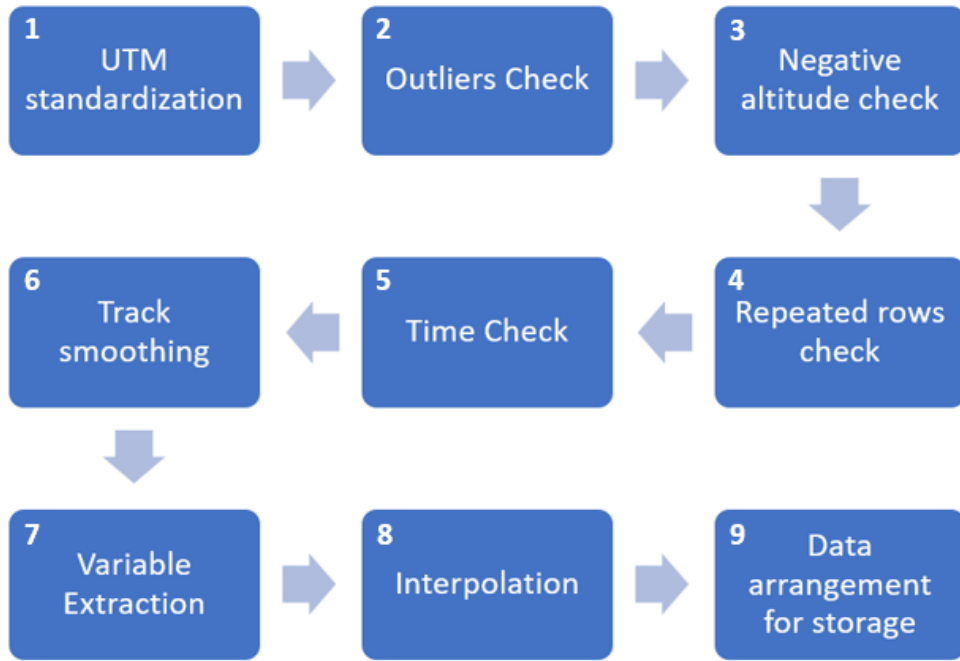


Figure 4: Stage 1 workflow (Steps 1-9)

### 6.1.1 Data Processing

**UTM Standardization:** To prevent potential conflicts arising from sudden changes in position caused by tracks crossing different UTM zones, it was necessary to standardize the values of the coordinates in the x-axis or UTM easting. This was accomplished using the "check\_UTM.m" function, which enforces a specific UTM zone in position to ensure the continuity of position information while preserving the original UTM zone value for future steps. Figure 5 displays the “before and after” effects of this process, demonstrating how the function helps maintain consistency in the position information of the tracks, while retaining the original values in the utmZone column. The UTM zone used to force the positions is saved in a separate variable.

	1	2	3	4	5	utmZone
	x	y	Altitude	Seconds		
519	7.0362e+05	5.6859e+06	26712	1.6043e+09	13 U	
520	7.0444e+05	5.6856e+06	26712	1.6043e+09	13 U	
521	7.0526e+05	5.6853e+06	26712	1.6043e+09	13 U	
522	7.0605e+05	5.6850e+06	26712	1.6043e+09	13 U	
523	7.0684e+05	5.6847e+06	26712	1.6043e+09	13 U	
524	7.0762e+05	5.6845e+06	26712	1.6043e+09	13 U	
525	7.0842e+05	5.6842e+06	26712	1.6043e+09	13 U	
526	7.0920e+05	5.6840e+06	26712	1.6043e+09	13 U	
527	2.9143e+05	5.6837e+06	26712	1.6043e+09	14 U	
528	2.9222e+05	5.6832e+06	26712	1.6043e+09	14 U	
529	2.9299e+05	5.6829e+06	26712	1.6043e+09	14 U	
530	2.9378e+05	5.6826e+06	26712	1.6043e+09	14 U	
531	2.9451e+05	5.6824e+06	26712	1.6043e+09	14 U	
532	2.9531e+05	5.6820e+06	26712	1.6043e+09	14 U	
533	2.9604e+05	5.6817e+06	26712	1.6043e+09	14 U	
534	2.9677e+05	5.6814e+06	26712	1.6043e+09	14 U	
535	2.9760e+05	5.6811e+06	26712	1.6043e+09	14 U	

	1	2	3	4	5	utmZone
	x	y	Altitude	Seconds		
519	7.0362e+05	5.6859e+06	26712	1.6043e+09	13 U	
520	7.0444e+05	5.6856e+06	26712	1.6043e+09	13 U	
521	7.0526e+05	5.6853e+06	26712	1.6043e+09	13 U	
522	7.0605e+05	5.6850e+06	26712	1.6043e+09	13 U	
523	7.0684e+05	5.6847e+06	26712	1.6043e+09	13 U	
524	7.0762e+05	5.6845e+06	26712	1.6043e+09	13 U	
525	7.0842e+05	5.6842e+06	26712	1.6043e+09	13 U	
526	7.0920e+05	5.6840e+06	26712	1.6043e+09	13 U	
527	7.0999e+05	5.6837e+06	26712	1.6043e+09	14 U	
528	7.1082e+05	5.6834e+06	26712	1.6043e+09	14 U	
529	7.1161e+05	5.6831e+06	26712	1.6043e+09	14 U	
530	7.1242e+05	5.6828e+06	26712	1.6043e+09	14 U	
531	7.1317e+05	5.6827e+06	26712	1.6043e+09	14 U	
532	7.1399e+05	5.6824e+06	26712	1.6043e+09	14 U	
533	7.1475e+05	5.6822e+06	26712	1.6043e+09	14 U	
534	7.1550e+05	5.6819e+06	26712	1.6043e+09	14 U	
535	7.1635e+05	5.6816e+06	26712	1.6043e+09	14 U	

Figure 5: (a) Before and (b) after of UTM Standardization Step

**Outliers Check:** In the original RDPS data, some observations were found to be outliers that did not fit the pattern of the tracks and seemed to be added or measured by a different sensor. Keeping such observations could adversely affect the results, particularly if this trend occurred repeatedly along a track. To ensure the integrity of the data, a process was developed to remove these outliers. It was found that this process does not impact the expected time interval between observations, as outliers are typically located between correlated observations, at a lower time interval than the one expected.

**Negative Altitude Check:** During the initial data cleaning phase, erroneous or missing altitude information was assigned a large negative value, and some of these instances have been carried over up to this stage. However, as altitude information is critical for further analysis, it was necessary to eliminate such observations from the dataset since failure to do so would prevent the progress of the analysis.

**Repeated Row Check:** This step of the data processing involved the removal of redundant rows identified in subsequent observations. The algorithm was specifically designed to identify repeated positions, rather than simply relying on time stamps, as cases were found where the time information changed while the position remained the same for several observations, extending up to over 30 seconds in the exact same location. Figure 6 shows the before and after of this process, exemplifying a case where time information is also repeated.

Figure 6 consists of two side-by-side Excel spreadsheets, labeled (a) and (b). Both spreadsheets have columns A through E. Column A contains row numbers, and columns B through E contain data fields: x, y, Altitude, Seconds, and Time difference. Red boxes highlight specific rows in both spreadsheets, primarily focusing on rows 2, 5, 6, 7, 8, 9, 10, 11, 12, 13, 14, 15, 16, 17, 18, 19, 20, 21, 22, 23, and 24. These highlighted rows represent data points that were identified as repeats and removed during the processing step. An arrow points from the right side of spreadsheet (a) towards the left side of spreadsheet (b), indicating the transformation from the 'before' state to the 'after' state.

	A	B	C	D	E
1	x	y	Altitude	Seconds	Time difference
2	588921.144	6033879.75	39231	1604246542	0
3	588921.144	6033879.75	39231	1604246542	0
4	588921.144	6033879.75	39231	1604246542	0
5	588921.144	6033879.75	39231	1604246542	5
6	588333.527	6032823.06	39231	1604246547	0
7	588333.527	6032823.06	39231	1604246547	0
8	588333.527	6032823.06	39231	1604246547	0
9	588333.527	6032823.06	39231	1604246547	4
10	587696.704	6031831.75	39231	1604246551	0
11	587696.704	6031831.75	39231	1604246551	0
12	587696.704	6031831.75	39231	1604246551	0
13	587696.704	6031831.75	39231	1604246551	5
14	587121.556	6030656.38	39231	1604246556	0
15	587121.556	6030656.38	39231	1604246556	0
16	587121.556	6030656.38	39231	1604246556	0
17	587121.556	6030656.38	39231	1604246556	5
18	586529.902	6029571	39231	1604246561	0
19	586529.902	6029571	39231	1604246561	0
20	586529.902	6029571	39231	1604246561	0
21	586529.902	6029571	39231	1604246561	5
22	585897.133	6028608.31	39231	1604246566	0
23	585897.133	6028608.31	39231	1604246566	0
24	585897.133	6028608.31	39231	1604246566	0

	A	B	C	D	E
1	x	y	Altitude	Seconds	Time difference
2	588921.144	6033879.75	39231	1604246542	5
3					
4					
5	588333.527	6032823.06	39231	1604246547	4
6					
7	585897.133	6028608.31	39231	1604246561	5
8					
9	585260.32	6027616.96	39231	1604246571	4
10	584660.254	6026678.86	39231	1604246575	5
11	584035.584	6025773.45	39231	1604246580	5
12	582766.016	6023819.33	39231	1604246590	5
13	582145.727	6022737.92	39231	1604246595	5
14	581537.579	6021742.47	39231	1604246600	4
15	580900.779	6020751.05	39231	1604246604	5
16	580272.072	6019816.92	39231	1604246609	5
17	579651.794	6018735.47	39231	1604246614	5
18	579048.039	6017564.01	39231	1604246619	5
19	578407.204	6016543.89	39231	1604246624	4
20	577782.892	6015433.75	39231	1604246628	5
21	577137.676	6014589.59	39231	1604246633	5
22	576517.414	6013508.08	39231	1604246638	5
23	575888.721	6012573.89	39231	1604246643	5
24	575268.119	6011697	39231	1604246648	5

Figure 6: Before (a) and after (b) of Repeated Row Check Step

**Time Check:** After performing the previous data checks, it was necessary to ensure that the observations were taken at an interval of 5 seconds, with a tolerance of  $\pm 2$  seconds for the purpose of this study. This verification guaranteed a suitable time gap between observations. If there were two consecutive points with a time difference of more than 7 seconds, a modified Akima piecewise cubic Hermite interpolation was applied. However, this was limited to a maximum of 30 seconds (6 observations) to avoid unrealistic predictions. The "check\_Time.m" function was utilized for this purpose, and the results are displayed in Figure 7.

**a**

	1	2	3	4	5
	x	y	Altitude	Seconds	Time difference
1	3.7526e+05	5.7448e+06	1869	1.6043e+09	10
2	3.7495e+05	5.7447e+06	1644	1.6043e+09	5
3	3.7480e+05	5.7447e+06	1575	1.6043e+09	4
4	3.7469e+05	5.7447e+06	1506	1.6043e+09	5
5	3.7454e+05	5.7446e+06	1438	1.6043e+09	5
6	3.7443e+05	5.7446e+06	1362	1.6043e+09	5
7	3.7429e+05	5.7446e+06	1362	1.6043e+09	28
8	3.7553e+05	5.7429e+06	2038	1.6043e+09	5
9	3.7560e+05	5.7427e+06	2138	1.6043e+09	5
10	3.7562e+05	5.7426e+06	2138	1.6043e+09	4
11	3.7564e+05	5.7424e+06	2238	1.6043e+09	5
12	3.7568e+05	5.7423e+06	2238	1.6043e+09	5
13	3.7573e+05	5.7421e+06	2238	1.6043e+09	5
14	3.7574e+05	5.7420e+06	2238	1.6043e+09	5
15	3.7582e+05	5.7418e+06	2338	1.6043e+09	5
16	3.7584e+05	5.7417e+06	2338	1.6043e+09	4
17	3.7591e+05	5.7415e+06	2438	1.6043e+09	5

**b**

	1	2	3	4	5
	x	y	Altitude	Seconds	Time difference
1	3.7526e+05	5.7448e+06	1869	1.6043e+09	5
2	3.7510e+05	5.7447e+06	1756	1.6043e+09	5
3	3.7495e+05	5.7447e+06	1644	1.6043e+09	5
4	3.7480e+05	5.7447e+06	1575	1.6043e+09	4
5	3.7469e+05	5.7447e+06	1506	1.6043e+09	5
6	3.7454e+05	5.7446e+06	1438	1.6043e+09	5
7	3.7443e+05	5.7446e+06	1362	1.6043e+09	5
8	3.7429e+05	5.7446e+06	1362	1.6043e+09	5
9	3.7451e+05	5.7443e+06	1482	1.6043e+09	5
10	3.7473e+05	5.7440e+06	1603	1.6043e+09	5
11	3.7495e+05	5.7437e+06	1724	1.6043e+09	5
12	3.7517e+05	5.7434e+06	1845	1.6043e+09	5
13	3.7539e+05	5.7431e+06	1965	1.6043e+09	3
14	3.7553e+05	5.7429e+06	2038	1.6043e+09	5
15	3.7560e+05	5.7427e+06	2138	1.6043e+09	5
16	3.7562e+05	5.7426e+06	2138	1.6043e+09	4
17	3.7564e+05	5.7424e+06	2238	1.6043e+09	5

Figure 7: (a) Before and (b) after of Time Check Step

**Displacement check** rejection is due to a change in position that is deemed unrealistic for an aircraft, indicating extremely high speeds.

Lastly, **few observations** rejection indicated too few observations exist after previous check and processing step.

Table 3: Summary of Subtrack Rejection Reasons at Data Processing

WTC	Potential Rejection Reasons					Counts	
	Altitude check	Displacement check	Few Observations	Repeated row check	Outlier check	Unique Rejections	Tracks Without Removals
<b>Heavy</b>	14766	4062	14485	5033	207855	219998	<b>705921</b>
<b>Medium</b>	38509	24809	18481	7708	100116	171862	<b>2014631</b>
<b>Light</b>	20646	9059	12935	14126	12977	61130	<b>1135147</b>
<b>Helicopter</b>	8629	918	5346	2255	2827	16995	<b>295858</b>
<b>Gyro</b>	3	8	5	0	2	14	<b>862</b>
<b>Ultralight</b>	874	1650	38	3	32	1890	<b>1325</b>
<b>Military</b>	473	61	278	192	696	1457	<b>15511</b>
<b>Unknown</b>	591041	10904	239298	121268	214760	987701	<b>4253054</b>
<b>Total</b>						1461047	<b>8422309</b>

In preclean, tracks which have 10 observations or fewer were rejected, corresponding to 49.1% of total number of tracks. In processing, track rejections due to the altitude check, displacement check, repeated row check, and outlier check further removed 7.3% of the total number of tracks. While those number may seem high, these track rejections correspond to tracks that are often very short and physically unrealistic, accounting for only 10.6% of deduplicated observations, which is significantly lower than implied by track rejection rate. Besides, these short tracks are likely to be the result of split tracks (multiple tracks initiated by the radar system for the same target), or false radar detections that were later rejected by the radar system.

For the purpose of building an airspace model, including such tracks has no benefits or could even adversely affect the model; using realistic high-quality data is crucial to build an accurate model.

The detailed rejection counts in processing stage are summarized in Table 4. *Potential Rejection Reasons* columns count the total number of subtrack rejections (here, subtracks are referred to parts of tracks). *Unique Rejections* column counts the total number of total tracks which have at least one subtrack rejection and *Tracks Without Removals* column counts the number of tracks with no rejections at processing. To clarify, when data inconsistencies found within a track, only parts of tracks were removed to maintain the highest number of observations possible.

Following these removals and interpolation, the data was ready for the next stage of the analysis.

### 6.1.2 Track smoothing

One of the biggest challenges of this project was to take the data provided by the radar, and to be able to remove the noise and uncertainty to obtain a position estimate as accurate and realistic as possible. To overcome this challenge, Kalman filters were employed to generate estimates of hidden variables, such as velocity, and acceleration, from the imprecise position measurements. This process effectively smoothed the track and produced data that closely reflects real-world conditions, which was essential for developing an accurate airspace model.

The Kalman filter consists of two main stages as described in literature [14]:

Firstly, the prediction stage utilizes the previous state of the system and the equations governing its evolution to predict the current state. The equations for this stage are as follows:

- Predicted state estimate:  $\hat{x}_{k|k-1} = F_k \hat{x}_{k-1|k-1}$
- Predicted error covariance:  $P_{k|k-1} = F_k P_{k-1|k-1} F_k^T + Q_k$

Where,  $F_k$  is the evolution matrix,  $\hat{x}_{k-1|k-1}$  the estimate the previous time step,  $P_{k-1|k-1}$  the covariance matrix the previous time step, and  $Q_k$  the process white noise matrix.

Secondly, the correction stage utilizes measured data from the sensors to refine the estimate produced by the prediction stage based on calculated gains. The equations for this stage are:

- Innovation measurement:  $nuk = z_k - H_k \hat{x}_{k|k-1}$
- Innovation covariance:  $S_k = H_k P_{k|k-1} H_k^T + R_k$
- Optimal Kalman Gain  $K_k = H_k P_{k|k-1} H_k^T S_k^{-1}$
- Corrected state estimate  $\hat{x}_{k|k} = \hat{x}_{k|k-1} + K_k * nuk$
- Corrected estimate covariance  $P_{k|k} = (I - K_k H_k) P_{k|k-1}$

Where,  $z_k$  is the measurement taken by the sensor,  $H_k$  the measurement matrix, and  $R_k$  the measurement white noise matrix.

In view of the flight dynamics of an aircraft, three models were chosen for implementation, inspired by the findings of previous research conducted by scholars like Genovese [15] and Watson & Blair [16], who have demonstrated the effectiveness of these models. The selected models comprise of the constant velocity model, constant acceleration model, and constant turn model - the implementation and results of which are presented in detail below.

**Constant Velocity Model (CV):** describes the behavior of tracks with a constant velocity.

- Initial state vector:  $x = \begin{bmatrix} x & y & z & \frac{dx}{dt} & \frac{dy}{dt} & \frac{dz}{dt} \end{bmatrix}$
- Initial covariance vector:  $P = 0_{6x6}$
- Evolution matrix:  $F = \begin{bmatrix} I_{3x3} & diag(T) \\ 0_{3x3} & I_{3x3} \end{bmatrix}$
- Measurement matrix:  $H = [I_{3x3} \quad 0_{3x3}]$
- Measurement noise matrix:  $R = [diag(\sigma_{3x3}^2)]$
- Process noise matrix:  $Q = q \begin{bmatrix} \frac{T^3}{m_{3x3}} & \frac{T^2}{m_{3x3}} \\ \frac{T^2}{m_{3x3}} & T_{3x3} \end{bmatrix}$

**Constant Acceleration Model (CA):** describe the behavior of tracks that undergo changes in velocity at a constant rate.

- Initial state vector:  $x = \begin{bmatrix} x & y & z & \frac{dx}{dt} & \frac{dy}{dt} & \frac{dz}{dt} & \frac{d^2x}{dt^2} & \frac{d^2y}{dt^2} & \frac{d^2z}{dt^2} \end{bmatrix}$
- Initial covariance vector:  $P = 0_{9x9}$
- Evolution matrix:  $F = \begin{bmatrix} I_{3x3} & diag(T) & diag\left(\frac{T^2}{2}\right) \\ 0_{3x3} & I_{3x3} & diag(T) \\ 0_{3x3} & 0_{3x3} & I_{3x3} \end{bmatrix}$
- Measurement matrix:  $H = [I_{3x3} \quad 0_{3x6}]$
- Measurement noise matrix:  $R = [diag(\sigma_{3x3}^2)]$
- Process noise matrix:  $Q = q \begin{bmatrix} 0_{3x3} & 0_{3x3} & 0_{3x3} \\ 0_{3x3} & 0_{3x3} & 0_{3x3} \\ 0_{3x3} & 0_{3x3} & T_{3x3} \end{bmatrix}$

**Constant Turn Model (CT):** describe the behavior of tracks performing turns at a constant rate.

- Initial state vector:  $x = \begin{bmatrix} x & y & z & \frac{dx}{dt} & \frac{dy}{dt} & \frac{dz}{dt} \end{bmatrix}$
  - Initial covariance vector:  $P = 0_{6x6}$
  - Evolution matrix:  $q = \begin{bmatrix} 1 & \frac{\sin \omega T}{\omega} & \frac{1-\cos \omega T}{\omega^2} \\ 0 & \cos \omega T & \frac{\sin \omega T}{\omega} \\ 0 & -\omega \sin \omega T & \cos \omega T \end{bmatrix}$
  - Measurement matrix:  $H = [I_{3x3} \quad 0_{3x3}]$
  - Measurement noise matrix:  $R = [diag(\sigma_{3x3}^2)]$
  - Process noise matrix:  $Q = q \begin{bmatrix} \frac{T^3}{3} & \frac{T^2}{2} \\ \frac{T^2}{2} & T_{3x3} \end{bmatrix}$
- $$f = \begin{bmatrix} I_{3x3} & diag(q_{12}) & diag(q_{13}) \\ 0_{3x3} & diag(q_{22}) & diag(q_{23}) \\ 0_{3x3} & diag(q_{32}) & diag(q_{33}) \end{bmatrix}$$

where  $x, y, \text{ and } z$  are the position coordinates in each axis,  $T$  represents the time interval,  $\sigma$  the noise covariance,  $\omega$  the turning rate, and  $I$  represent the identity matrix.

**Interacting Multiple Models algorithm:** The use of the three models CA, CV, and CT allowed for the management of different stages of flight; however, to achieve the desired performance, it was crucial to efficiently manage all of them. This was accomplished by applying an Interactive Multiple Models (IMM)

algorithm, which enabled the combination of state estimates from the different models to produce a more realistic estimate, considering the changing dynamics of the flight. This was achieved through an underlying Markov chain that governs the interaction between the different models, given more weight to the model that best fits the aircraft dynamics in the estimated state [14].

Similar to the individual Kalman filters, determining the appropriate initial conditions for the IMM algorithm was crucial for its performance. The initial set up of the matrices, which were determined using the first two observations of the flight track, are presented below:

- Initial state vector:  $x = \begin{bmatrix} x & y & z & \frac{dx}{dt} & \frac{dy}{dt} & \frac{dz}{dt} & 0 & 0 & 0 \\ x & y & z & \frac{dx}{dt} & \frac{dy}{dt} & \frac{dz}{dt} & \frac{d^2x}{dt^2} & \frac{d^2y}{dt^2} & \frac{d^2z}{dt^2} \\ x & y & z & \frac{dx}{dt} & \frac{dy}{dt} & \frac{dz}{dt} & 0 & 0 & 0 \end{bmatrix}^T$
- Transition probability:  $p = \begin{bmatrix} p_{11} & p_{12} & p_{13} \\ p_{21} & p_{22} & p_{23} \\ p_{31} & p_{32} & p_{33} \end{bmatrix}$
- Model Probability:  $\mu = [\mu_1 \quad \mu_2 \quad \mu_3]^T$

The other required matrices are the same as the ones shown for each model but each one set as an element in a 3-dimensional array for each variable (P, F, H, R, Q). Once the initial conditions were defined and the matrices built, it was possible to execute the algorithm combining the estimations of the 3 different Kalman filter models. As a result, the smoothed track and information on speed and acceleration in each axis was determined.

To ensure that the Interacting Multiple Model (IMM) approach was effective in improving tracking results, it was necessary to determine the noise levels of both the sensor observations and the process noise (R, Q). The International Civil Aviation Organization (ICAO) standards [17], as outlined in Table 4, were chosen as the benchmark for this analysis, given that radar systems are expected to comply with these standards. Accordingly, the measurement noise matrix was adjusted to optimize the results obtained. Additionally, simulated flights were utilized to evaluate the performance of the Kalman filter and refine its parameters, to which noise was added in a similar fashion as the RDPS data.

To further minimize errors across all variables, a multi-objective optimization algorithm called the Strength

Pareto Evolutionary Algorithm (SPEA2) was utilized. [18] This algorithm allowed for the selection of parameter values that would yield the most accurate results possible, as determined through an iterative process that focussed on reducing the error between the truth values and the estimated values, the results obtained are shown in [27].

Then, the refined parameter values were then used to apply the IMM approach to all tracks, resulting in significant improvements in results across various aircraft types and stages of flight, as illustrated in Figure 8 to 11. The data obtained from this process is presented in Figure 12 and was utilized in the subsequent stages to extract the relevant information necessary for creating airspace models.

**Table 4: Radar Performance Characteristics ICAO (2007)**

Range		Accuracy	Revisit rate
<b>Primary surveillance radar (PSR)</b>	S-band typically 60-80 NM  L-band 160-220 NM	In range: 0.1 NM rms or 0.2 NM $2\sigma$ In azimuth: 0.15 degrees rms or 0.3 degrees $2\sigma$	5 seconds
<b>Secondary surveillance radar (SSR)</b>	200 NM-250 NM	For monopulse radar  In range: 0.03 NM rms  In azimuth: 0.07 degrees rms or 0.14 degrees $2\sigma$ for random errors.  At 50 NM range the 0.14-degree error results in a position error of 0.12 NM. At 100 NM range: 0.24 NM At 200 NM: 0.48 NM At 250 NM: 0.60 NM	5 seconds
<b>Automatic Dependent Surveillance-Broadcast (ADS-B)</b>	200 NM-250 NM	Determined by the aircraft avionics and independent of range from sensor.  For GPS, typically: 95% less than 0.1 NM	Typically, 1 second from ground station.

**Table 5: IMM Calculated Error**

Variable	RMSE	Average Error	Standard Deviation
<b>Speed (knots)</b>	7.6290	5.7722	7.4089
<b>Acceleration (knots/sec)</b>	1.3640	1.1191	1.3724
<b>Vertical Rate (feet/sec)</b>	5.8942	3.9958	5.7898
<b>Turn Rate (deg/sec)</b>	3.6721	2.5685	3.4038
<b>X-Axis (meter)</b>	58.8577	47.8442	44.7376
<b>Y-Axis (meter)</b>	48.2647	38.7624	41.4567
<b>Z-Axis (feet)</b>	22.7493	15.6588	19.1113

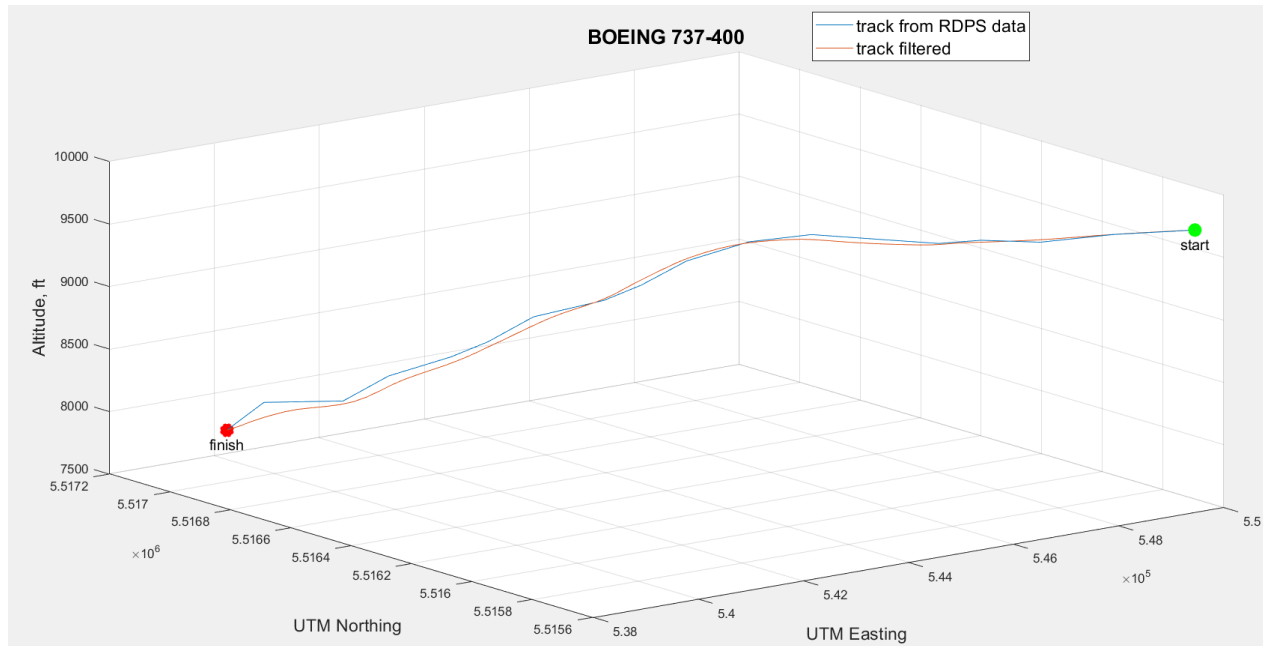


**Figure 8: Track of Boeing 737-400- Commercial aircraft commencing a descent**

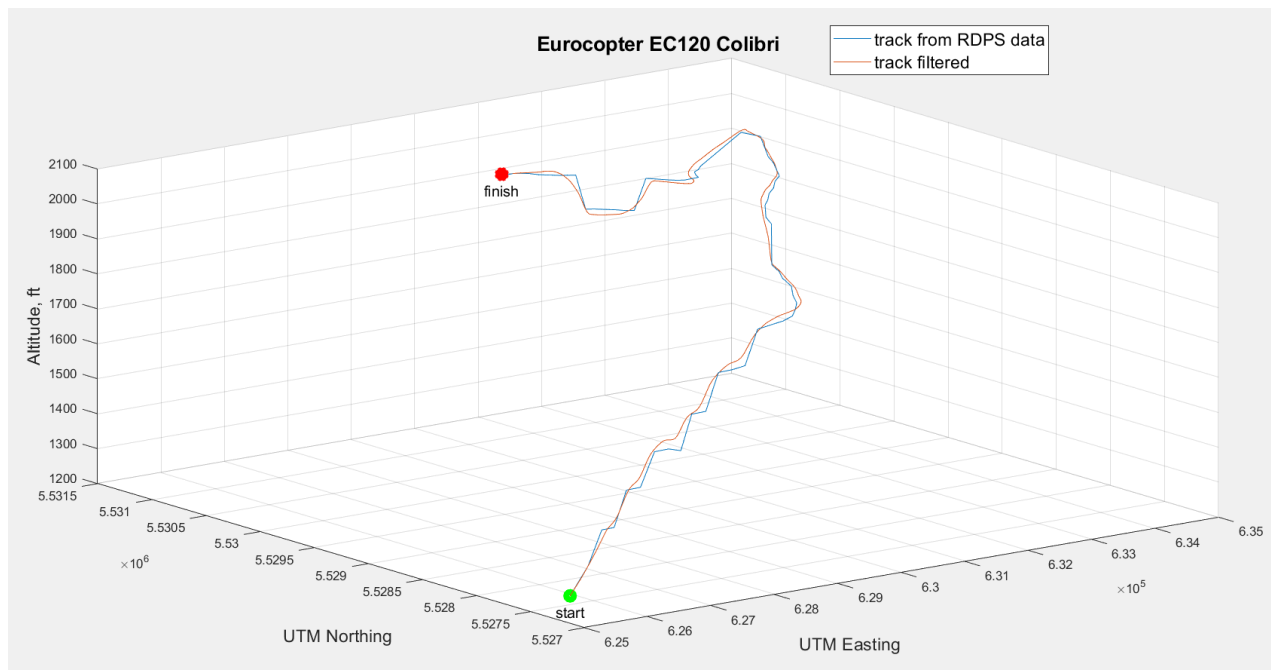


**Figure 9: Track of Eurocopter EC120 Colibri- Helicopter in ascent**

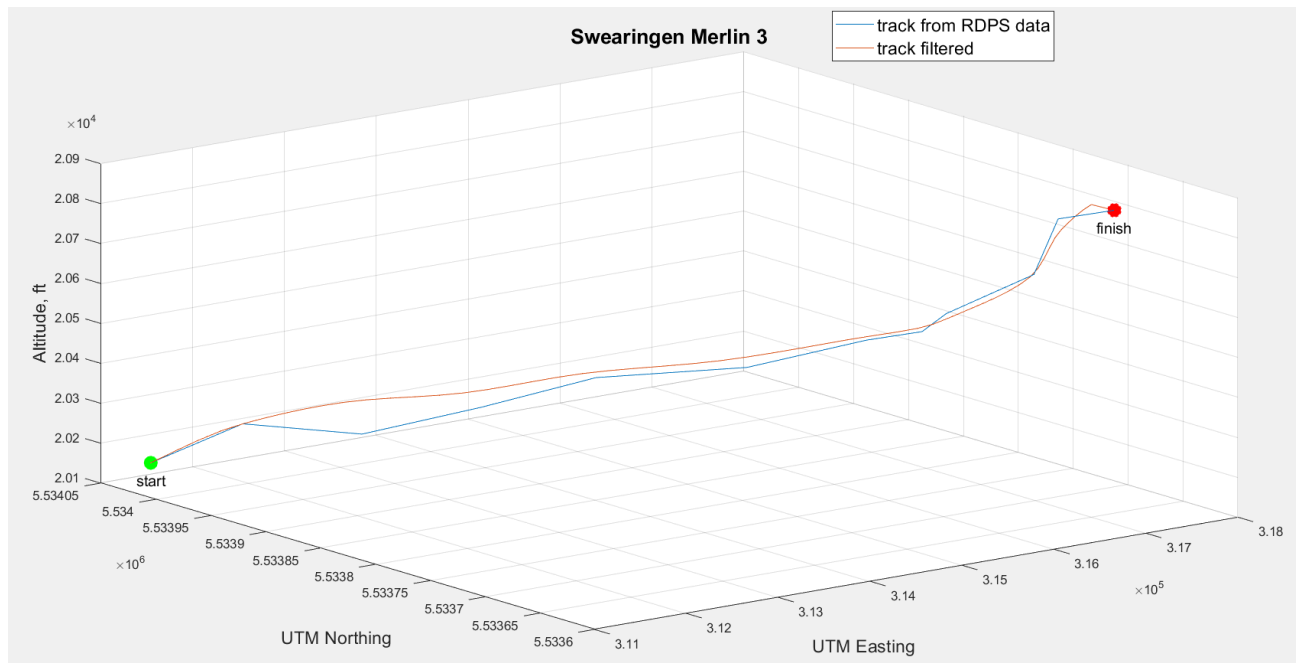


**Figure 10: Track of Swearingen Merlin 3-Business Turboprop in ascent**

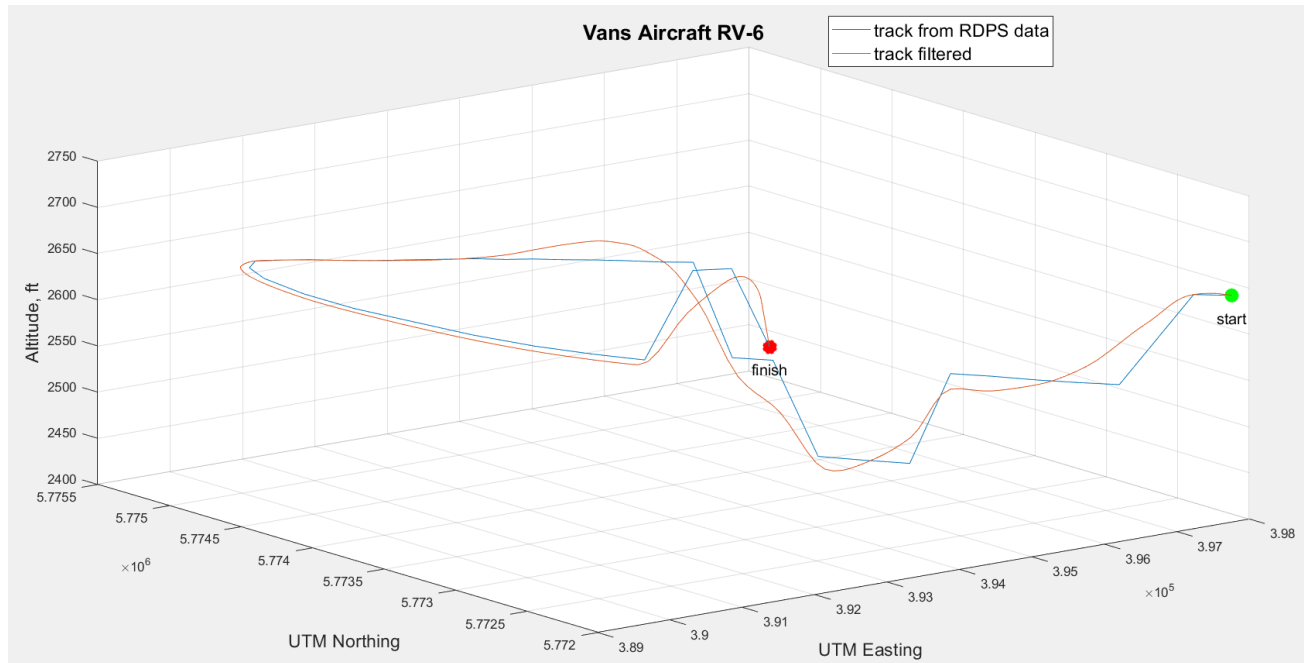


**Figure 11: Track of Vans Aircraft RV-6- Light aircraft performing turns**

	1 x	2 y	3 z	4 velocity-x	5 velocity-y	6 velocity-z	7 acceleration-x	8 acceleration-y	9 acceleration-z	10 Time
1	6.4800e+05	5.5409e+06	2031	34.2071	24.1499	0	0	-1.3068e-04	0	1.6042e+09
2	6.4803e+05	5.5409e+06	2031	34.1113	24.0487	0	-0.0145	-0.0156	0	1.6042e+09
3	6.4806e+05	5.5409e+06	2031	34.0588	23.9928	0	-0.0239	-0.0257	0	1.6042e+09
4	6.4810e+05	5.5409e+06	2031	34.0541	23.9869	0	-0.0261	-0.0281	0	1.6042e+09
5	6.4813e+05	5.5410e+06	2031	34.1021	24.0358	0	-0.0188	-0.0207	0	1.6042e+09
6	6.4817e+05	5.5410e+06	2031	34.2074	24.1443	0	0	-0.0012	0	1.6042e+09
7	6.4821e+05	5.5410e+06	2031	34.4025	24.3487	0	0.0331	0.0334	0	1.6042e+09
8	6.4826e+05	5.5410e+06	2031	34.6951	24.6569	0	0.0775	0.0798	0	1.6042e+09
9	6.4831e+05	5.5411e+06	2031	35.0527	25.0312	0	0.1268	0.1315	0	1.6042e+09
10	6.4835e+05	5.5411e+06	2031	35.4427	25.4340	0	0.1746	0.1816	0	1.6042e+09
11	6.4839e+05	5.5411e+06	2031	35.8830	25.9261	0	0.2226	0.2363	0	1.6042e+09
12	6.4843e+05	5.5412e+06	2031	36.3888	26.5303	0	0.2739	0.2991	0	1.6042e+09
13	6.4847e+05	5.5412e+06	2031	36.9233	27.1520	0	0.3243	0.3589	0	1.6042e+09
14	6.4851e+05	5.5412e+06	2031	37.4498	27.6967	0	0.3696	0.4046	0	1.6042e+09

Figure 12: Data obtained and track smoothing process

### 6.1.3 Overview of Simulated Flights

As radar data is typically noisy and has an update period of 4-15 seconds, information of the reported location of an aircraft will contain positional uncertainty. To determine the effect of these factors on the accuracy of the tracks and to test the robustness of the developed filter, realistic flights were flown in the X-Plane flight simulator engine. This provided noise-free tracks that could be run through a radar model, outputting data similar to real radar to assess the filter accuracy.

14 flights have been flown, providing close to 15 hours of flight data recordings. The majority of these flights were conducted in small civil aircraft, such as the Cessna 172 and the Beechcraft Baron 58, and were flown to recreate typical flight-training flights as these are highly sporadic and unpredictable in movement when compared to typical commercial flights. These types of flights were the most extreme cases that the filter would encounter and thus were the best test of its robustness. These flights included manoeuvres such as stalls, spins, spiral dives, steep turns, lazy eights, and more. For each flight, a detailed flight plan was created, outlining each manoeuvre that was to be performed. The start and stop time of each manoeuvre was recorded allowing for them to be identified in the datasets, such that they could be extracted and analysed independently. The flights were flown at various locations including Toronto (CYYZ), Winnipeg (CYWG), and Montreal (CYUL), as this allowed for differing radar location scenarios to be applied to the datasets. In addition, several flights have been conducted in medium aircraft such as the Boeing 737.

### 6.1.4 Variable Extraction

The next step consisted of the selection of variables for describing the trajectory of an aircraft with the goal of enabling the generation of new trajectories that accurately reflect the behavior of aircraft in a given airspace. These variables were chosen with consideration given to their potential use in a Bayesian network structure, which will be explored in later steps of the process.

- **Airspace Class:** This variable is a crucial factor as an aircraft's behavior is dependent on the class of airspace it is operating in. The Canadian airspace is classified into seven classes, designated by the letters A to G. However, for the purpose of the model, they were denoted by the numbers 1 to 7, respectively. To determine this variable, a file developed by the NRC using NAV CANADA's airspace data was employed [3]. An algorithm was developed that compared the aircraft's position (x, y, z coordinates) with the database of airspace types, as illustrated in Figure 13. If the aircraft

was within the designated airspace, the corresponding identifier was assigned. If not, the altitude was evaluated, and depending on that, the airspace class was assigned. For instance, if the aircraft was between FL180 and FL600, it was assigned as 1 (Class A); if below FL180, it was assigned as 7 (Class G); and if above FL600, it was assigned as 5 (Class E) airspace established in Canada, and although these are designated by the letters A to G, for the purpose of the model, they were designated by the numbers 1 to 7 respectively.

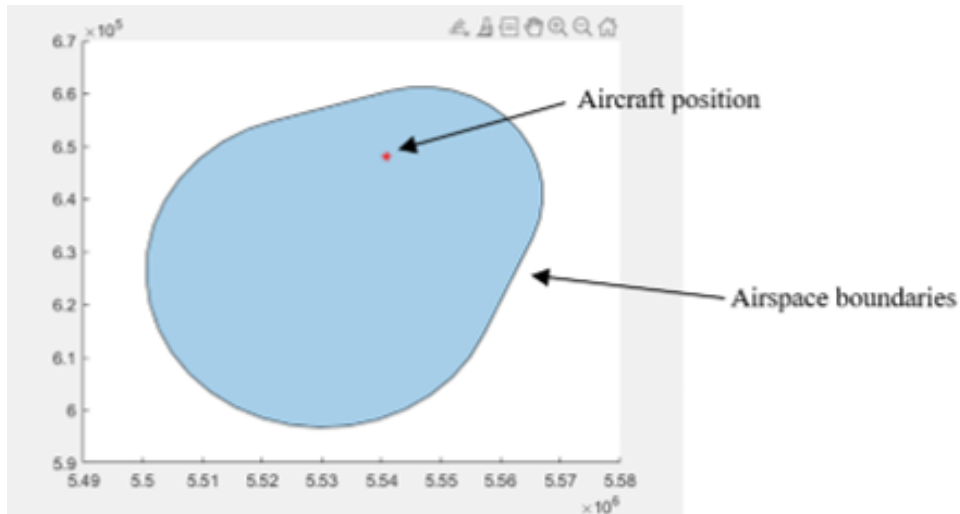


Figure 13: Airspace Class determination Algorithm Visualization

- **Altitude layer (feet):** This variable plays a crucial role in characterizing the aircraft's behavior during different phases of flight. It is presented in units of feet and readily available in the third column of the table obtained from the IMM, eliminating the need for further computations.
- **Speed (knots):** To obtain this variable, the data in Columns 4 to 6 of the IMM algorithm's resulting table, which represent the aircraft's speed in the x, y, and z axes, are utilized and subjected to the following mathematical expression:

$$v = \sqrt{v_x^2 + v_y^2 + v_z^2}$$

It is worth noting that this variable is expressed in knots and is subject to change every second, reflecting the ground speed of the aircraft; however, the effects of wind have not been accounted for.

- **Acceleration (knots/sec):** The computation of this variable involves taking Columns 7 to 9 from the data table derived from the IMM algorithm, which correspond to the acceleration in the x, y, and z-axis. The calculation is performed by utilizing the following formula:

$$a = \sqrt{a_x^2 + a_y^2 + a_z^2}$$

It is worth noting that this variable is expressed in knots per second and may vary every second.

- **Vertical Speed (feet/min):** Can be obtained directly from the result of the IMM algorithm, specifically from the third column which represents the velocity on the Z-axis. However, the result is expressed in meters per second, so unit conversion is necessary to express it in feet/min. The variation of this variable is allowed every second to achieve a more accurate description of the aircraft dynamics.

- **Turn rate (degree/sec):** Represents the rate of heading change per unit of time. In this model, the variation of this variable is also allowed every second. An algorithm was developed to calculate the heading of the aircraft by considering the direction it was heading an instant before and after the analyzed point, thus calculating the heading variation.
- **Wake Turbulence Category (WTC):** Variable exclusive to the mixed model and was included to improve the accuracy of the flight dynamics representation for various types of aircraft. To classify this variable, the ICAO standard [19] was adopted, with additional categories created for helicopters, gyrocopters, ultralights, and military aircraft due to their unique flight characteristics. Moreover, an unknown category was also introduced to classify and analyze flight tracks that could not be categorized due to insufficient information in the database but was still desired to be included as part of the airspace. Table 66 shows a summary of this information, and this classification is done in the previous data storing process using the maximum take-off weight field in the RDPS dataset.

**Table 6: Data classification according to aircraft characteristics**

Classification	Description
<b>Light aircraft</b>	Maximum Takeoff Weight lower or equal to 7,000 kg
<b>Medium aircraft</b>	Maximum Takeoff Weight higher than 7,000 kg and lower than 136,000 kg
<b>Heavy aircraft</b>	Maximum Takeoff Weight higher or equal to 136,000 kg
<b>Helicopter</b>	Rotorcraft that is lifted and propelled by rotors
<b>Gyrocopter</b>	Rotorcraft that uses an unpowered rotor in autorotation to develop lift, and a separate power source to provide thrust
<b>Ultralight</b>	Maximum take-off mass of 454 kg
<b>Military</b>	Aircraft that are designed for use by military forces
<b>Unknown</b>	Tracks that were not possible to classify

Once all the necessary variables were defined, a MATLAB function called "*Variable\_Extraction.m*" was developed to extract and process the results obtained from the IMM algorithm. This function carries out all the calculations described earlier and generates a table containing all the required variables. The output of this algorithm (Figure 14) was saved as a .csv file that included the additional information from the input data, as well as, the estimated positions of the smoothed track, for further processing in the subsequent steps. Reference [27] presents the accuracy achieved by the filter in predicting each variable, which was calculated using simulated flights and is expected to be replicated in the RDPS tracks.

The diagram illustrates a data processing workflow. At the top, a table titled "Track\_Final" (2464x10 table) contains 14 rows of data. An arrow points down to a script file named "Variables\_Extraction.m". Another arrow points down to a table titled "Variables(1, 1)" (Variables(1, 1)). This table has 14 rows and 7 columns, labeled 1 through 7. The columns represent variables: WTC, Airspace Class, Altitude ft, Airspeed kt, Acceleration kt/s, Vertical rate ft/min, and Turn rate deg/s.

	1	2	3	4	5	6	7	8	9	10
	x	y	z	velocity-x	velocity-y	velocity-z	acceleration-x	acceleration-y	acceleration-z	Time
1	6.4800e+05	5.5409e+06	2031	34.2071	24.1499	0	0	-1.3068e-04	0	1.6042e+09
2	6.4803e+05	5.5409e+06	2031	34.1113	24.0487	0	-0.0145	-0.0156	0	1.6042e+09
3	6.4806e+05	5.5409e+06	2031	34.0588	23.9928	0	-0.0239	-0.0257	0	1.6042e+09
4	6.4810e+05	5.5409e+06	2031	34.0541	23.9869	0	-0.0261	-0.0281	0	1.6042e+09
5	6.4813e+05	5.5410e+06	2031	34.1021	24.0358	0	-0.0188	-0.0207	0	1.6042e+09
6	6.4817e+05	5.5410e+06	2031	34.2074	24.1443	0	0	-0.0012	0	1.6042e+09
7	6.4821e+05	5.5410e+06	2031	34.4025	24.3487	0	0.0331	0.0334	0	1.6042e+09
8	6.4826e+05	5.5410e+06	2031	34.6951	24.6569	0	0.0775	0.0798	0	1.6042e+09
9	6.4831e+05	5.5411e+06	2031	35.0527	25.0312	0	0.1268	0.1315	0	1.6042e+09
10	6.4835e+05	5.5411e+06	2031	35.4427	25.4340	0	0.1746	0.1816	0	1.6042e+09
11	6.4839e+05	5.5411e+06	2031	35.8830	25.9261	0	0.2226	0.2363	0	1.6042e+09
12	6.4843e+05	5.5412e+06	2031	36.3888	26.5303	0	0.2739	0.2991	0	1.6042e+09
13	6.4847e+05	5.5412e+06	2031	36.9233	27.1520	0	0.3243	0.3589	0	1.6042e+09
14	6.4851e+05	5.5412e+06	2031	37.4498	27.6967	0	0.3696	0.4046	0	1.6042e+09

	1	2	3	4	5	6	7
	WTC	Airspace Class	Altitude ft	Airspeed kt	Acceleration kt/s	Vertical rate ft/min	Turn rate deg/s
1	1	5	2031	81.3943	0	0	0
2	1	5	2031	81.1288	-0.0414	0	0
3	1	5	2031	80.9827	-0.0682	0	-0.4290
4	1	5	2031	80.9686	0.0746	0	-0.2834
5	1	5	2031	81.0996	0.0544	0	-0.1826
6	1	5	2031	81.3884	0.0023	0	-0.1067
7	1	5	2031	81.9275	0.0914	0	-0.0689
8	1	5	2031	82.7380	0.2163	0	-0.1243
9	1	5	2031	83.7263	0.3551	0	-0.2109
10	1	5	2031	84.7985	0.4897	0	-0.3386
11	1	5	2031	86.0521	0.6311	0	-0.6514
12	1	5	2031	87.5376	0.7884	0	-0.5399
13	1	5	2031	89.0899	0.9403	0	-0.0669
14	1	5	2031	90.5420	1.0652	0	0.4332

Figure 14: Before (Above) and after (Below) of Variable extraction Process

### 6.1.5 Variable interpolation and data arrangement

The final two steps of this stage are combined into a single process. The input for this process is the file generated in the previous step, to which an Akima cubic piecewise Hermite interpolation [20] was applied for both positions and variables. The purpose of this interpolation was to increase the resolution of the radar data observations to 1-second, since, as mentioned before and shown in Table 4, they are typically available at 5-second intervals. This type of interpolation was chosen because it maintained the shape of the track and performed faster compared to other types of interpolation or using Kalman filer predictions. Finally, an algorithm was developed the UTM zone standardization and data arrangement as required by the server, to save space (see Section 5.2 on disk space optimization).

## **6.2 Stage 2: Determination of Statistical Characteristics and Arrangement of the Dataset**

During this stage, the primary focus was on analyzing the variables and gaining insights into aircraft behavior within the airspace. Effective visualization of the variable distributions played a crucial role in achieving this objective. However, considering the extensive volume of data, loading it into a data visualization software to create histograms would be impractical.

To overcome this challenge, a MATLAB function was developed specifically for this purpose. This function utilized information on edges and counts obtained directly from the database to generate histograms and calculate significant statistical measures. The input data summarized the dataset by identifying the minimum and maximum values for each variable, and then incrementing them by a fixed unit to establish the edges. The counts represented the number of observations falling within each bin or edge.

To enhance the clarity of the pie charts, a simplification was made by merging the categories "Gyrocopter," "Ultralight," and "Military" into a single category labeled as "Others." This consolidation facilitates a more coherent visualization of the data.

These visualizations were generated for 12 selected airspace areas around different Canadian airports, ranging from large international airports to small regional ones, and considering tracks from the surface up to 10,000 feet ASL to observe the differences in aircraft behavior under different conditions. While this section presents the results for only three airport regions - Ottawa/Macdonald–Cartier International Airport-CYOW (Figure 15-Table 7), Victoria International Airport-CYJJ (Figure 16-Table 8), and Montréal-Trudeau International Airport CYUL (Figure 17-Table 9) - the results obtained for the remaining nine airports are included in Appendix A.

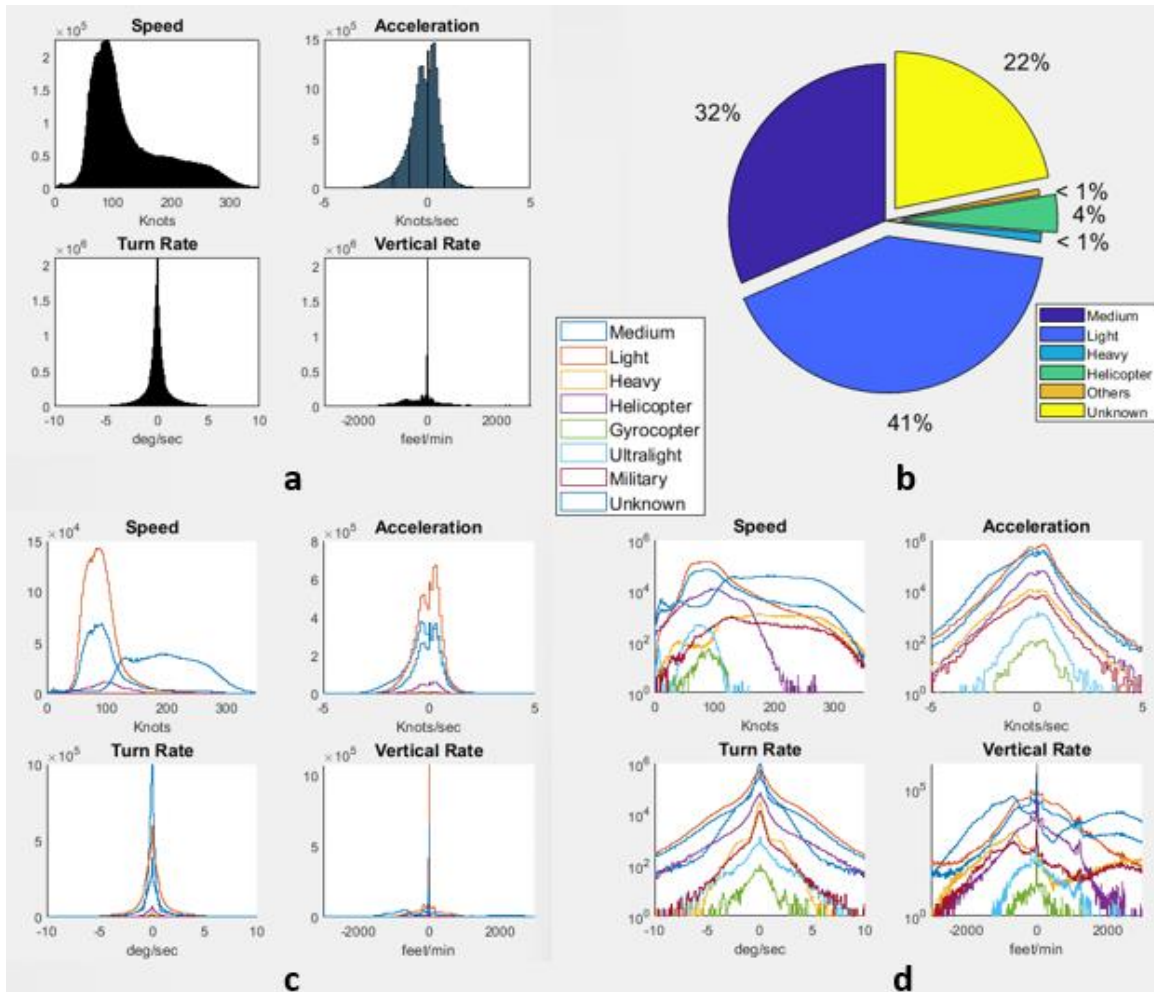


**Figure 15: Ottawa/Macdonald–Cartier International Airport Model (CYOW) 0-10,000 ft ASL**  
**(a) Mixed model distribution (b) Aircraft categories percentages (c) Variables distributions by aircraft category (d) Underlying distributions shape**

**Table 7: Descriptive Statistics of Variable Distributions for CYOW (0-10,000 ft ASL): Mean, Mode, and Standard Deviation**

Variable	Mean	Mode	Standard Deviation
Speed (knots)	128.0975	91	67.4141
Turn Rate (deg/sec)	-0.0258	0	1.5993
Vertical Rate (feet/sec)	73.5145	0	991.9793
Acceleration (knots/sec)	-0.1978	0.3	0.7641

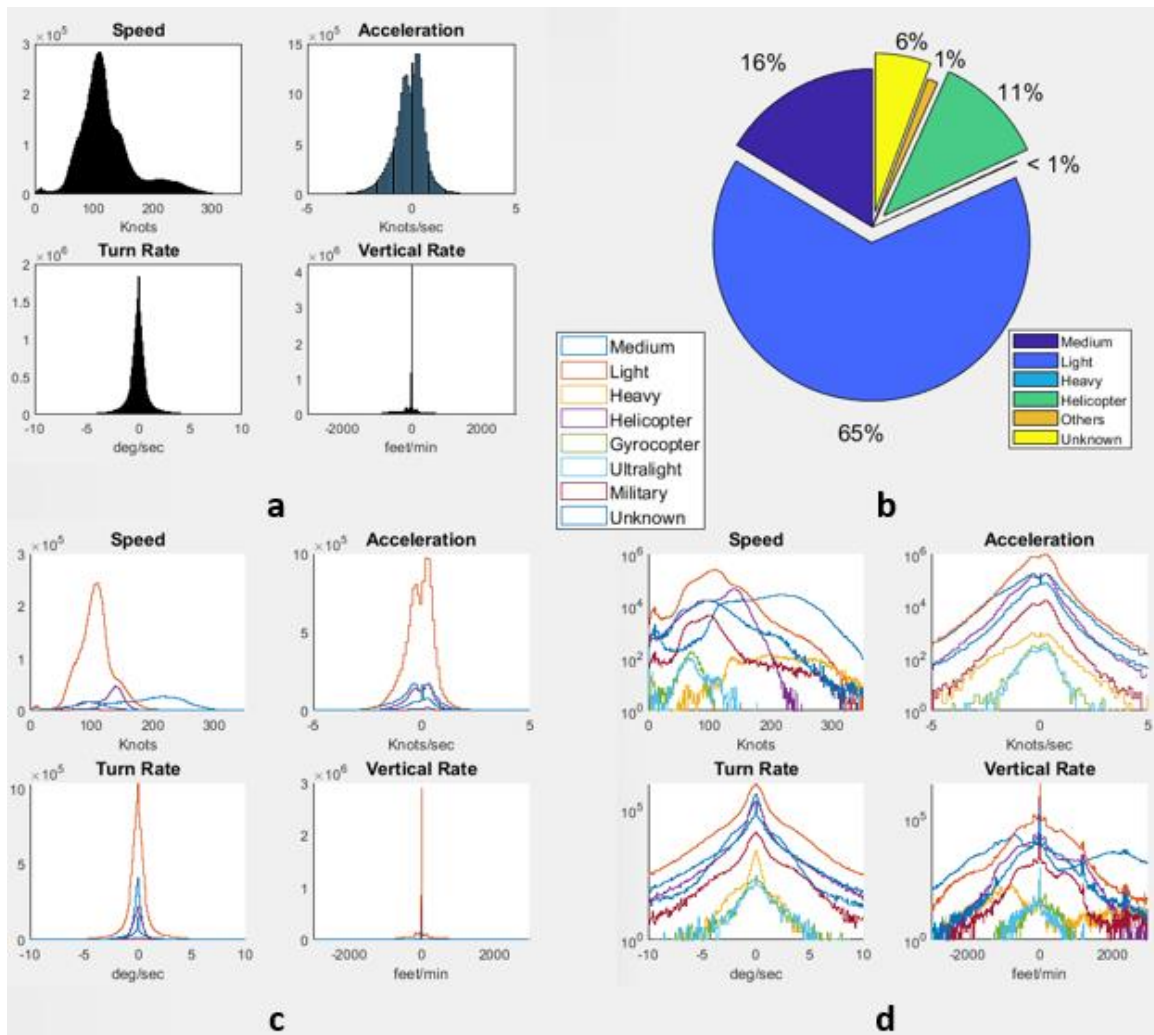


Figure 16: Victoria International Airport Model (CYYJ) 0-10,000 ft ASL

(a) Mixed model distribution (b) Aircraft categories percentages (c) Variables distributions by aircraft category (d) Underlying distributions shape

Table 8: Descriptive Statistics of Variable Distributions for CYYJ (0-10,000 ft ASL): Mean, Mode, and Standard Deviation

Variable	Mean	Mode	Standard Deviation
Speed (knots)	122.3824	108	48.2432
Turn Rate (deg/sec)	-0.0571	0	1.4048
Vertical Rate (feet/sec)	-14.5177	0	650.2516
Acceleration (knots/sec)	-0.1741	0.3	0.7816

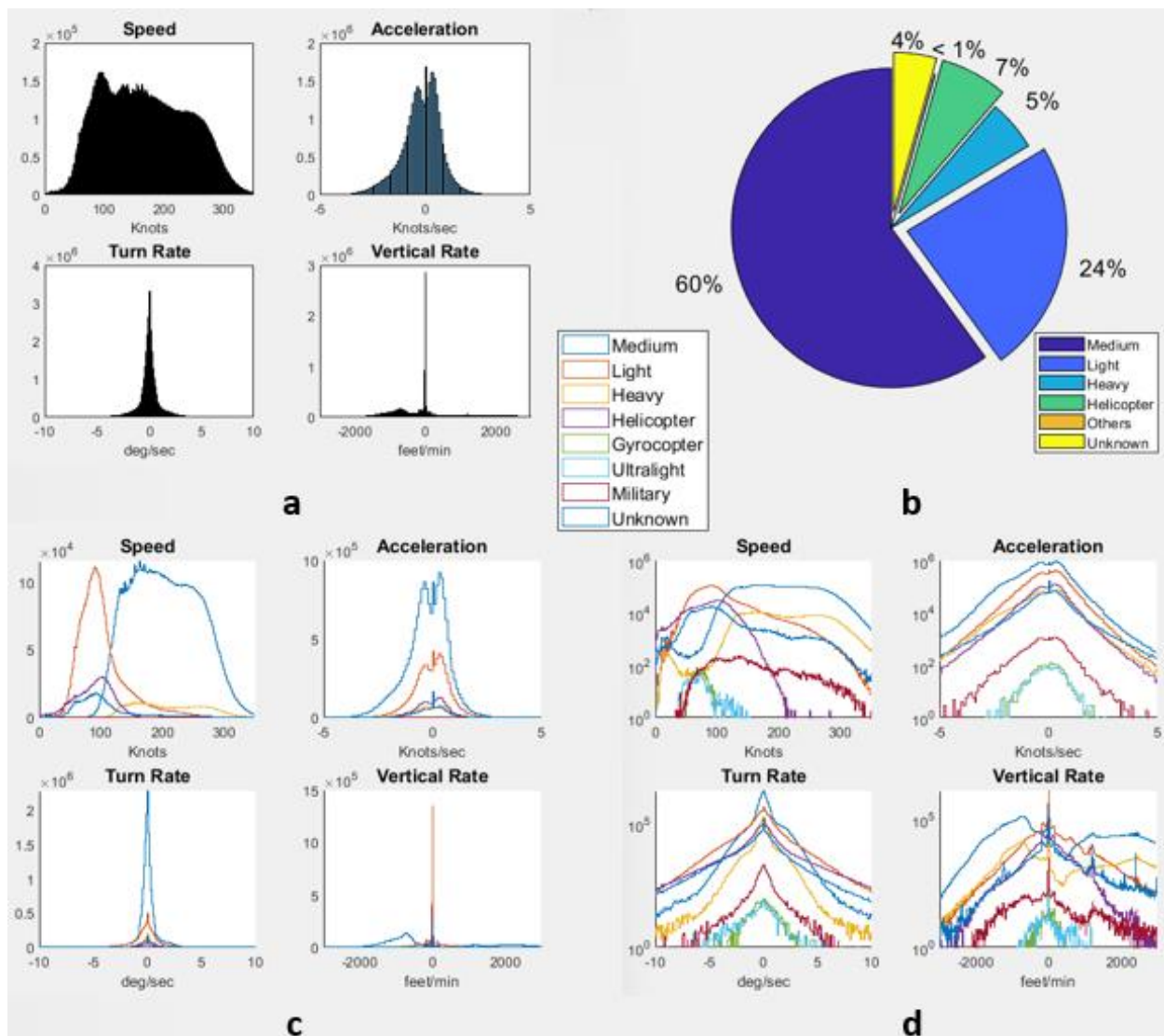


Figure 17: Montréal-Trudeau International Airport (CYUL) 0-10,000 ft ASL

(a) Mixed model distribution (b) Aircraft categories percentages (c) Variables distributions by aircraft category (d) Underlying distributions shape

Table 9: Descriptive Statistics of Variable Distributions for CYUL (0-10,000 ft ASL): Mean, Mode, and Standard Deviation

Variable	Mean	Mode	Standard Deviation
Speed (knots)	167.7059	91	70.9853
Turn Rate (deg/sec)	-0.0579	0	1.3291
Vertical Rate (feet/sec)	61.4624	0	1179.4987
Acceleration (knots/sec)	-0.2158	0	0.9579

To obtain a comprehensive understanding of aircraft behavior across all categories and altitudes, an analysis was conducted on Canada-wide data (mixed model). The analysis provided a comprehensive view of the observed ranges across all variables, as well as the percentage of observations within each selected category. The results of the model obtained are presented in Figure 18 and Table 10.

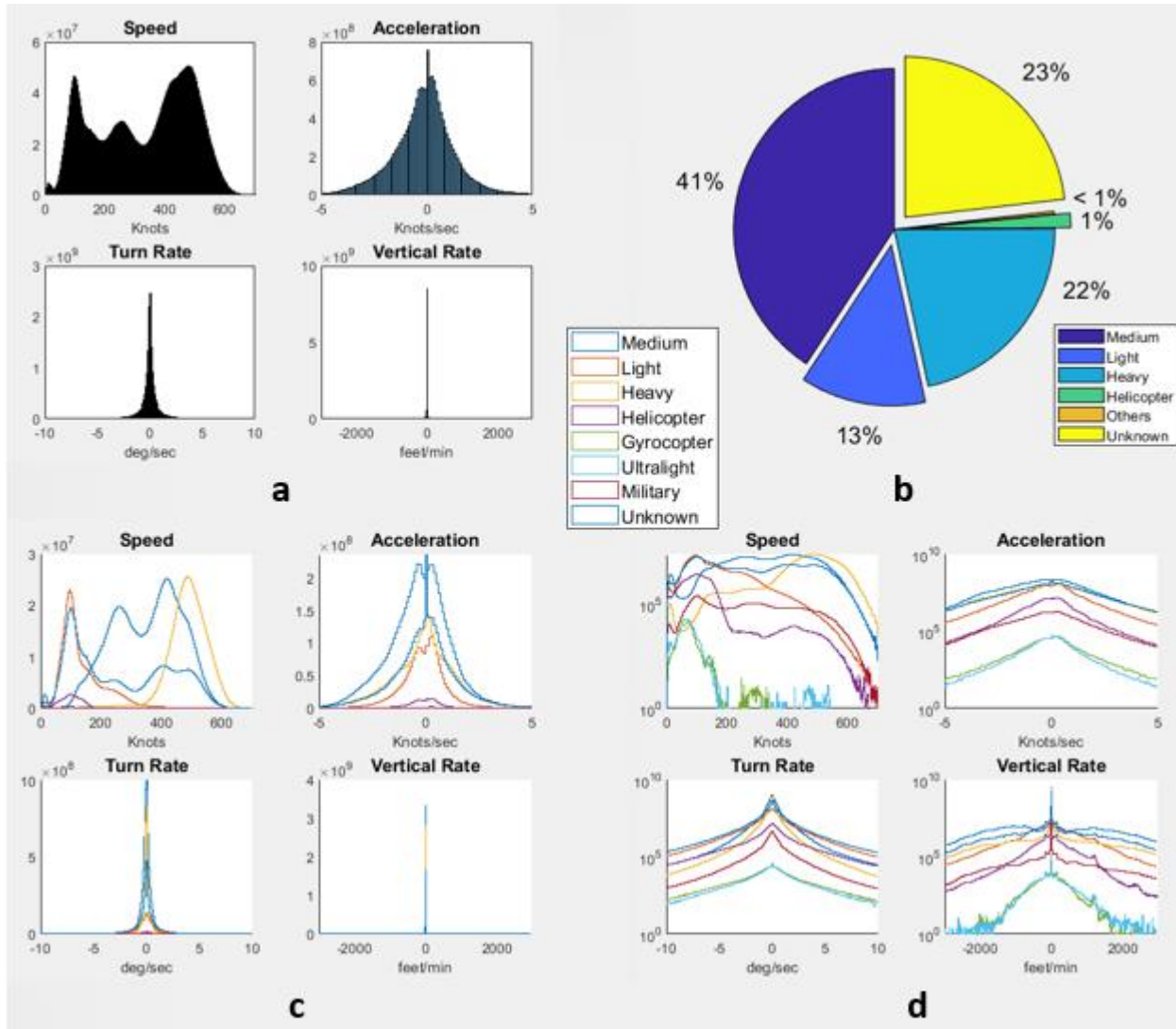


**Figure 18: Canada Wide 2017 - All Altitudes**

- (a) Mixed model distribution
- (b) Aircraft categories percentages
- (c) Variables distributions by aircraft category
- (d) Underlying distributions shape

**Table 10: Descriptive Statistics of Variable Distributions for Canada (All altitudes): Mean, Mode, and Standard Deviation**

Variable	Mean	Mode	Standard Deviation
Speed (knots)	330.6401	476.5	214.5086
Turn Rate (deg/sec)	-0.1595	0.05	1.5410
Vertical Rate (feet/sec)	-0.5975	0	778.8337
Acceleration (knots/sec)	-0.0104	0.05	1.2208

The first three models were developed for the airports of different sizes: a medium-sized airport CYOW, a small airport CYJJ, and a large airport CYUL, with all data being considered at altitudes below 10,000 feet ASL. The histograms and statistical descriptions provided interesting insights into the behavior of aircraft in different airport categories. For example, the mean speed at CYOW was lower than that of CYUL, which could be attributed to the difference in airport size and the higher number of commercial flights at CYUL. Similarly, the standard deviation of the vertical rate at CYOW was considerably higher than the other two airports, indicating greater variability in the rate of climb or descent of aircraft at the medium-sized airport.

Conversely, the fourth model offers an overview of the variables for Canadian airspace at all altitude ranges, providing a broader perspective on the behavior of aircraft in Canadian airspace. The mean speed observed was significantly higher than that observed at individual airports, which was expected due to the variety of aircraft types and higher altitudes included in this model. Additionally, the standard deviation of vertical rate was also noticeably higher, highlighting the greater variability of altitude changes in Canada-wide airspace.

Overall, these models provide valuable insights into the behavior of aircraft in specific areas and altitude ranges, as well as, in general, given that the ability to identify trends and patterns in aircraft behavior provides crucial information for decision-makers in the aviation industry, allowing all interested parties to make informed decisions to ensure the safety and efficiency of air operations of all types. A more detailed analysis of the models would be useful in various applications including, but not limited to, risk assessment and collision mitigation, development of regulatory frameworks, and optimization of airspace among other users.

### **6.2.1 Cut-Point Determination**

If further processing of the models was desired to generate realistic tracks that accurately represent aircraft behavior, it was necessary to determine the Bayesian network structure. To achieve this, identifying cut-points and discretizing the data was required. Regarding altitude, it was decided to adopt the same cut-points utilized by the MIT-LL, while also including additional values for higher altitudes. However, when it comes to variables such as velocity, acceleration, vertical rate, and turn rate, the determination of cut-points for data discretization is a required step. Currently, there is no universally accepted standard method for this application, and the selection of a specific method depends on the desired outcomes [21].

A Maximum Likelihood Estimation (MLE) approach was chosen for data discretization [22]. This method involves selecting cut points in a manner that preserves the underlying distribution shape of the variables to be discretized. To implement it, a Nelder-Mead simplex algorithm was used, utilizing built-in MATLAB functions [23]. The algorithm ingested the same counts and edges file used in the previous step, and a default number of desired cut-points for each variable was selected based on the values that yielded the best results.

The MLE method was selected because it is a widely used technique in data discretization and has been shown to perform well in various applications. Moreover, it is computationally efficient, can handle large amounts of data, and is able to preserve the shape of the distribution of the variables being discretized. Furthermore, the use of a default number of cut-points helps to reduce subjectivity and bias in the discretization process. Figure 19 shows an example of the results.

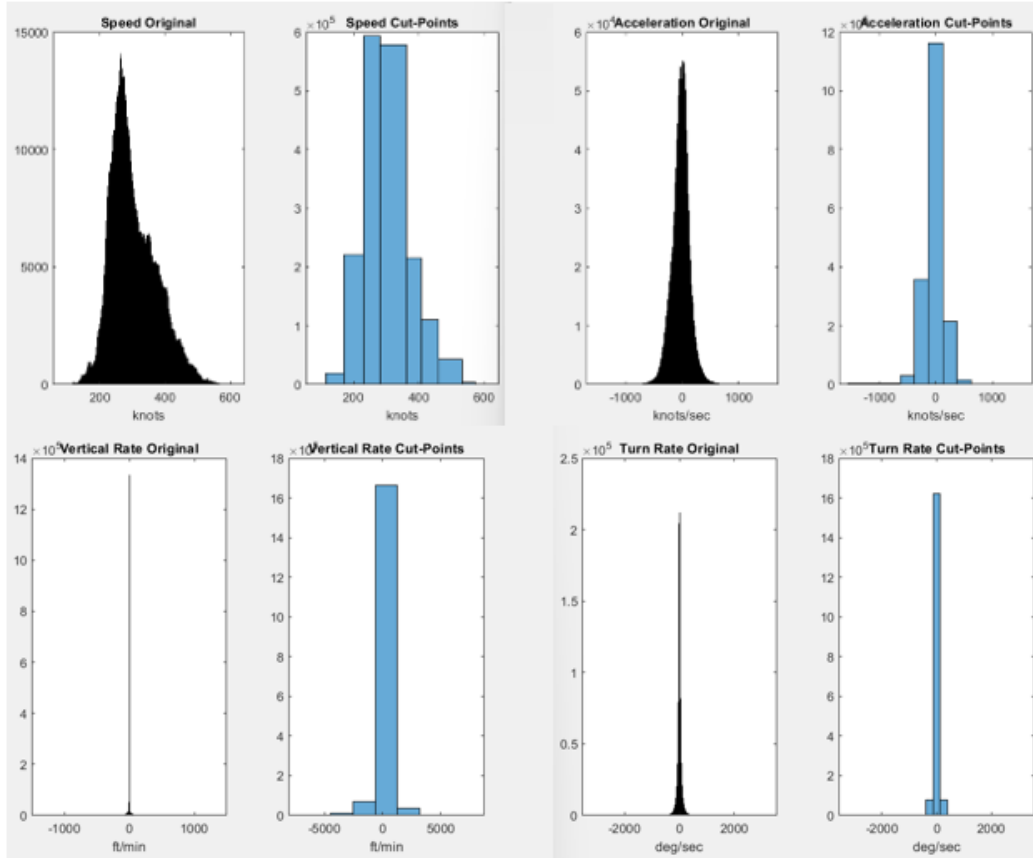


**Figure 19: Sample of cut-point selections results**

This process was implemented for 9 models, one for each aircraft category (light, medium, and heavy), with each model divided according to altitude layers:

- Below 10,000 ft ASL to account for the regulatory speed restriction of 250 kts.
- Between 10,000 ft and 25,000 ft ASL to consider low altitude operations.
- Above 25,000 ft ASL to consider high altitude operations.

In addition, a 10th model was created with helicopter tracks only in the altitude layer below 10,000 ft ASL.

The following subsections present the results for the light model below 10,000 ft ASL (Figure 20 and Table 11) and the medium aircraft model between 10,000 ft and 25,000 ft ASL (Figure 21 and Table 12), while the remaining results for the other models can be found in Appendix B.

### 6.2.1.1 Light Aircraft Model Results:

**Table 11: Light aircraft model cut point for tracks below 10,000 ft ASL**

Light Aircraft Model from 0-10,000 ft ASL	
Variable	Cut-Points
<b>Altitude</b>	1200, 3000, 5000
<b>Speed</b>	26, 77, 128, 179, 230, 281, 332
<b>Acceleration</b>	-6.3, -3.8, -1.3, 1.3, 3.8, 6.3
<b>Vertical Rate</b>	-6510, -4570, -2620, -680, 1260, 3200, 5150, 7090
<b>Turn Rate</b>	-6.7, -4.0, -1.3, 1.3, 4.0, 6.70

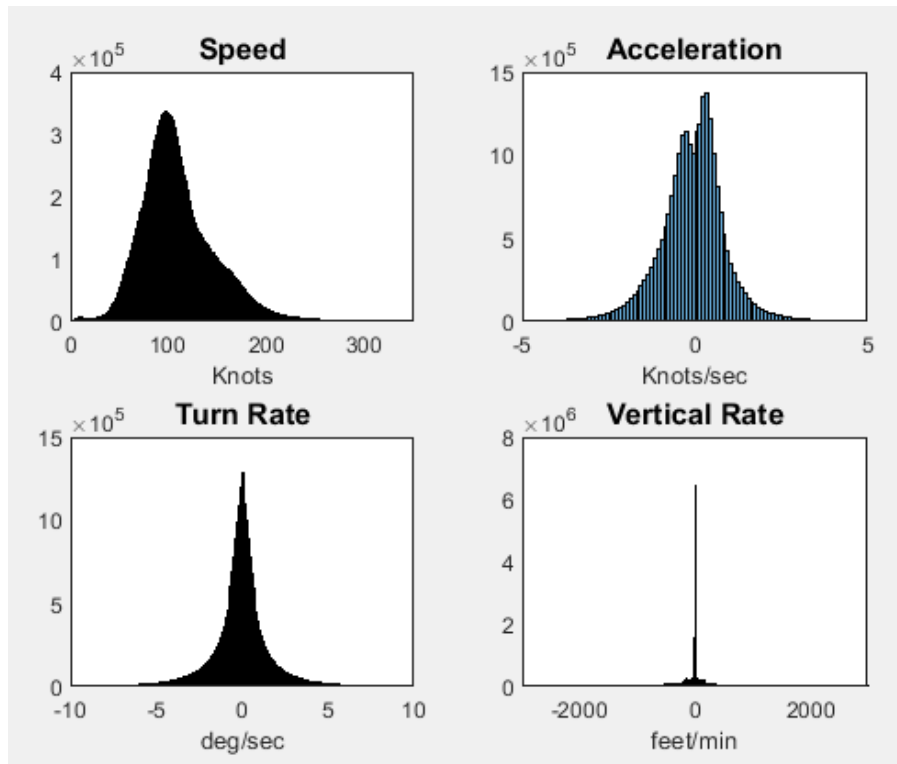


**Figure 20: Light aircraft model histograms below 10,000 ft ASL**

### 6.2.1.2 Medium Aircraft Model Results:

**Table 12: Medium aircraft model cut point for tracks between 10,000 and 25,000 ft ASL**

Medium Aircraft Model from 10,000-25,000 ft ASL	
Variable	Cut-Points
<b>Altitude</b>	12500, 18000
<b>Speed</b>	41, 118, 183, 249, 323, 395, 504, 539, 568
<b>Acceleration</b>	-6.3, -3.8, -1.3, 1.3, 3.8, 6.3
<b>Vertical Rate</b>	-6970, -4950, -2930, -910, 1120, 3140, 5160, 7180
<b>Turn Rate</b>	-6.7, -4.0, -1.3, 1.3, 4.0, 6.7

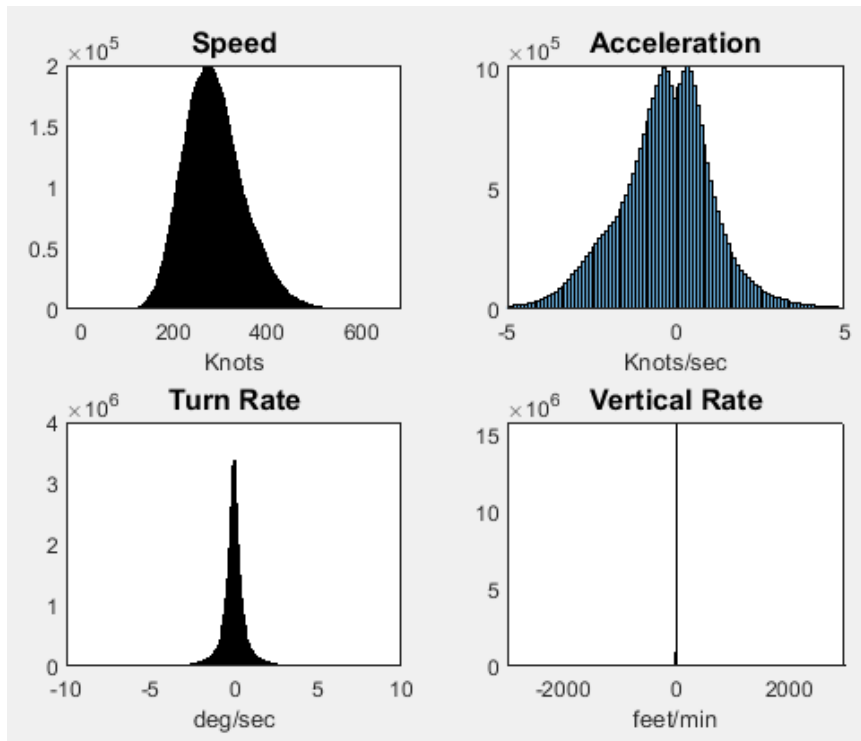


**Figure 21: Medium aircraft model histograms below 10,000 ft ASL**

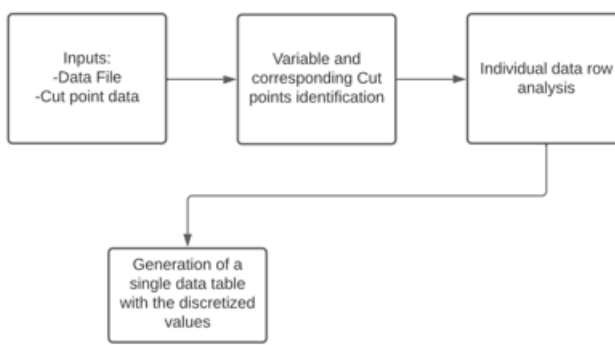
The results of the analysis reveal that each model accurately captures the characteristics of different categories of aircraft and altitudes of operation. Specifically, the light aircraft model demonstrates a speed concentration of approximately 100 knots, which aligns with the types of aircraft being analyzed and the altitude with speed limitation. Additionally, there is a significant variation observed in the acceleration, vertical rate, and turn rate variables. These findings are expected at lower altitudes as the aircraft are in the process of takeoff, climb, approach, and landing.

In contrast, the medium aircraft model displays a notable concentration of speeds at higher values, approximately 300 knots, which is to be expected at higher altitudes. The acceleration variable reveals a broader range, which can be attributed to the greater power and higher speed characteristics of medium-sized aircraft, as well as the increased wind and turbulence present at higher altitudes. Conversely, the turn rate and vertical rate variables demonstrate less variation, as is typical during established cruising or altitude transition phases of flight.

## 6.2.2 Data Discretization and Distributions Set Up

From this step moving forward, the analysis required to consider the full dataset that contained relevant information about the area of interest. The reason was because the conditional probability and relationships between variables needed to be considered, as opposed to earlier steps where the variables were analyzed independently, and simple count files were sufficient. However, the full data set was too large to be processed by the software; therefore, a smaller representative sample dataset was extracted and ensured to have the same characteristics and distributions as the full dataset.

After defining the cut points, the next step involved discretizing the data for all continuous variables, namely altitude, speed, acceleration, vertical rate, and turn rate. The goal was to determine the counts of each bin, which is crucial for subsequent steps. To achieve this, two functions were implemented, namely "*Data\_Discretization\_Initial.m*" for initial distribution files and "*Data\_Discretization\_Transition.m*" for transition distribution files. The workflow of this process is depicted in Figure 22a, and the results are illustrated in Figure 22b.

**a**

The figure shows the results of data discretization. On the left, a screenshot of a MATLAB script named "Data\_Discretization.m" is shown, indicating the execution of the function. To its right is a table of raw data, and further right is a table showing the discretized data. The raw data table has columns: Altitude, Airspeed, Acceleration, VerticalRate, and TurnRate. The discretized data table has columns: Altitude, Airspeed, Acceleration, Vertical rate, and Turn rate, with values ranging from 2 to 5.

Altitude	Airspeed	Acceleration	VerticalRate	TurnRate
981	90.9901	1.7372e-04	0	0
977.3359	91.2940	0.0663	-27.3624	0
973.6719	91.5993	0.1327	-54.7249	0
970.0078	91.9060	0.1991	-82.0873	1.2400e-10
966.3437	92.2141	0.2655	-109.4497	-1.2400e-10
962.6796	92.5235	0.3319	-136.8122	-1.1600e-10
959.0156	92.8342	0.3984	-164.1746	1.1600e-10
955.3515	93.1463	0.4648	-191.5371	1.2400e-10
951.6874	93.4597	0.5312	-218.8995	-1.2400e-10
948.0234	93.7744	0.5976	-246.2619	0
933.2639	93.9908	0.6604	-301.4796	1.1252
918.5044	94.2107	0.6164	-356.6973	-1.3500e-10
903.7449	94.4342	0.6276	-411.9150	2.8200e-10
888.9854	94.6611	0.6397	-467.1327	-1.4700e-10
874.2259	94.8915	0.6529	-522.3504	-1.3500e-10

Altitude	Airspeed	Acceleration	Vertical rate	Turn rate
5	7	3	3	2
5	7	3	3	2
5	7	3	3	2
5	7	4	3	2
5	7	4	3	2
5	7	4	3	2
5	7	4	3	2
5	7	4	3	2
5	7	4	3	2
5	7	4	3	2
5	7	4	3	2
5	7	4	3	2
5	7	4	3	2
5	7	4	3	2
5	7	4	3	2
5	7	4	3	2
5	7	4	3	2
5	7	4	3	2

**b**

**Figure 22: (a) Data Discretization Workflow and (b) results**

The next step after obtaining the discretized data was to generate the data distribution files. It is important to note that the model consists of two types of variables: those that represent the initial state of the aircraft, and dynamic variables that describe the trajectory's evolution based on the initial conditions. Therefore, two types of data distributions needed to be created for the subsequent determination of Bayesian structures.

The first was the initial distribution, which includes all variables and determines the initial conditions of the trajectory. The second was the transition distribution, which, based on the initial conditions, described how the motion will evolve over time. The transition distribution included all variables plus three additional columns of acceleration, vertical rate, and turn rate data at the next time step.

As described earlier in this report, the file structure was modified to optimize storage by storing rows in 5-second intervals and storing observations for each second in between the columns. Thus, it was required to develop an algorithm to return the data to its original structure, where each row displayed the observations for every second, with no additional columns. With the modified file, a different algorithm was implemented to create the distributions mentioned above. The process flow is depicted in Figure 23 and the outcomes are presented in Figure 24.

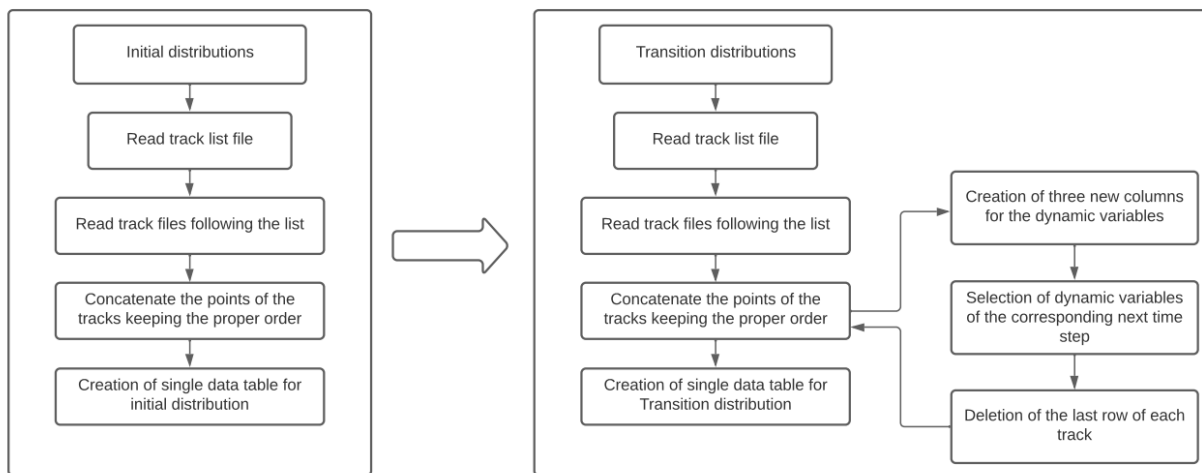


**Figure 23: Initial and transition distributions algorithm workflow**

	1	2	3	4	5	6
	Airspace Class	Altitude	Airspeed	Acceleration	Vertical rate	Turn rate
1		7	4	6	4	4
2		7	4	6	4	4
3		7	4	6	4	4
4		7	4	6	4	4
5		7	4	6	4	4
6		7	4	6	4	4
7		7	4	6	4	4
8		7	4	6	4	4
9		7	4	6	4	4

	1	2	3	4	5	6	7	8	9
	Airspace Class	Altitude	Airspeed	Acceleration	Vertical rate	Turn rate	Acceleration(t+1)	Vertical rate(t+1)	Turn rate(t+1)
1	7	4	6	4	4	1	4	4	1
2	7	4	6	4	4	1	4	4	1
3	7	4	6	4	4	1	4	4	1
4	7	4	6	4	4	1	4	4	1
5	7	4	6	4	4	1	4	4	1
6	7	4	6	4	4	1	4	4	1
7	7	4	6	4	4	1	4	4	1
8	7	4	6	4	4	1	4	4	1
9	7	4	6	4	4	1	4	4	1

**Figure 24: Initial (above) and transition (below) distributions file example**

With the completion of this step, the Stage 2 has reached its conclusion and has successfully accomplished all the necessary data processing and statistical analysis required to proceed towards the final stage. As part of this stage, several crucial data processing techniques were implemented, which included the creation of histograms, extraction of data statistical characteristics such as mean, mode, and standard deviation, determination of cut points, and data discretization.

The outputs generated from this stage were the data insights, and the initial and transition distributions file, which are essential for the next stage of the analysis.

### **6.3 Stage 3: Determination of the Bayesian Network Structure and Generation of Frequency Tables**

The final stage of this process involved determining the initial and transition distributions of the Bayesian network structures. The initial distribution allows for the generation of realistic initial conditions for a track, while the transition distribution enables the track to evolve over subsequent time steps, showcasing its progression over time. A Bayesian network is a type of Direct Acyclic Graph (DAG) that shows the relationship between different variables based on their conditional probabilities.

There are different methods to determine the structure that best fits the data. One approach is an exhaustive search that analyzes all possible structures, while other approaches involve search algorithms and scoring methods that allow for the determination of the best graph. Given the number of variables and the huge number of possible structure combinations in this research project, the second approach was selected.

The implementation of the search algorithms and scoring methods was done in Python, using the "*pgmpy*" and "*bnlearn*" libraries. A hill climbing algorithm was employed, working with the K2 metric [24] and the Bayesian Information Criterion (BIC) score [25] [26]. Three structures were determined for each distribution, and these were then compared against four other structures selected based on previous work, such as the MIT-LL and general aircraft dynamic knowledge. An exhaustive search was performed among the seven candidates, and the structure that yielded the best scores was selected.

The same approach was followed for both the initial and transition distributions, with the only difference being that a restriction was imposed on the transition distributions. Specifically, only the variables on the next time step (Columns 7 to 9 in Figure 24) were allowed to be dependent on others, while the others (Columns 1 to 6) had to be completely independent, as their relationship is determined by the initial distribution.

The results obtained for the initial and transition distributions of both the light and medium aircraft models are shown in Figure 25 and 26. Overall, this approach provided a robust methodology to determine the most appropriate Bayesian network structure for the given dataset.

By analysing the initial distributions, these two structures show the relationships between different variables for light and medium aircraft models. For both cases, all variables including altitude, airspace, turn rate, speed, acceleration, and vertical rate were considered, and the structures suggest that different variables may be more important for different types of aircraft and altitudes, with some variables appearing more frequently in one structure versus the other. For example, acceleration has two parents and 3 children in the light aircraft model structure, while this is not the case for the medium aircraft model structure.

Upon analyzing the transition distribution structures, it became evident that the light aircraft model has a simpler structure with fewer nodes and edges as compared to the medium aircraft model. This indicates a more straightforward and direct relationship between the variables. It is noteworthy that the medium aircraft model includes the altitude variable while the light model does not. This observation is interesting, especially since the regulatory speed restriction for the altitudes considered in the light model may limit the variation of all variables and nullify its effects.

The results of the remaining 8 models are included in Appendix B, along with the corresponding histograms and cut-point tables as mentioned in a previous section.

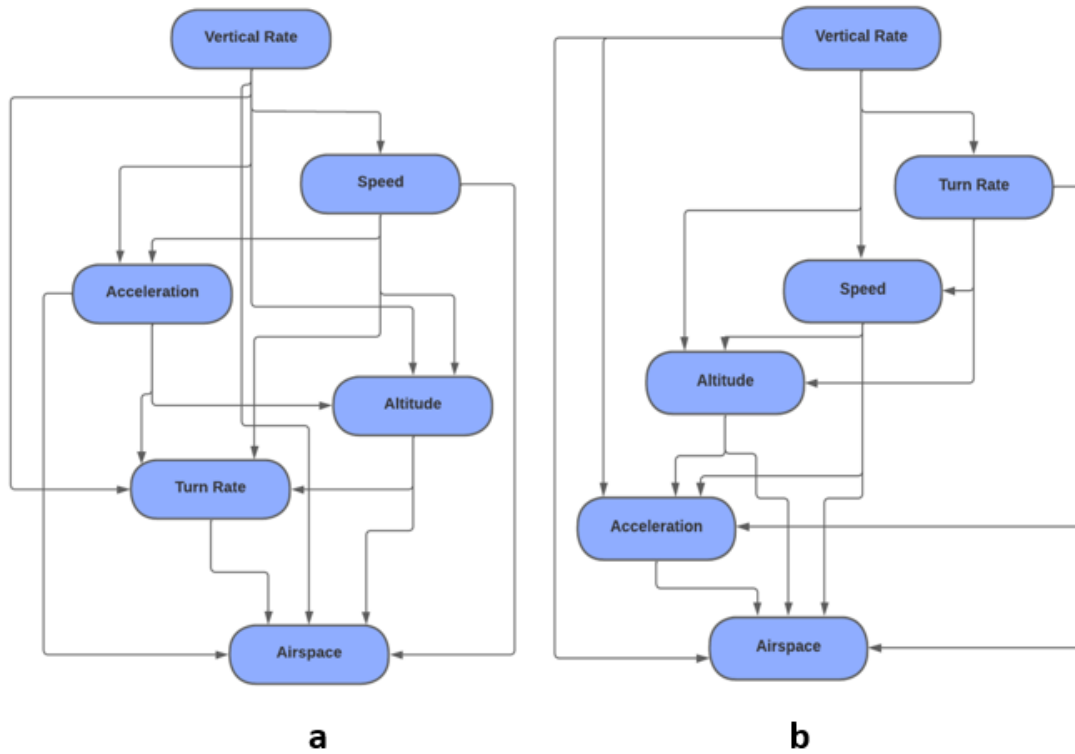


Figure 25: Initial Distributions for (a) Light aircraft model and (b) Medium aircraft model

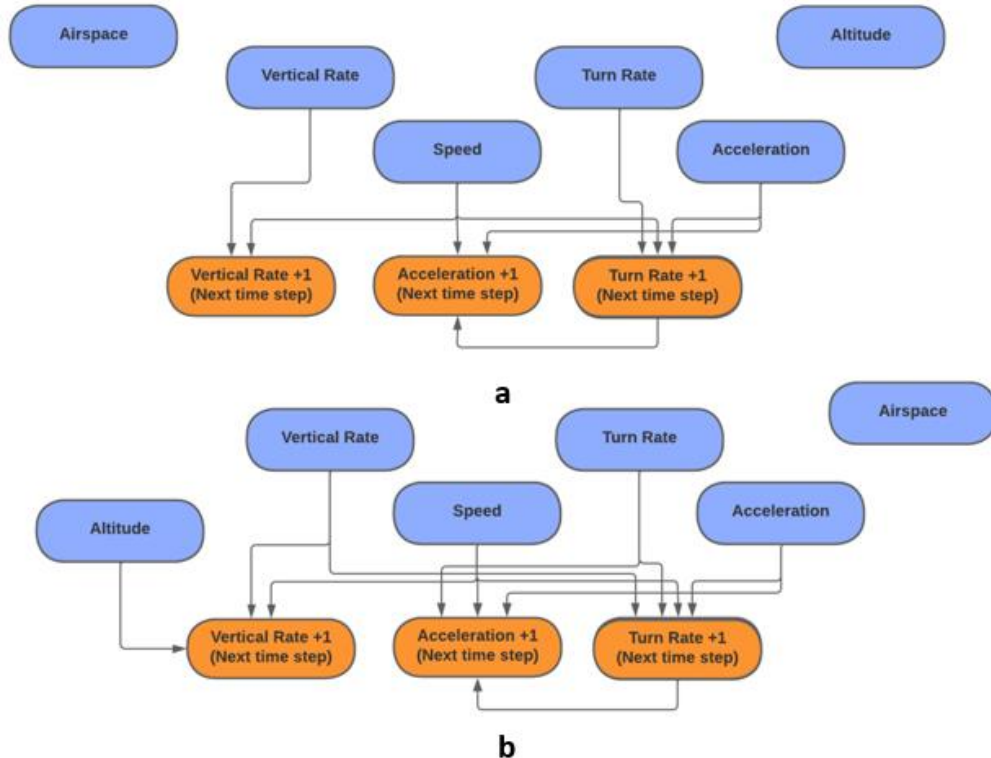
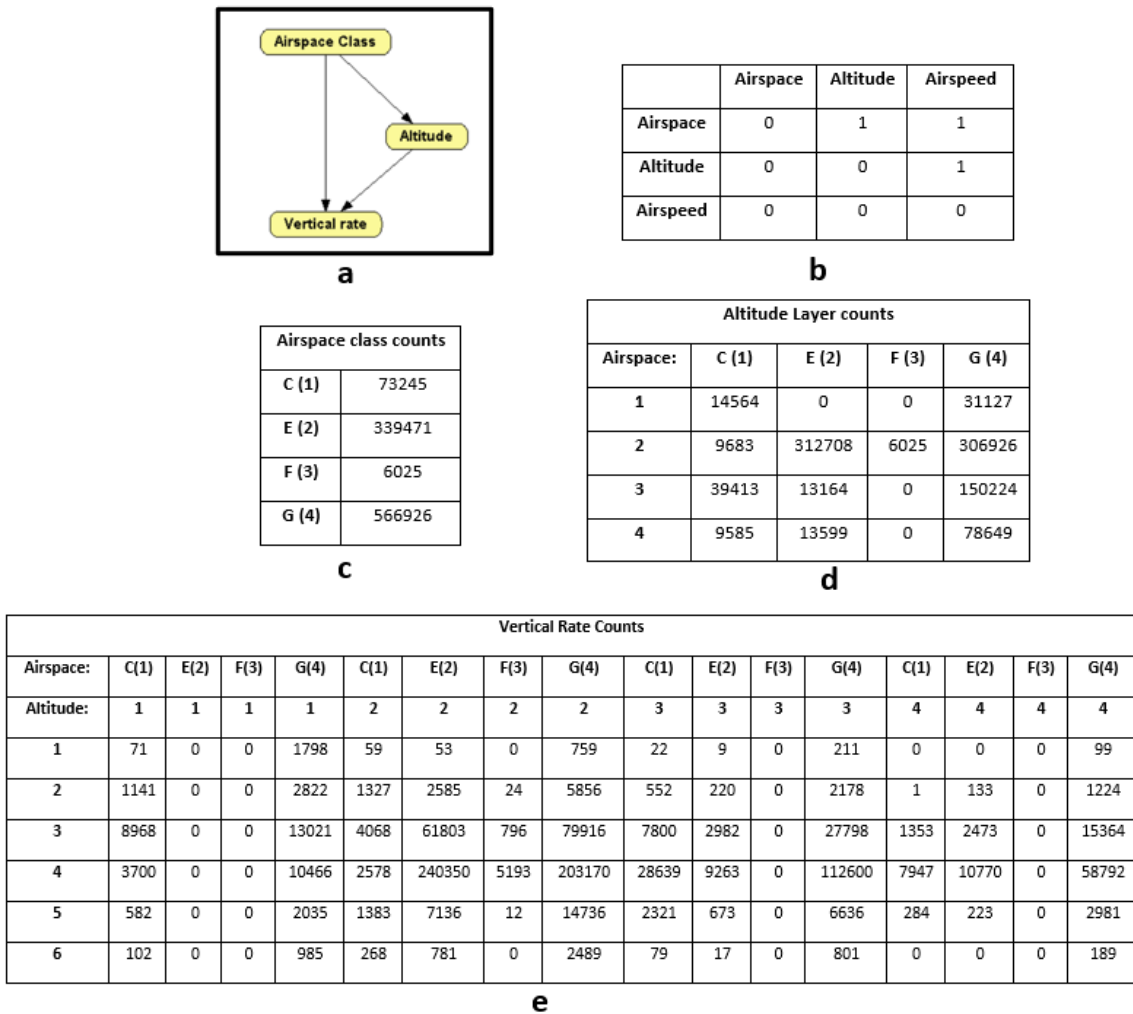


Figure 26: Transition Distributions for (a) Light aircraft model and (b) Medium aircraft model

### 6.3.1 Data Count File Generation

The selected Bayesian structures enable the creation of quantified tables for the dataset, which provide sufficient statistics to estimate the model parameters. To create these tables, a MATLAB algorithm was developed. The algorithm takes the distribution tables and the direct acyclic graph of the Bayesian structure as input, sorts the data of each variable based on parent-child dependencies, and performs data counts for each bin. An example of the data frequency tables for the first three variables of a random initial distribution structure, according to the Bayesian structure, is shown in Figure 27.



**Figure 27: The Bayesian network structure is shown in (a), along with its corresponding distribution table in (b). Frequency tables for the first, second, and third variables of the network are presented in (c), (d), and (e), respectively.**

The frequency tables above enable the generation of representative aircraft tracks that can be utilized in a variety of simulation methods, including Monte-Carlo simulations, and can be employed to calculate the probability of mid-air collisions, as well as other analytical applications. Figures 28 and 29 display sample results.

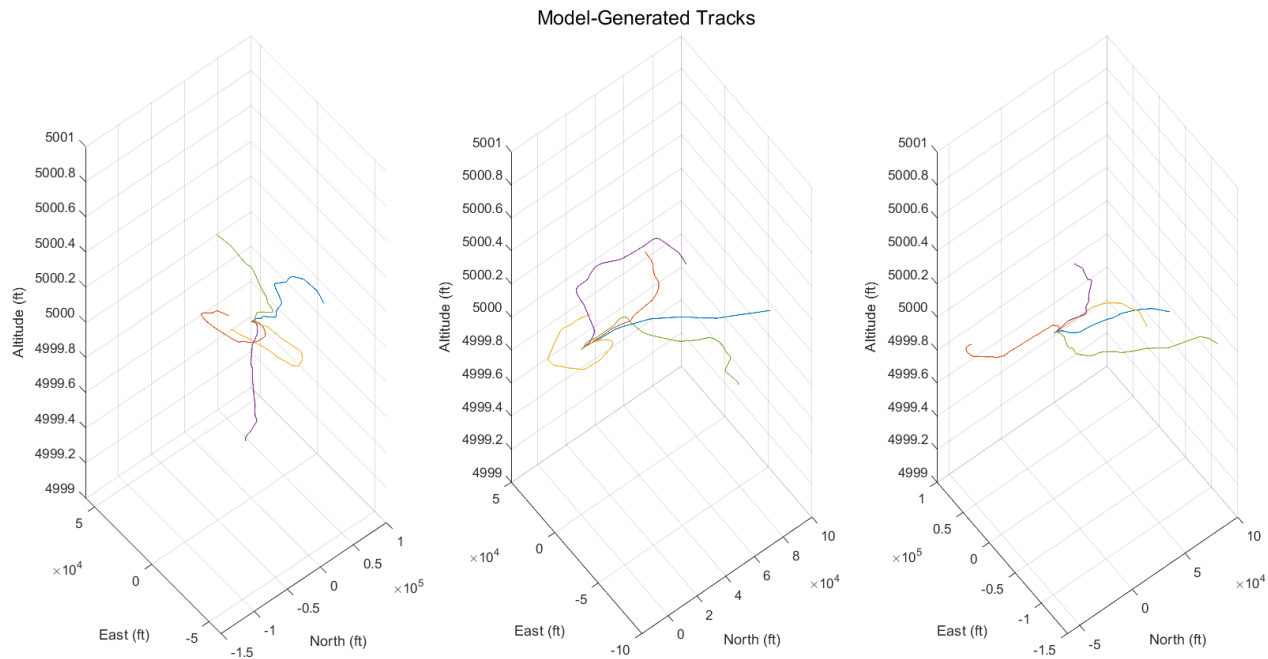


**Figure 28: Generated tracks with identical initial conditions**

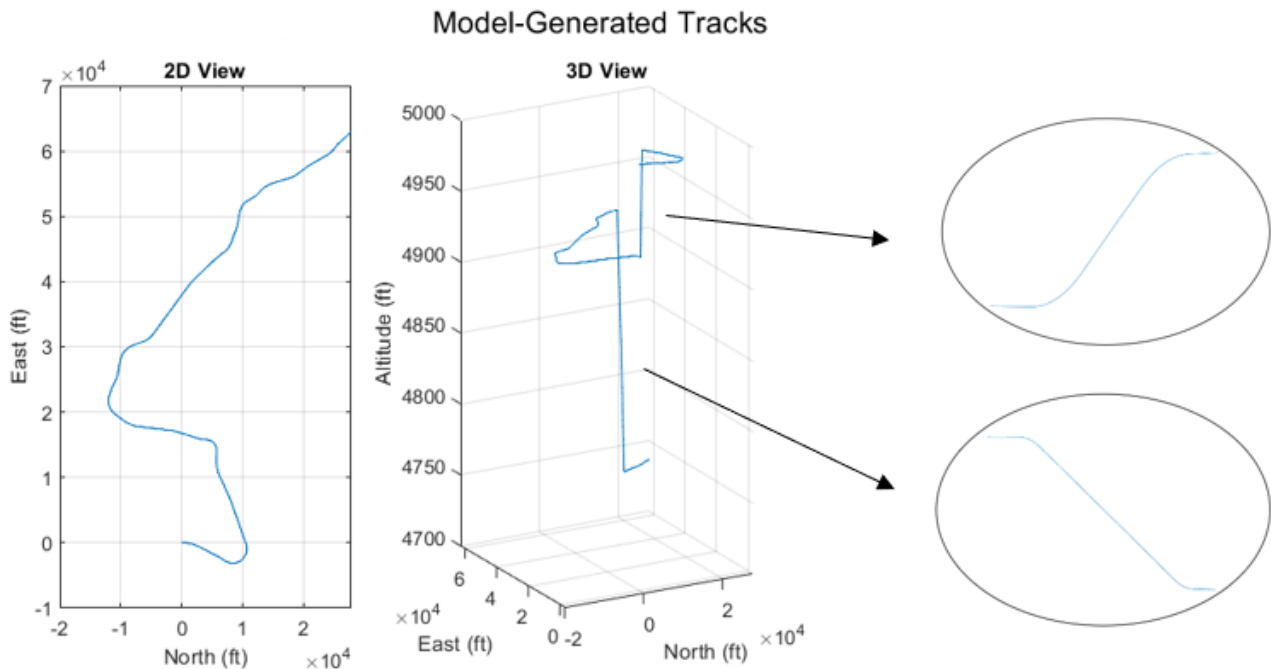


**Figure 29: Flight Path Visualization - 2D and 3D visualization with vertical section zoom**

## 7.0 CONCLUSION

This report provides a comprehensive overview of the data processing pipeline developed to enable the Canadian statistical airspace model development. First, the RDPS aircraft track data was pre-processed, followed by the application of a custom-developed track smoothing filter. Next, a selection of variables was made, and data interpolation was conducted to enhance the overall data resolution. Statistical analysis was then conducted to generate the Bayesian network structures and frequency tables, which are essential for generation of realistic aircraft tracks.

To enable further long-term applications of the works presented in this report, the server configuration was set up to enable target data queries for the 2017 RDPS dataset based on several factors including, but not limited to, location, time, and aircraft WTC. The development of the data processing and management procedures highlighted in the report enables similar airspace studies to be conducted at target geographical locations across Canada in a streamlined process.

To optimize the speed and extract useful information from the data, external functionalities were incorporated that take advantage of the server querying system. These functionalities enabled the plotting of histograms and calculation of descriptive statistics, providing better understanding and insights into the data. The valuable insights generated from these analyses are useful for various applications, including developing models for improving airspace safety and BVLOS RPAS regulations development in Canada.

Ongoing improvements and updates to the developed models are being made, with a focus on implementing additional functionalities that enable direct querying of the server for Bayesian network structure determination.

## **8.0 FUTURE WORK**

With the tools developed over the duration of the CAM project, the research team has identified several new areas of research that can leverage this data processing pipeline. While the focus of the developed airspace statistical models presented in this report was placed on both a Canada-wide overview and 12 selected airports, these represent broad models that can provide an informative, base-level overview of the expected traditional crewed aircraft behavior. As more and more operators seek to incorporate the use of RPAS to enable various use cases, the research team believes that regional airspace statistical models should be assessed, specific to identified operational environments. Moreover, there is a growing demand for the development of an RPAS mission planning tool that would enable operators to effectively plan the route. This tool would provide operators with the necessary functionalities to plan and optimize the RPAS mission, ensuring safe and efficient operations.

### **8.1 Data processing for the 2020 RDPS Dataset**

In continued partnership with TC and NAV CANADA, the research group aims to leverage the tools developed to ingest the 2020 RDPS dataset, to further enhance the capabilities of the airspace statistical model development. Besides, it would be of interest to study the effects of Pandemic on aircraft movements, as well as compare the 2017 models (before Pandemic) to 2020 models (during Pandemic).

### **8.2 Assessment of RDPS Dataset Suitability for Low-Level Altitude Statistical Airspace Models**

The primary goal of the CAM was to provide key statistical data to TC to enable data-driven decision making for the safe integration of RPAS into the national airspace. The airspace statistical models developed to date have been focused on wider altitude bands, to capture key statistical characteristics of various airports in Canada, as well as, various aircraft types that are operated in Canada. To further enhance the data and statistical models specific to RPAS operations, the research team recommends a focus on identifying the suitability of this specific dataset for low-level altitudes in the specific geographic regions, considering holding patterns, attitude and altitude of aircraft for both VFR and IFR traffic. As discussed in Section 8.1, the incorporation of the 2020 RDPS dataset will be a key factor in this determination moving forward, as the dataset also includes the field indicating contributing sensor technology for each datapoint in the base dataset. This will enable the assessment of the data quality based on known capabilities of each aircraft tracking sensor technology, and its known limitations for tracking aircraft at various altitudes and distances.

### **8.3 Traffic Density Modelling**

The flight track data contained in the RDPS dataset is also capable of being leveraged to enable the modelling of airspace traffic density in a given geographic region. As the dataset is a historical record of all flight tracks that have taken place over a period of time, the temporal aspect of the data enables accurate placement of a given aircraft in both space and time. The research team believes that the development of airspace traffic density models will also play a key factor in the assessment of an airspace when looking to analyze the risks associated with an RPAS operation, and the likelihood of encounter with a manned intruder aircraft based on historical records of aircraft (if any) present in the vicinity of the proposed flight area.

## **8.4 Terminal and Enroute Statistical Airspace Model**

Typically, it is expected that aircraft have a more predictable enroute flight behavior. This is in contrast with aircraft flight patterns near a terminal, as there is additional coordination required with Air Traffic Control to ensure that the takeoff, landing, and flight paths of the various aircraft operating in the vicinity can be conducted in a safe manner. The research team is looking to conduct a study on the differences between aircraft behavior based on the developed statistical models for both terminal and enroute flight track data.

## **8.5 Development of Statistical Models for RPAS Flight Data**

Several airports across Canada are currently running trials of various technologies that enable the detection and collection of RPAS flight track data within the detection range of the system. It is the research team's belief that the collected data can also be used in a similar manner to generate and develop statistical models for RPAS flight behavior as presented, which can provide additional insight to the expected behavior of different RPAS types.

## 9.0 REFERENCES

- [1] Joint Authority for Rulemaking on UAS, "JARUS Guidelines on Specific Operations Risk Assessment (SORA)," 30 January 2019. [Online]. Available: [http://jarus-rpas.org/sites/jarusrpas.org/files/jar\\_doc\\_06\\_jarus\\_sora\\_v2.0.pdf](http://jarus-rpas.org/sites/jarusrpas.org/files/jar_doc_06_jarus_sora_v2.0.pdf). [Accessed 3 February 2023].
- [2] Transport Canada, Civil Aviation, Remotely Piloted Aircraft Systems Task Force, "Advisory Circular (AC) No. 903-002," Transport Canada, 21 June 2021. [Online]. Available: <https://tc.canada.ca/en/aviation/reference-centre/advisory-circulars/advisory-circular-ac-no-903-001>. [Accessed 02 February 2023].
- [3] D. Nelson, T. Krings, J. Chang, A. Basawanal, S. Kingma, B. Ooi, I. Borshchova and J. Laliberte, "Canadian Airspace and Aircraft Equipment Requirements," Transport Canada, Ottawa, 2023.
- [4] K. Ellis and I. Borshchova, "Towards a Quantitative Approach for Determining DAA System Risk Ratio," *Drones*, vol. 7, no. 2, p. 127, 2023.
- [5] T. Krings, I. Borshchova and J. Laliberte, "Development of Methods for Statistical Modeling of Air Traffic Demonstrated through a Winnipeg-Area Case Study," *Drone Systems and Applications*, 2023.
- [6] M. Kochenderfer, J. Kuchar, K. Espindle and J. Griffith, "Uncorrelated Encounter Model of the National Airspace System, Version 1.0," Massachusetts Institute of Technology Lexington Lincoln Lab, 2008.
- [7] M. Kochenderfer, L. Espindle, J. Kuchar and J. Griffith, "Correlated Encounter Model for Cooperative Aircraft in the National Airspace System, Version 1.0," Massachusetts Institute of Technology Lincoln Laboratory, Lexington, 2008.
- [8] A. J. Weinert, E. G. J. Harkleroad, M. W. Edwards and M. J. Kochenderfer, "Uncorrelated Encounter Model of the National Airspace System, Version 2.0," Massachusetts Institute of Technology Lexington Lincoln Lab.
- [9] N. Underhill, E. Harkleroad, R. Guendel, D. Maki and M. Edwards, "Correlated Encounter Model for Cooperative Aircraft in the National Airspace System, Version 2.0," Massachusetts Institute of Technology Lincoln Laboratory, Lexington, 2018.
- [10] M. Edwards, M. Kochenderfer, J. Kuchar and L. Espindle, "Encounter Models for Unconventional Aircraft," Massachusetts Institute of Technology Lincoln Laboratory, Lexington, 2009.
- [11] M. Edwards, "Encounter Models for the Littoral Regions of the National Airspace System," Massachusetts Institute of Technology Lincoln Laboratory, Lexington, 2010.
- [12] A. Weinert, N. Underhill and A. Wicks, "Developing a Low Altitude Manned Encounter Model Using ADS-B Observations," *IEEE Aerospace Conference*, pp. 1-8, 2019.
- [13] MIT Lincoln Lab, "Airspace Encounter Models," [Online]. Available: <https://github.com/Airspace-Encounter-Models>.

- [14] Y. Bar-Shalom, X. Li and T. Kirubarajan, *Estimation with Applications to Tracking and Navigation: Theory Algorithms and Software*, John Wiley & Sons, 2004.
- [15] A. F. Genovese, "The Interacting Multiplemodel Algorithm for Accurate State Estimation of Maneuvering Targets," *Johns Hopkins APL Technical Digest*, vol. 22, no. 4, pp. 614-623, 2001.
- [16] G. A. Watson and W. Blair, "IMM Algorithm for Tracking Targets that Maneuver Through Coordinated Turns," *Signal and Data Processing of Small Targets*, vol. 1698, pp. 236-247, 1992.
- [17] International Civil Aviation Organization, "Guidance Material on Comparison of Surveillance Technologies (GMST)," September 2007. [Online]. Available: [https://www.icao.int/APAC/Documents/edocs/cns/gmst\\_technology.pdf](https://www.icao.int/APAC/Documents/edocs/cns/gmst_technology.pdf). [Accessed May 2021].
- [18] E. Zitzler, M. Laumanns and L. Thiele, "SPEA2: Improving the Strenght Pareto Evolutionary Algorithm," TIK-report.
- [19] ICAO, "Aircraft Type Designators," [Online]. Available: <https://www.icao.int/publications/DOC8643/Pages/Search.aspx>.
- [20] F. Fritsch and J. Butland, "A Method for Constructing Local Monotone Piecewise Cubic Interpolants," *SIAM Journal on Scientific and Statistical Computing*, vol. 5, no. 2, pp. 300-304, 1984.
- [21] L. Fu and I. Tsamardinos, "A Comparison of Bayesian Network Learning Algorithms from Continuous Data," *AMIA Annual Symposium Proceedings*, vol. 2005, p. 960.
- [22] I. J. Myung, "Tutorial on Maximum Likelihood Estimation," *Journal of Mathematical Psychology*, vol. 47, no. 1, pp. 90-100, 2003.
- [23] D. Olsson and L. Nelson, "The Nelder-Mead Simplex Procedure for Function Minimization," *Technometrics*, vol. 17, no. 1, pp. 45-51, 1975.
- [24] G. Cooper and E. Herskovits, "A Bayesian Method for the Induction of Probabilistic Networks from Data," *Machine Learning*, vol. 9, pp. 309-347, 1992.
- [25] J. Suzuki, "Bayesian Networks and Decision Graphs," *Springer Science & Business Media*, 1993.
- [26] J. Suzuki, "Bayesian Methods and Probabilistic Programming," *Electronic Notes in Theoretical Computer Science*, vol. 29, no. 4, pp. 181-200, 1999.
- [27] T. Krings, "Statistical Modelling of Air Traffic: Development of Methods and Application Through a Canadian Case Study". [Thesis]. Carleton University, 2023.

## A Results of analysis of statistical characteristics by airports

### A.1 Billy Bishop Toronto City Airport (CYTZ)

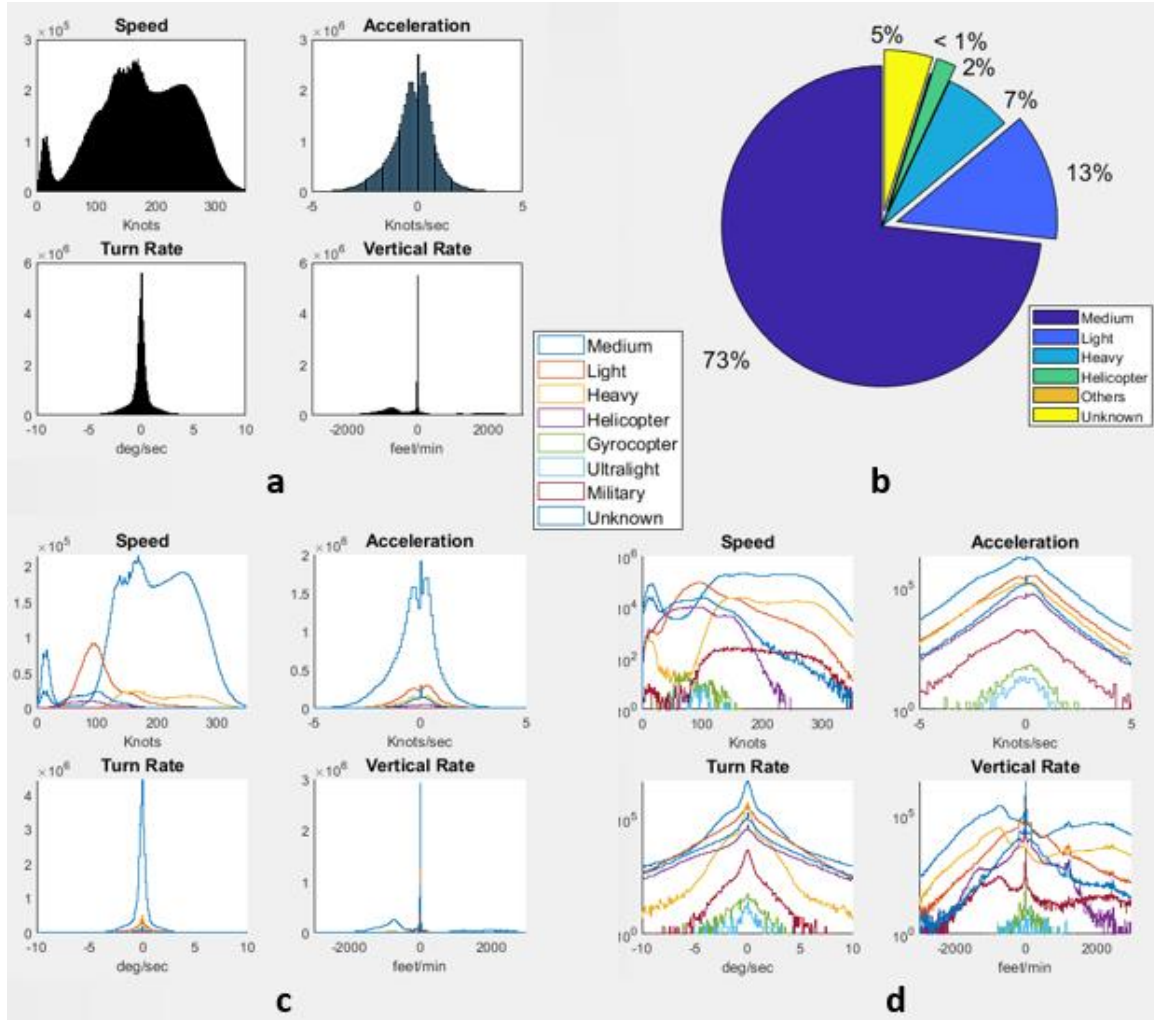


Figure 30: Billy Bishop Toronto City Airport (CYTZ) 0-10,000 ft ASL

(a) Mixed model distribution (b) Aircraft categories percentages (c) Variables distributions by aircraft category (d) Underlying distributions shape

Table 13: Descriptive Statistics of Variable Distributions for CYTZ (0-10,000 ft ASL): Mean, Mode, and Standard Deviation

Variable	Mean	Mode	Standard Deviation
Speed (knots)	177.6844	169	72.8179
Turn Rate (deg/sec)	-0.1177	0	1.5477
Vertical Rate (feet/sec)	1.1308	0	1174.8327
Acceleration (knots/sec)	-0.2646	0	1.0836

## A.2 Lester B. Pearson International Airport (CYYZ)

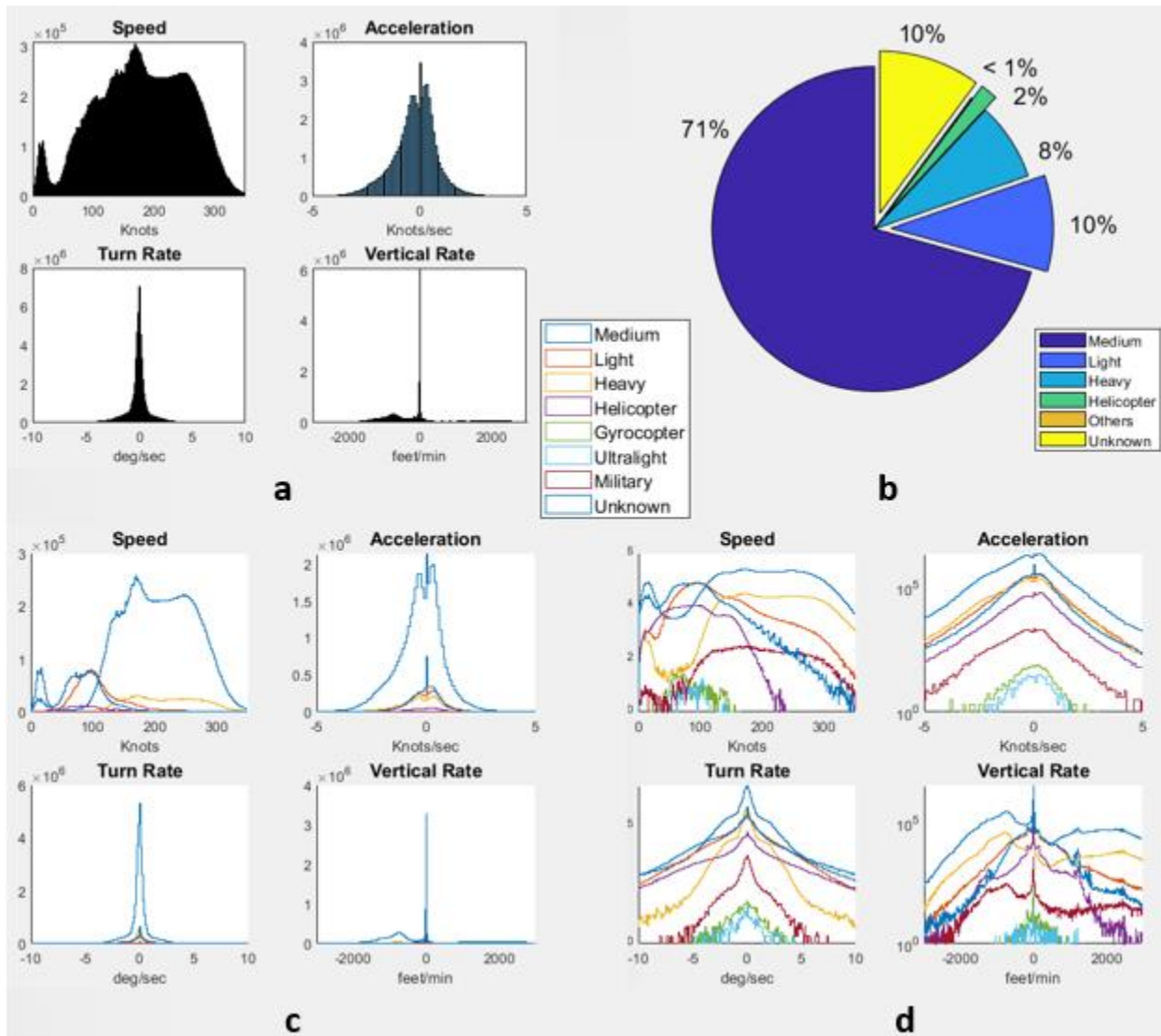


Figure 31: Lester B. Pearson International Airport (CYYZ) 0-10,000 ft ASL

(a) Mixed model distribution (b) Aircraft categories percentages (c) Variables distributions by aircraft category (d) Underlying distributions shape

Table 14: Descriptive Statistics of Variable Distributions for CYYZ (0-10,000 ft ASL): Mean, Mode, and Standard Deviation

Variable	Mean	Mode	Standard Deviation
Speed (knots)	179.0510	169	74.0729
Turn Rate (deg/sec)	-0.1341	0	1.5495
Vertical Rate (feet/sec)	0.8921	0	1177.6274
Acceleration (knots/sec)	-0.2678	0	1.0543

### A.3 Ottawa Macdonald-Cartier International (CYOW)

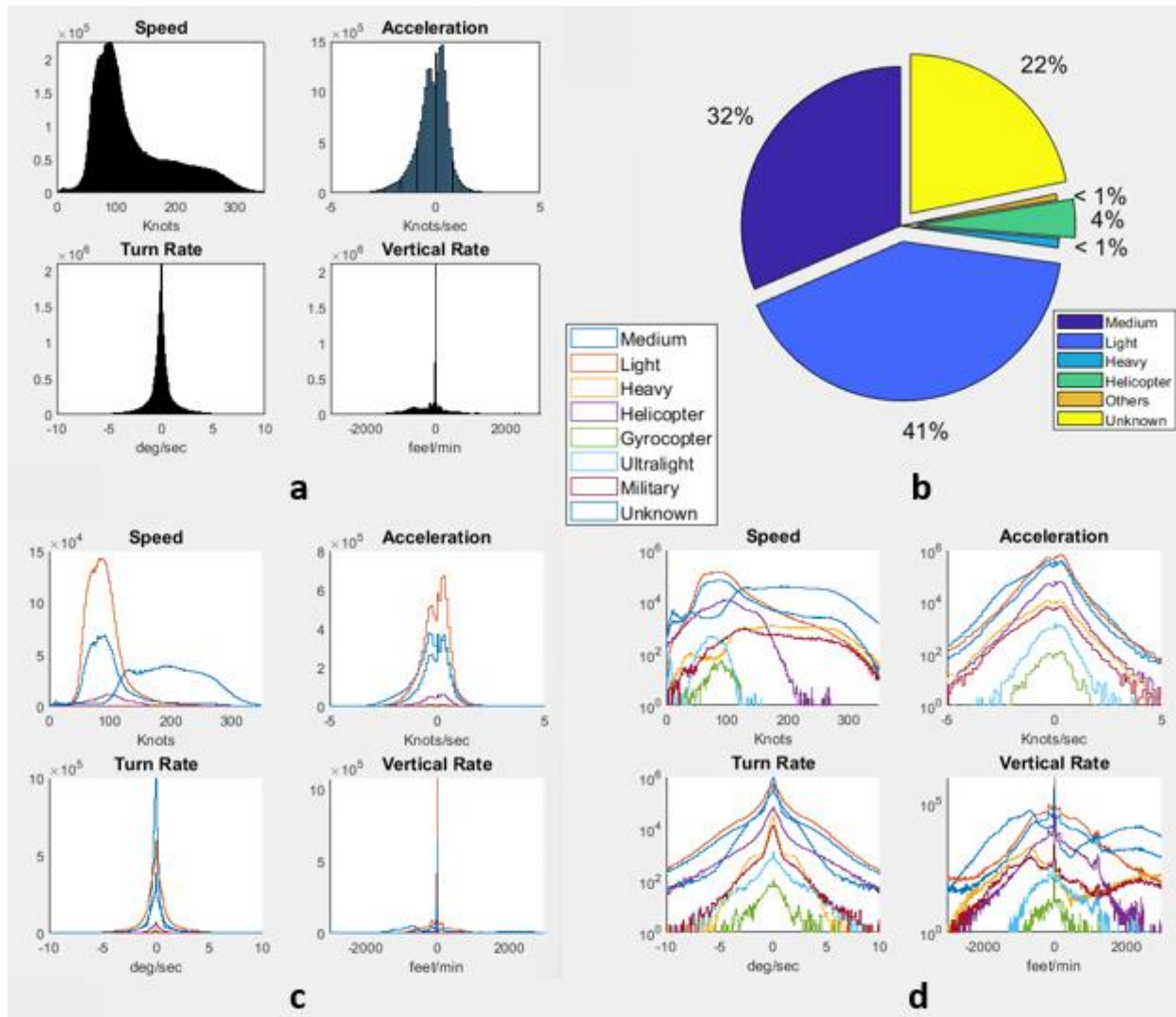


Figure 32: Ottawa Macdonald-Cartier International (CYOW) 0-10,000 ft ASL

- (a) Mixed model distribution
- (b) Aircraft categories percentages
- (c) Variables distributions by aircraft category
- (d) Underlying distributions shape

Table 15: Descriptive Statistics of Variable Distributions for CYYZ (0-10,000 ft ASL): Mean, Mode, and Standard Deviation

Variable	Mean	Mode	Standard Deviation
Speed (knots)	128.0975	91	67.4141
Turn Rate (deg/sec)	-0.0258	0	1.5993
Vertical Rate (feet/sec)	73.5145	0	991.9793
Acceleration (knots/sec)	-0.1978	0.3	0.7641

#### A.4 Montréal–Trudeau International Airport (CYUL)

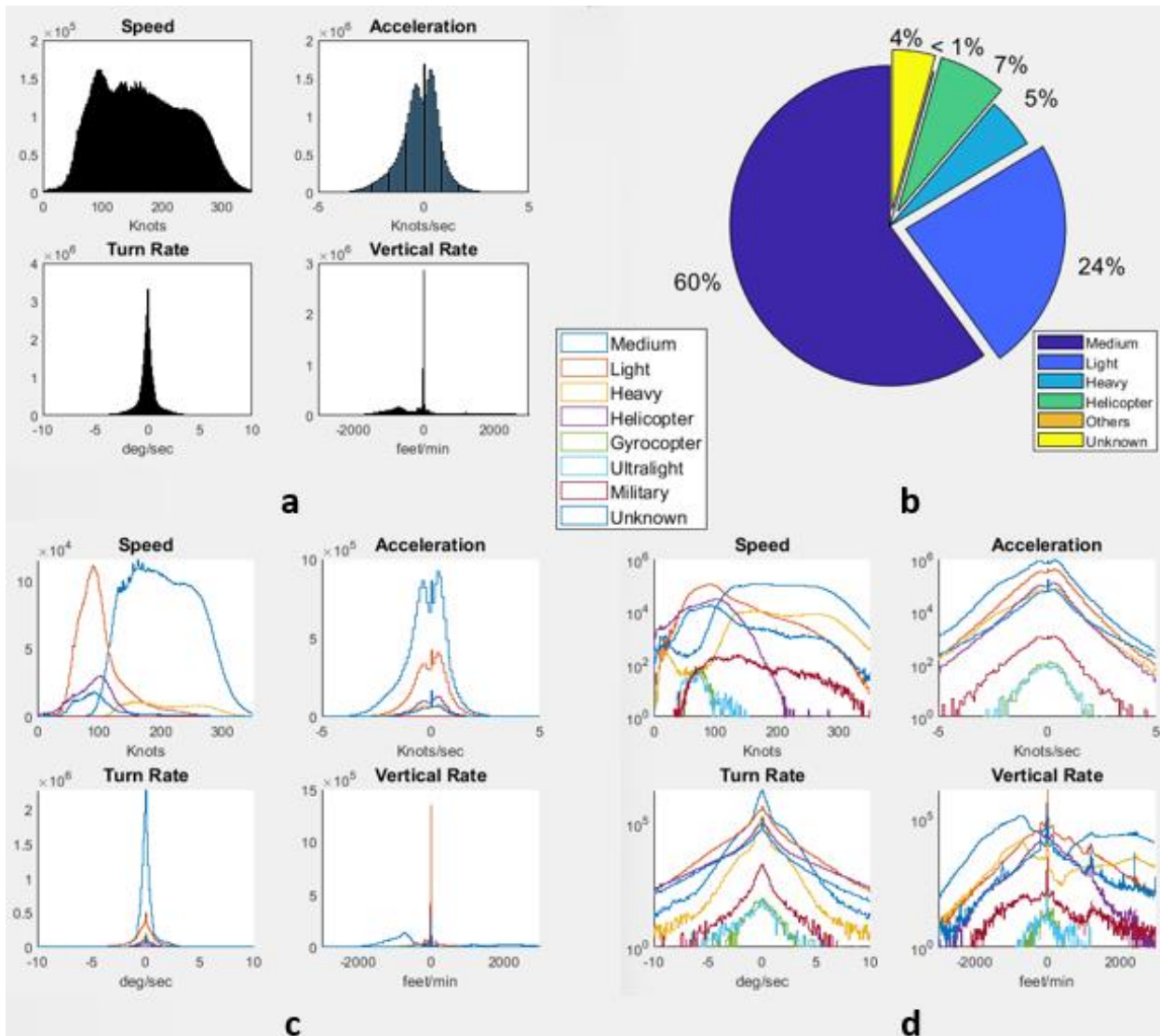


Figure 33: Montréal–Trudeau International Airport (CYUL) 0-10,000 ft ASL

- (a) Mixed model distribution
- (b) Aircraft categories percentages
- (c) Variables distributions by aircraft category
- (d) Underlying distributions shape

Table 16: Descriptive Statistics of Variable Distributions for CYUL (0-10,000 ft ASL): Mean, Mode, and Standard Deviation

Variable	Mean	Mode	Standard Deviation
Speed (knots)	167.7059	91	70.9853
Turn Rate (deg/sec)	-0.0579	0	1.3291
Vertical Rate (feet/sec)	61.4624	0	1179.4987
Acceleration (knots/sec)	-0.2158	0	0.9579

### A.5 Montréal–Mirabel International Airport (CYMX)

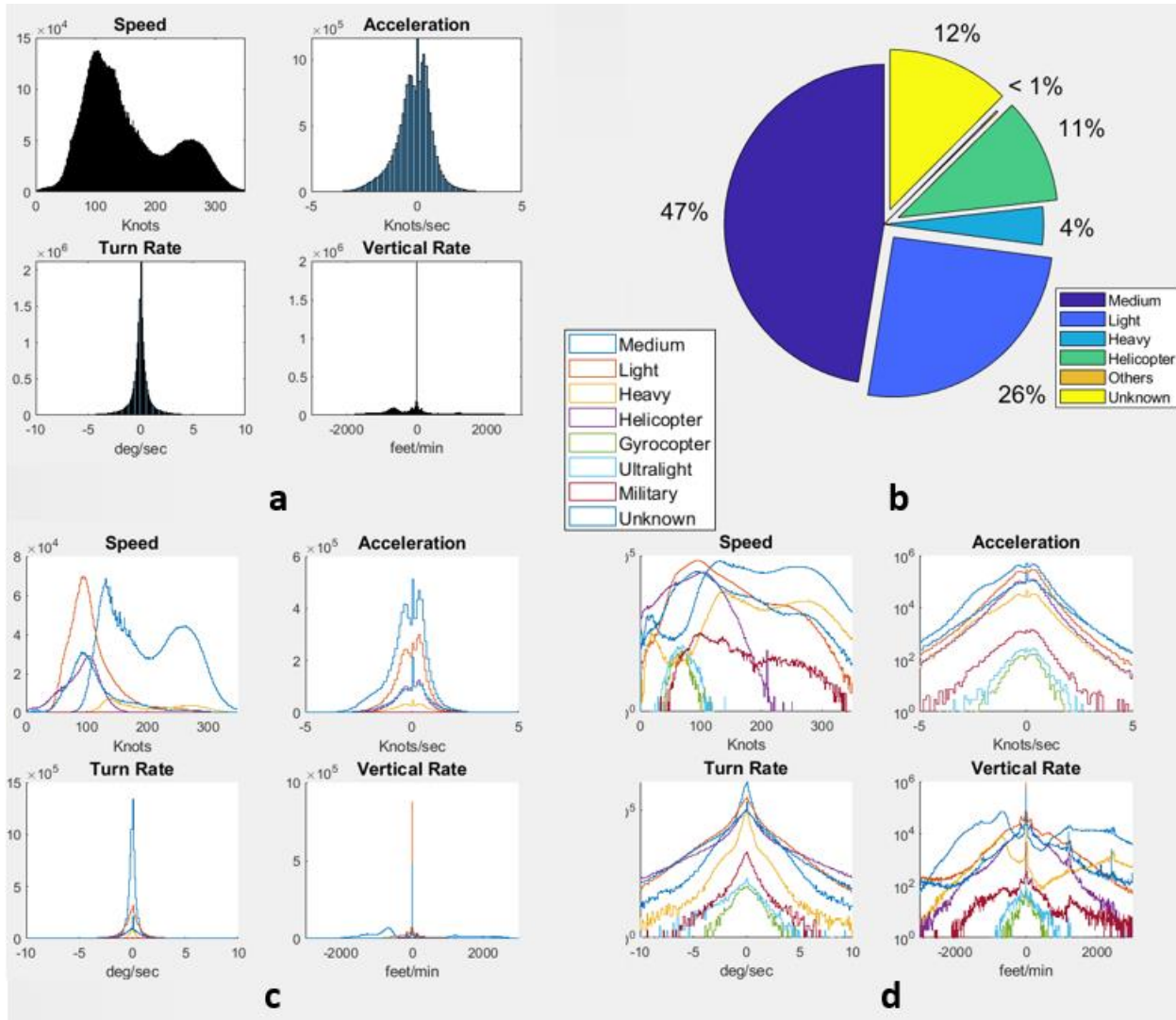


Figure 34: Montréal–Mirabel International Airport (CYMX) 0-10,000 ft ASL

(a) Mixed model distribution (b) Aircraft categories percentages (c) Variables distributions by aircraft category (d) Underlying distributions shape

Table 17: Descriptive Statistics of Variable Distributions for CYMX (0-10,000 ft ASL): Mean, Mode, and Standard Deviation

Variable	Mean	Mode	Standard Deviation
Speed (knots)	154.0661	102	72.3375
Turn Rate (deg/sec)	-0.0807	0	1.3908
Vertical Rate (feet/sec)	69.3392	0	1118.4679
Acceleration (knots/sec)	-0.1929	0	0.9045

### A.6 Timmins Victor M. Power Airport (CYTS)

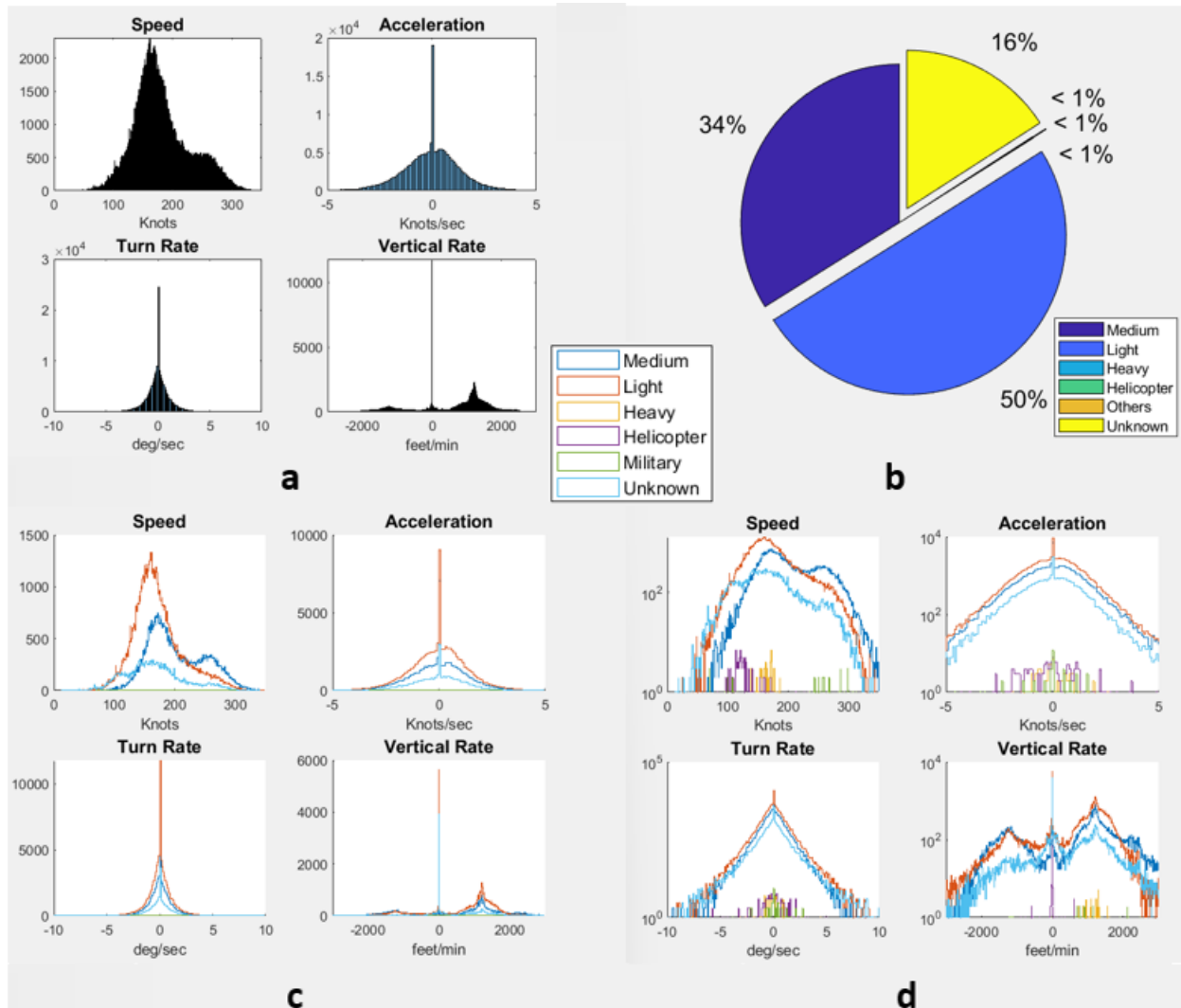


Figure 35: Timmins Victor M. Power Airport (CYTS) 0-10,000 ft ASL

(a) Mixed model distribution (b) Aircraft categories percentages (c) Variables distributions by aircraft category (d) Underlying distributions shape

Table 18: Descriptive Statistics of Variable Distributions for CYTS (0-10,000 ft): Mean, Mode, and Standard Deviation

Variable	Mean	Mode	Standard Deviation
Speed (knots)	180.9853	161	47.2474
Turn Rate (deg/sec)	-0.0351	0	1.2819
Vertical Rate (feet/sec)	614.6108	0	1135.7023
Acceleration (knots/sec)	-0.0597	0	1.3827

### A.7 Victoria International Airport Model (CYYJ)

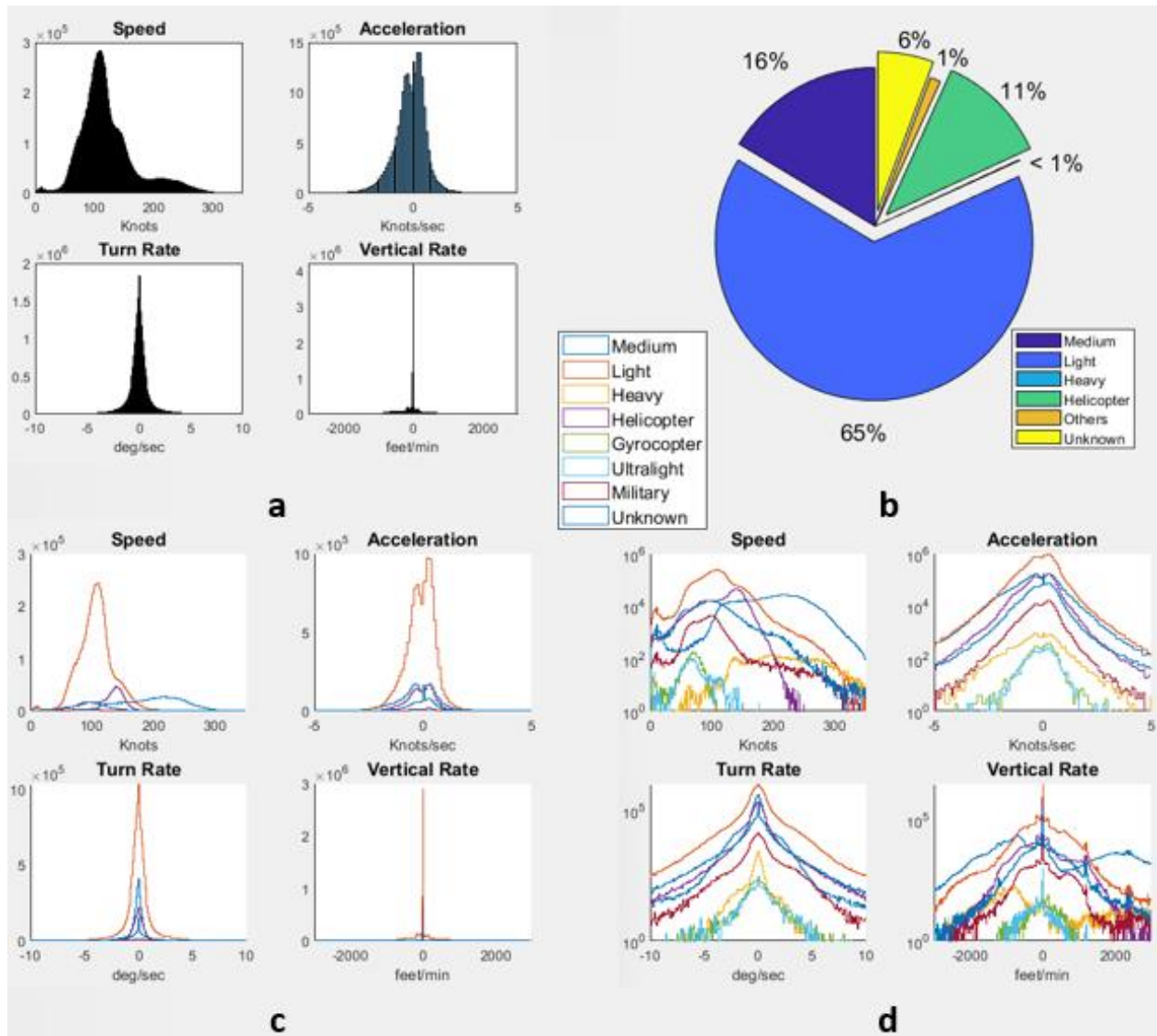


Figure 36: Victoria International Airport Model (CYYJ) 0-10,000 ft ASL

(a) Mixed model distribution (b) Aircraft categories percentages (c) Variables distributions by aircraft category (d) Underlying distributions shape

Table 19: Descriptive Statistics of Variable Distributions for CYYJ (0-10,000 ft ASL): Mean, Mode, and Standard Deviation

Variable	Mean	Mode	Standard Deviation
Speed (knots)	122.3824	108	48.2432
Turn Rate (deg/sec)	-0.0571	0	1.4048
Vertical Rate (feet/sec)	-14.5177	0	650.2516
Acceleration (knots/sec)	-0.1741	0.3	0.7816

### A.8 Vancouver International Airport (CYVR)

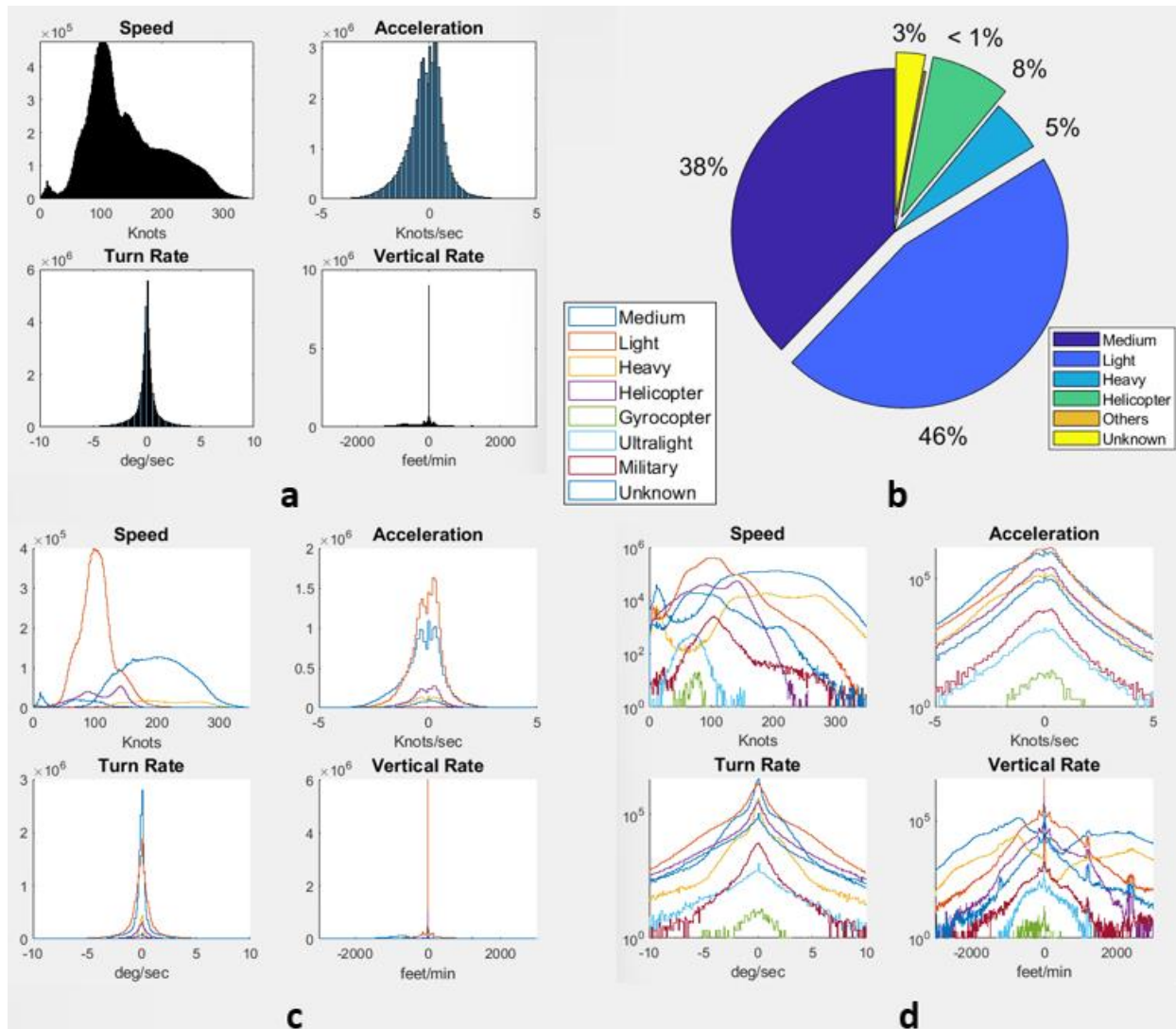


Figure 37: Vancouver International Airport (CYVR) 0-10,000 ft ASL

(a) Mixed model distribution (b) Aircraft categories percentages (c) Variables distributions by aircraft category (d) Underlying distributions shape

Table 20: Descriptive Statistics of Variable Distributions for CYVR (0-10,000 ft ASL): Mean, Mode, and Standard Deviation

Variable	Mean	Mode	Standard Deviation
Speed (knots)	142.3572	104	63.9610
Turn Rate (deg/sec)	-0.0969	0	1.4334
Vertical Rate (feet/sec)	35.8128	0	992.4206
Acceleration (knots/sec)	-0.2105	0.2	0.8937

### A.9      Winnipeg James Armstrong Richardson International Airport (CYWG)

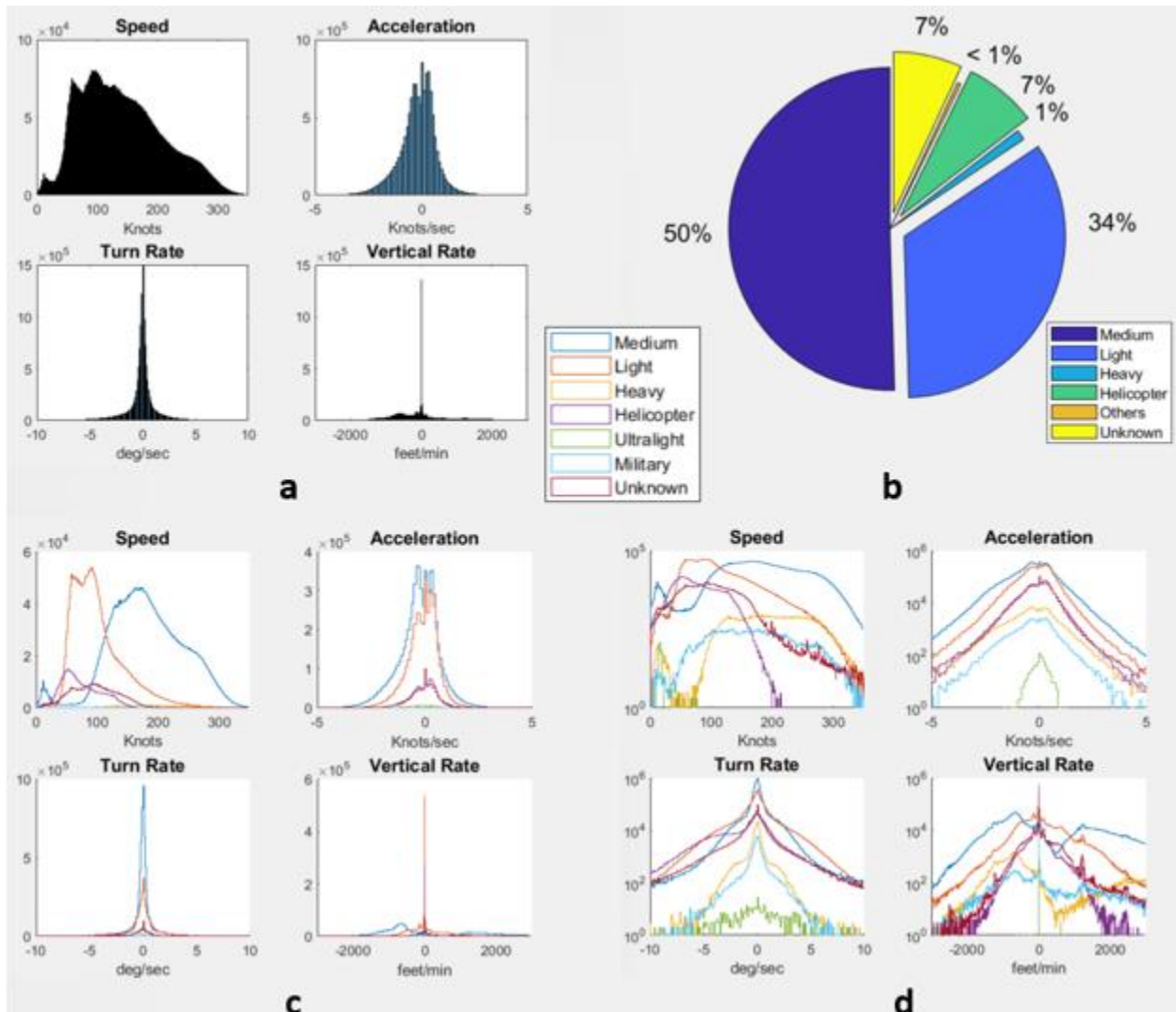


**Figure 38:** Winnipeg James Armstrong Richardson International Airport (CYWG) 0-10,000 ft ASL  
 (a) Mixed model distribution (b) Aircraft categories percentages (c) Variables distributions by aircraft category (d) Underlying distributions shape

**Table 21:** Descriptive Statistics of Variable Distributions for CYWG (0-10,000 ft ASL): Mean, Mode, and Standard Deviation

Variable	Mean	Mode	Standard Deviation
Speed (knots)	140.2516	96	67.5845
Turn Rate (deg/sec)	-0.1508	0	1.6314
Vertical Rate (feet/sec)	69.9812	0	1017.2109
Acceleration (knots/sec)	-0.2211	0	0.8580

### A.10 Canadian Forces Base Goose Bay (CYYR)

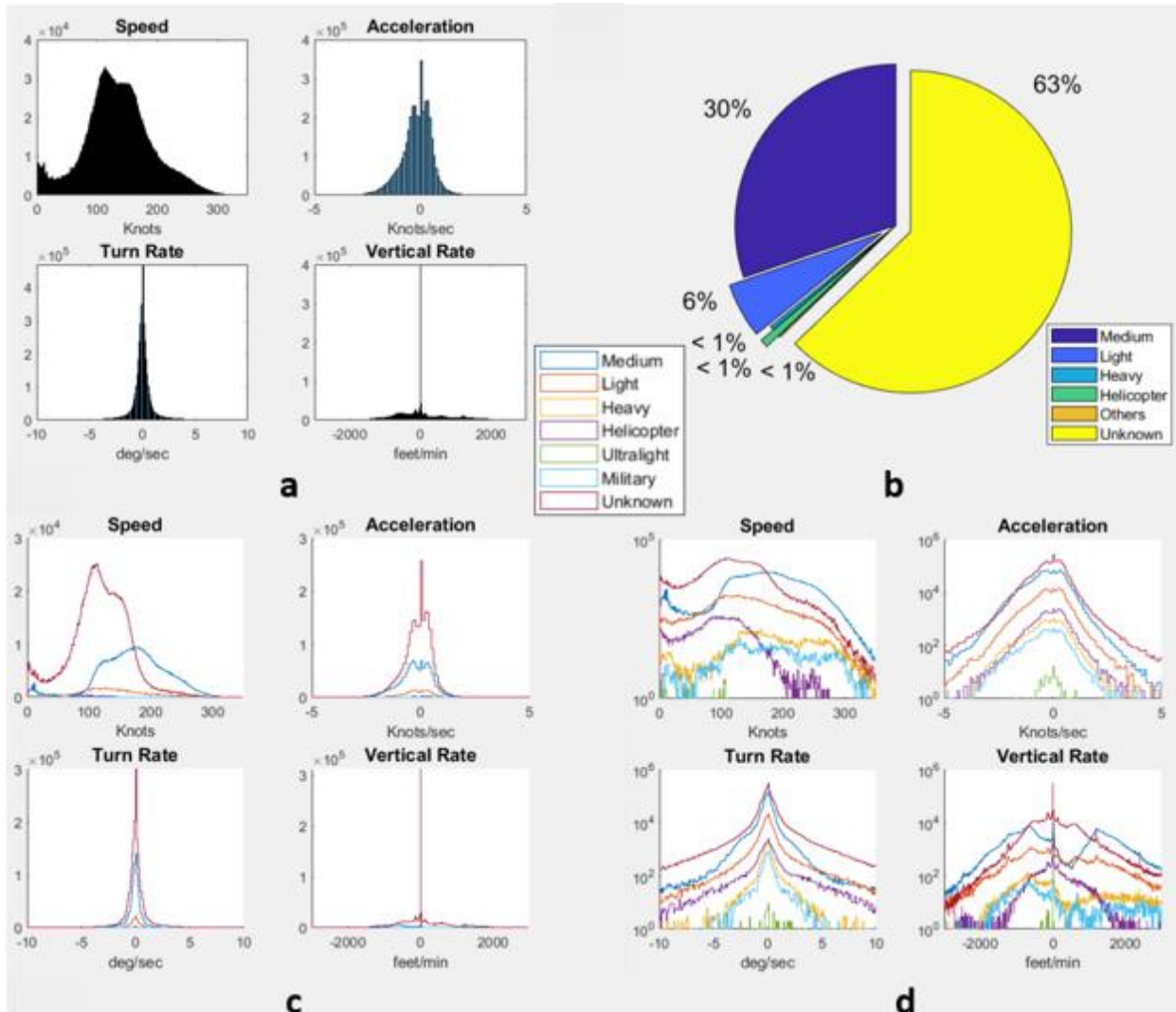


Figure 39: Canadian Forces Base Goose Bay (CYYR) 0-10,000 ft ASL

(a) Mixed model distribution (b) Aircraft categories percentages (c) Variables distributions by aircraft category (d) Underlying distributions shape

Table 22: Descriptive Statistics of Variable Distributions for CYYR (0-10,000 ft ASL): Mean, Mode, and Standard Deviation

Variable	Mean	Mode	Standard Deviation
Speed (knots)	134.9248	113	55.6636
Turn Rate (deg/sec)	-0.0234	0	1.8993
Vertical Rate (feet/sec)	80.4449	0	884.6254
Acceleration (knots/sec)	-0.2203	0	0.7162

### A.11 Yellowknife Airport (CYZF)

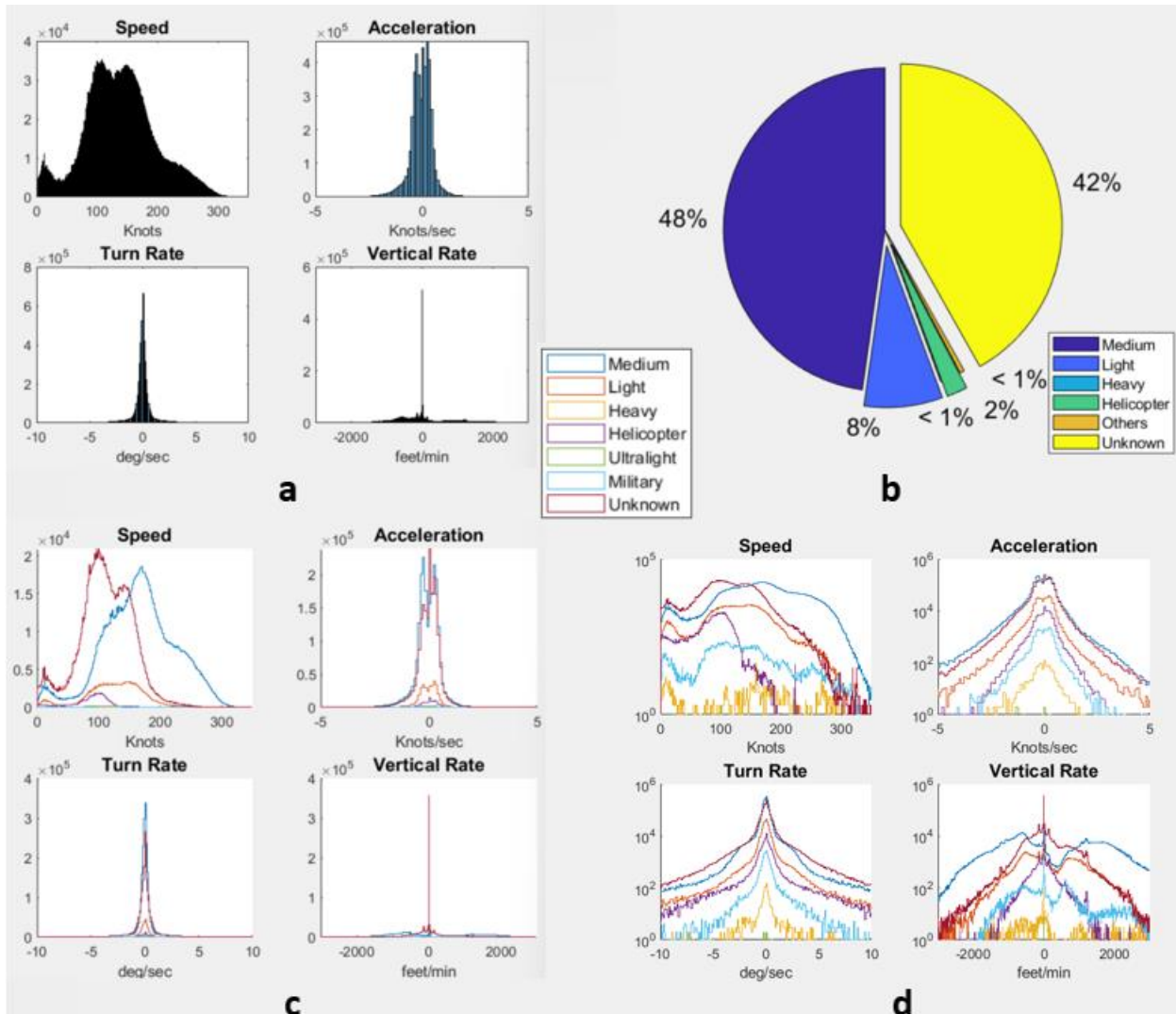


Figure 40: Yellowknife Airport (CYZF) 0-10,000 ft ASL

(a) Mixed model distribution (b) Aircraft categories percentages (c) Variables distributions by aircraft category (d) Underlying distributions shape

Table 23: Descriptive Statistics of Variable Distributions for CYZF (0-10,000 ft): Mean, Mode, and Standard Deviation

Variable	Mean	Mode	Standard Deviation
Speed (knots)	137.7508	108	57.5463
Turn Rate (deg/sec)	-0.0383	0	1.8254
Vertical Rate (feet/sec)	96.9906	0	952.6550
Acceleration (knots/sec)	-0.0842	0.2	0.5613

### A.12 Iqaluit International Airport (CYFB)

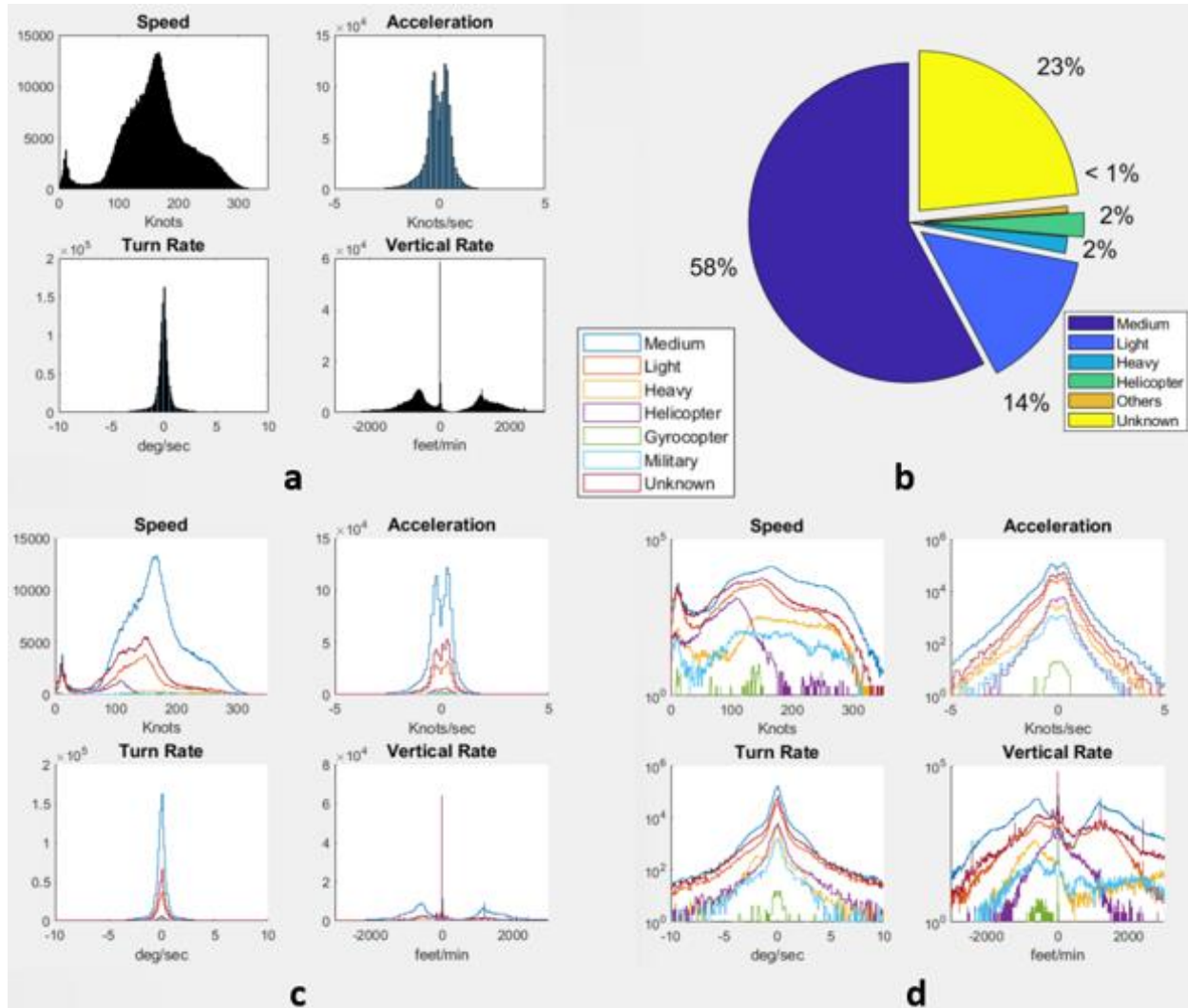


**Figure 41: Iqaluit International Airport (CYFB) 0-10,000 ft ASL**  
**(a) Mixed model distribution (b) Aircraft categories percentages (c) Variables distributions by aircraft category (d) Underlying distributions shape**

**Table 24: Descriptive Statistics of Variable Distributions for CYFB (0-10,000 ft ASL): Mean, Mode, and Standard Deviation**

Variable	Mean	Mode	Standard Deviation
Speed (knots)	161.5010	167	55.7930
Turn Rate (deg/sec)	-0.0650	0	1.3013
Vertical Rate (feet/sec)	260.4277	0	1266.4781
Acceleration (knots/sec)	-0.1084	0.2	0.6096

## B Cut-Points and Bayesian Network Structure Determination

### B.1 Light aircraft below 10,000 ft ASL

Table 25: Light aircraft model cut point for tracks below 10,000 ft

Light Aircraft Model from 0-10,000 ft	
Variable	Cut-Points
Altitude	1200, 3000, 5000
Speed	26, 77, 128, 179, 230, 281, 332
Acceleration	-6.3, -3.8, -1.3, 1.3, 3.8, 6.3
Vertical Rate	-4570, -2620, -680, 1260, 3200, 5150
Turn Rate	-6.7, -4.0, -1.3, 1.3, 4.0, 6.7

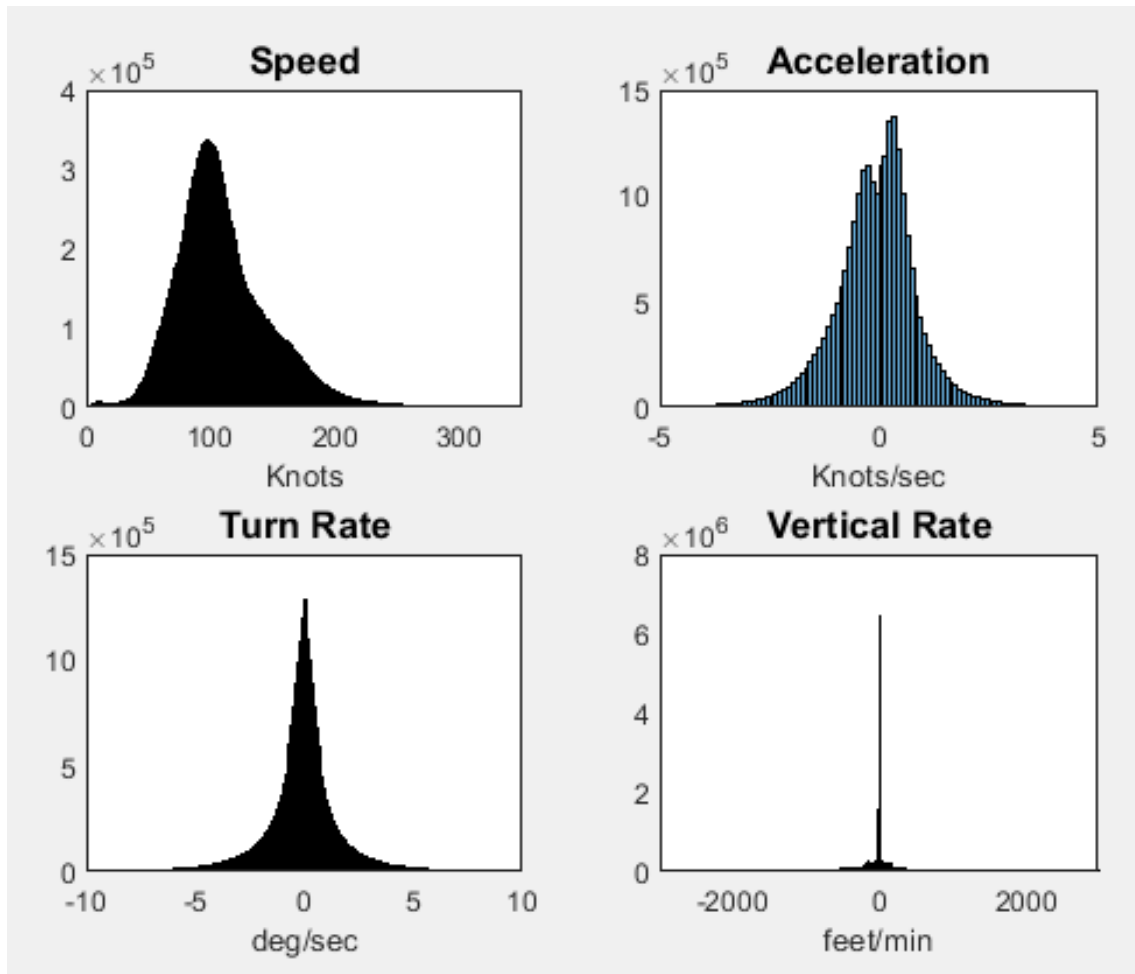


Figure 42: Light aircraft model histograms below 10,000 ft

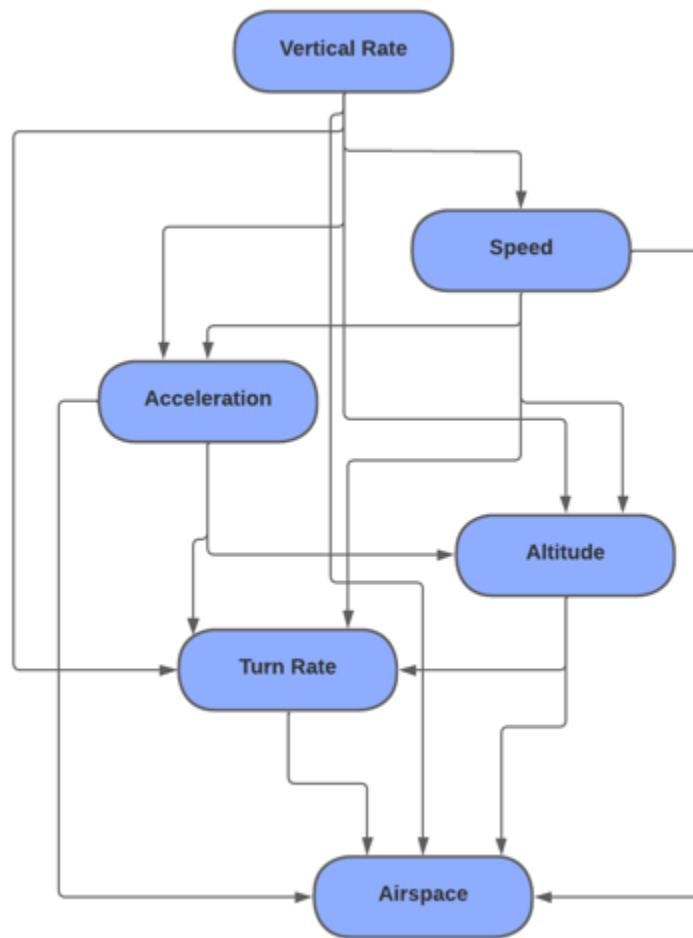


Figure 43: Initial Distributions for Light aircraft model below 10,000 ft

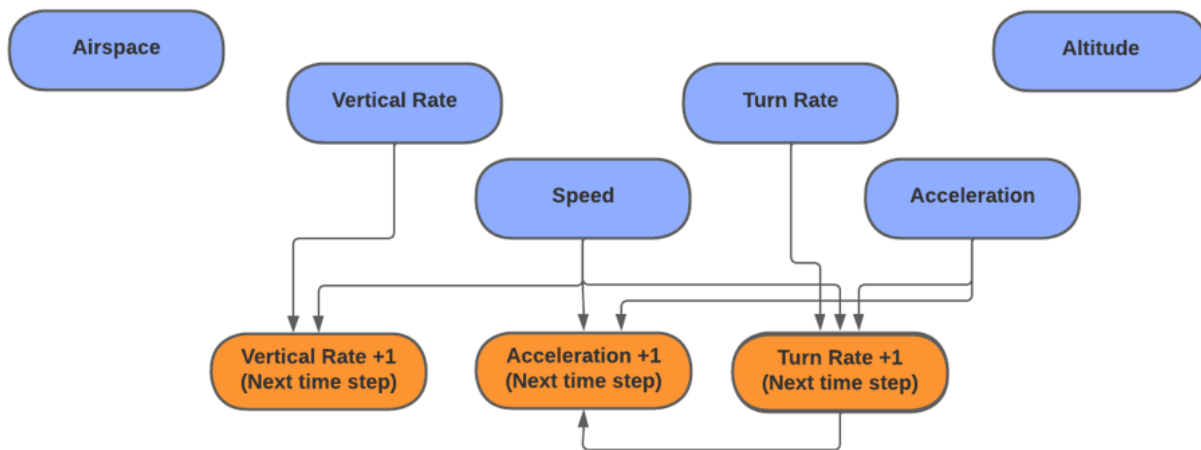


Figure 44: Transition Distributions for Light aircraft model below 10,000 ft

## B.2 Light aircraft between 10,000 and 25,000 ft ASL

Table 26: Light aircraft model cut point for tracks between 10,000-25,000 ft ASL

Light Aircraft Model from 10,000-25,000 ft	
Variable	Cut-Points
Altitude	12500, 18000
Speed	57, 112, 165, 228, 286, 332, 363, 463, 495
Acceleration	-6.3, -3.8, -1.3, 1.3, 3.8, 6.3
Vertical Rate	-5320, -3560, -1800, -50, 1710, 3470, 5230
Turn Rate	-6.7, -4.0, -1.3, 1.3, 4.0, 6.7

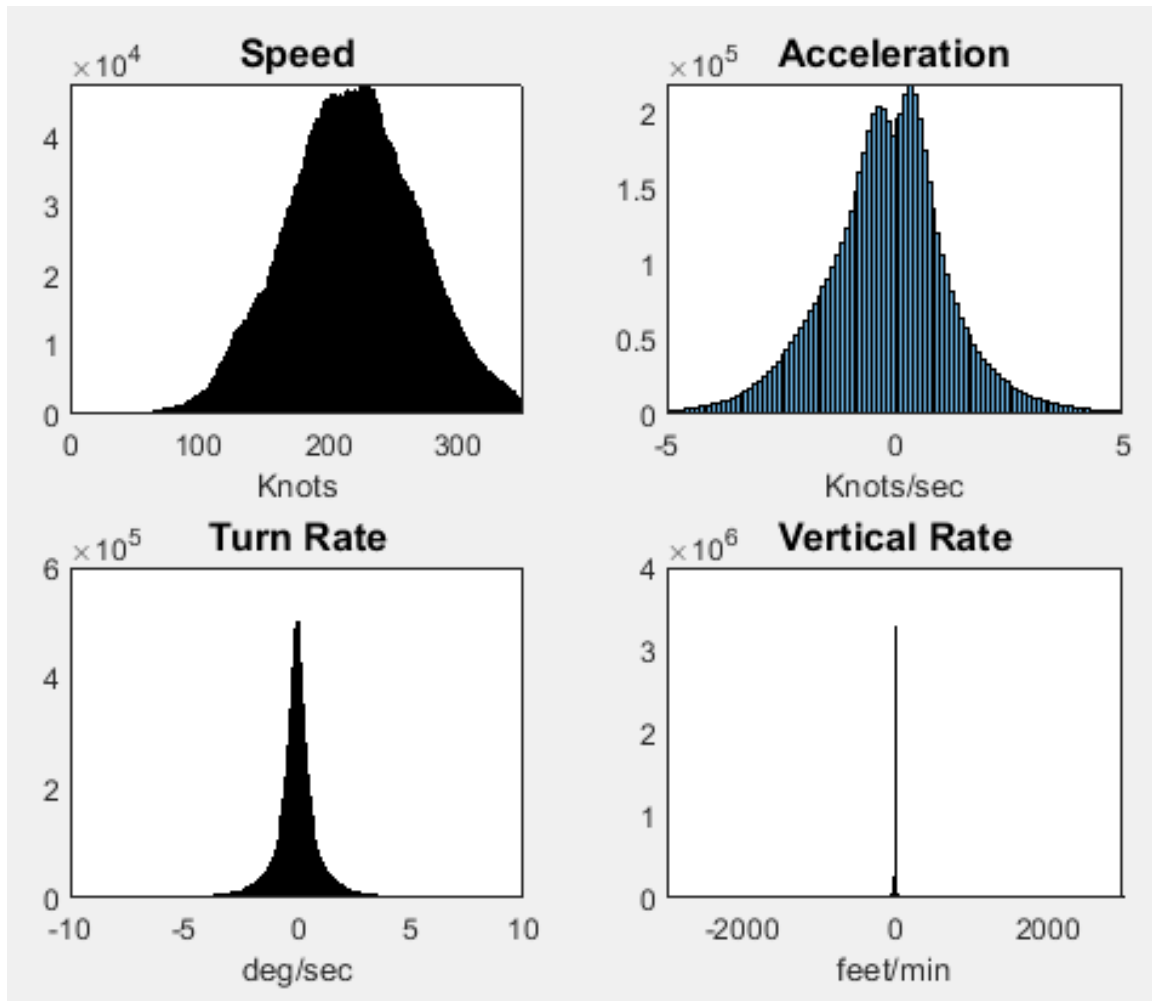


Figure 45: Light aircraft model histograms between 10,000-25,000 ft ASL

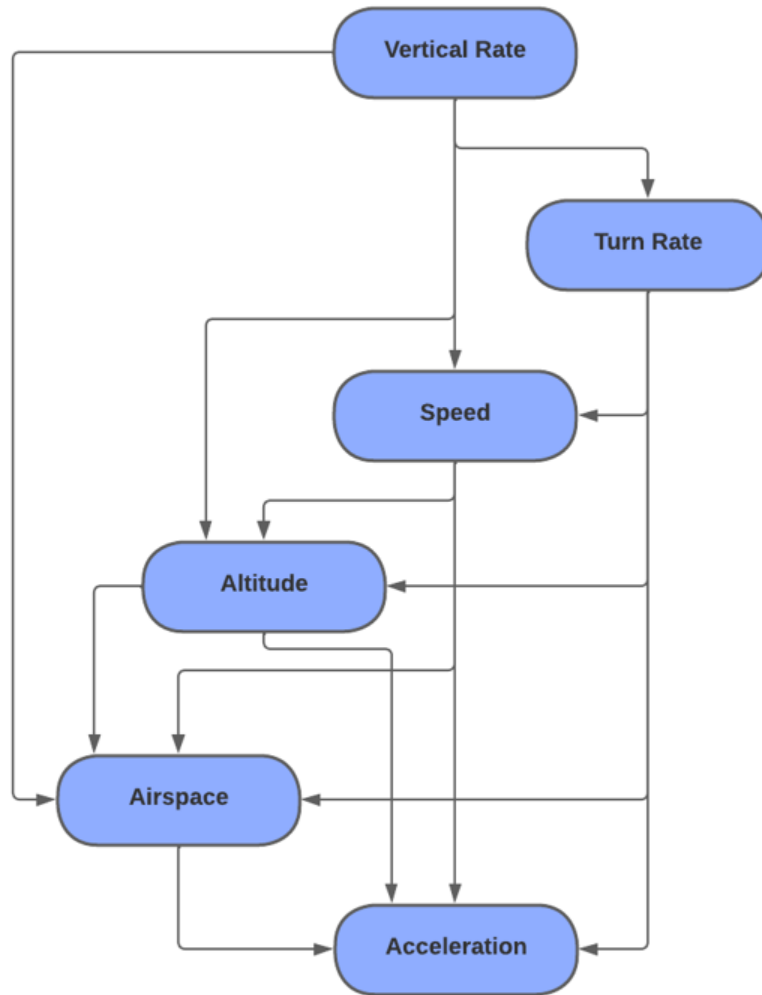


Figure 46: Initial Distributions for Light aircraft model between 10,000-25,000 ft ASL

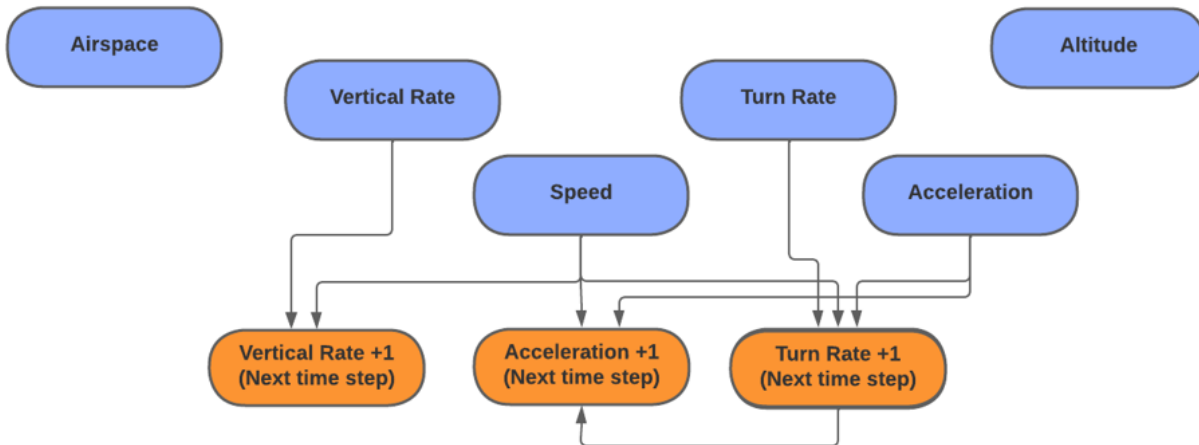


Figure 47: Transition Distributions for Light aircraft model between 10,000-25,000 ft ASL

### B.3 Light aircraft above 25,000 ft ASL

Table 27: Light aircraft model cut point for tracks above 25,000 ft ASL

Light Aircraft Model above 25,000 ft	
Variable	Cut-Points
Altitude	35000, 40000, 60000
Speed	115, 171, 232, 282, 361, 408, 460, 534, 572
Acceleration	-6.3, -3.8, -1.3, 1.3, 3.8, 6.3
Vertical Rate	-6390, -4470, -2550, -630, 1280, 3200, 5120, 7040
Turn Rate	-6.7, -4.0, -1.3, 1.3, 4.0, 6.7

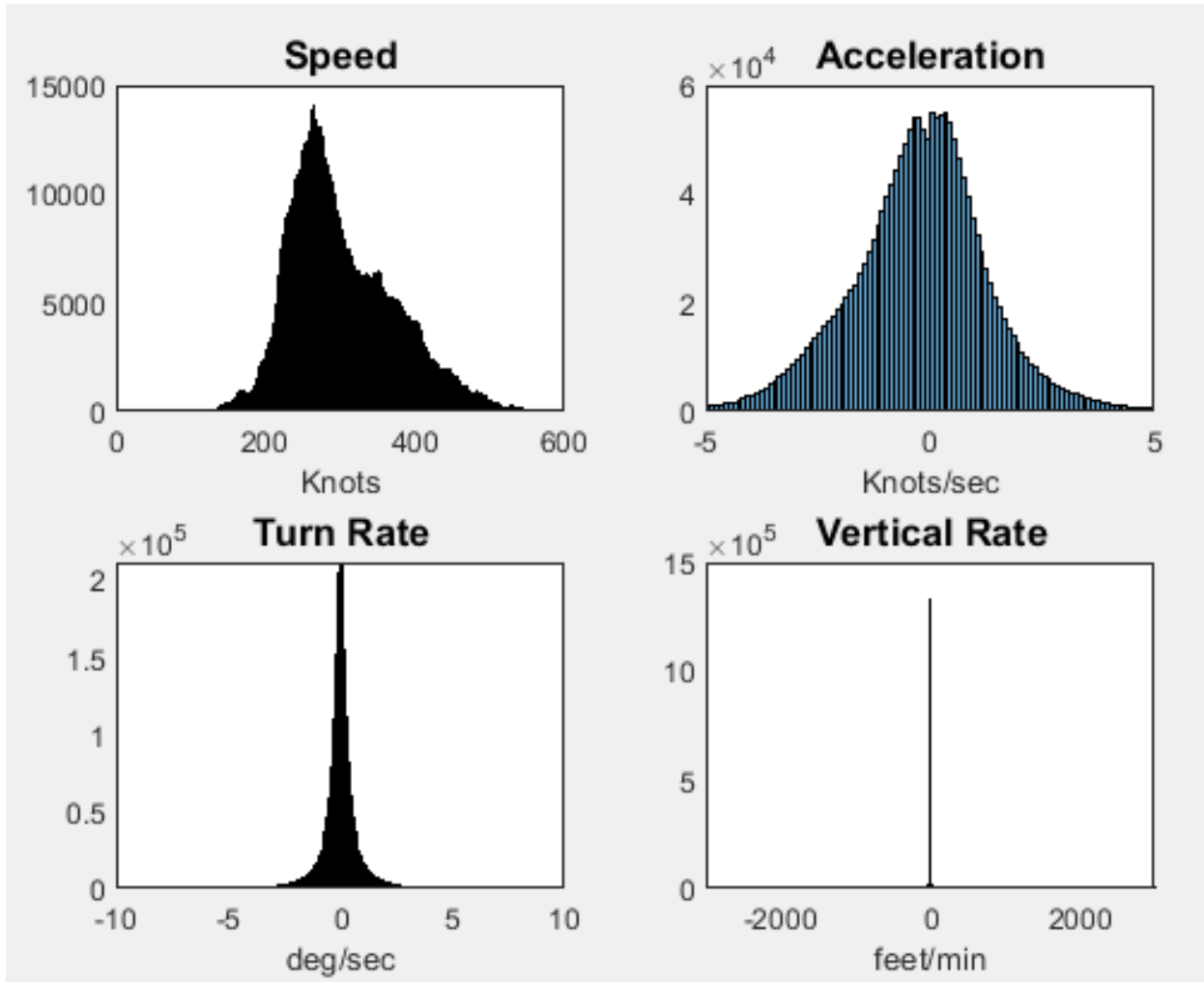


Figure 48: Light aircraft model histograms above 25,000 ft ASL

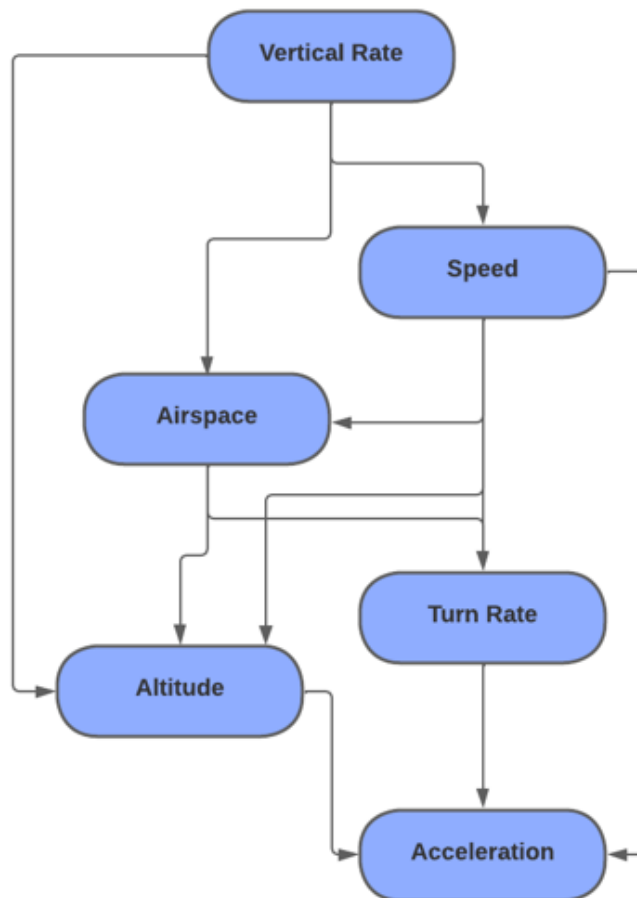


Figure 49: Initial Distributions for Light aircraft model above 25,000 ft ASL

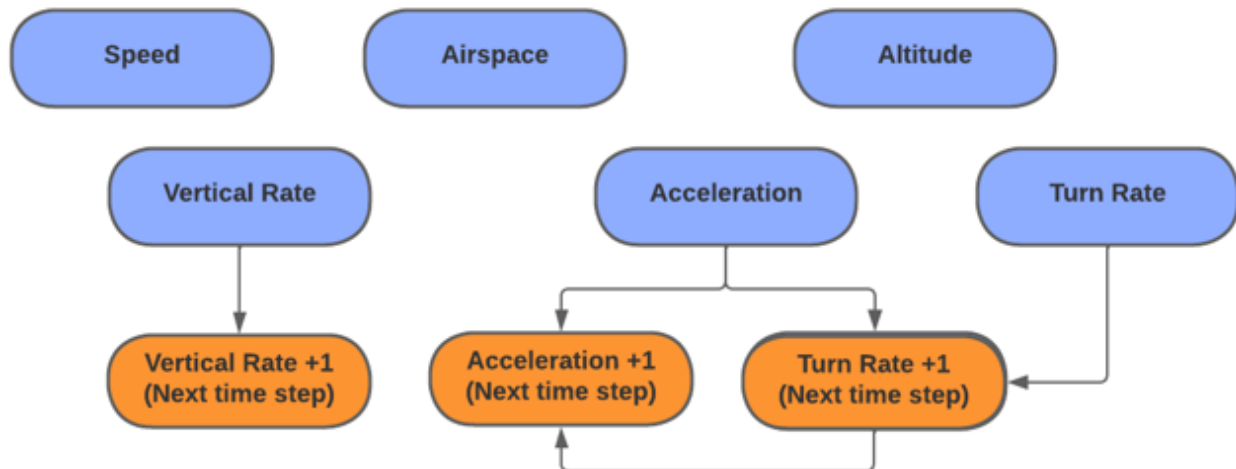
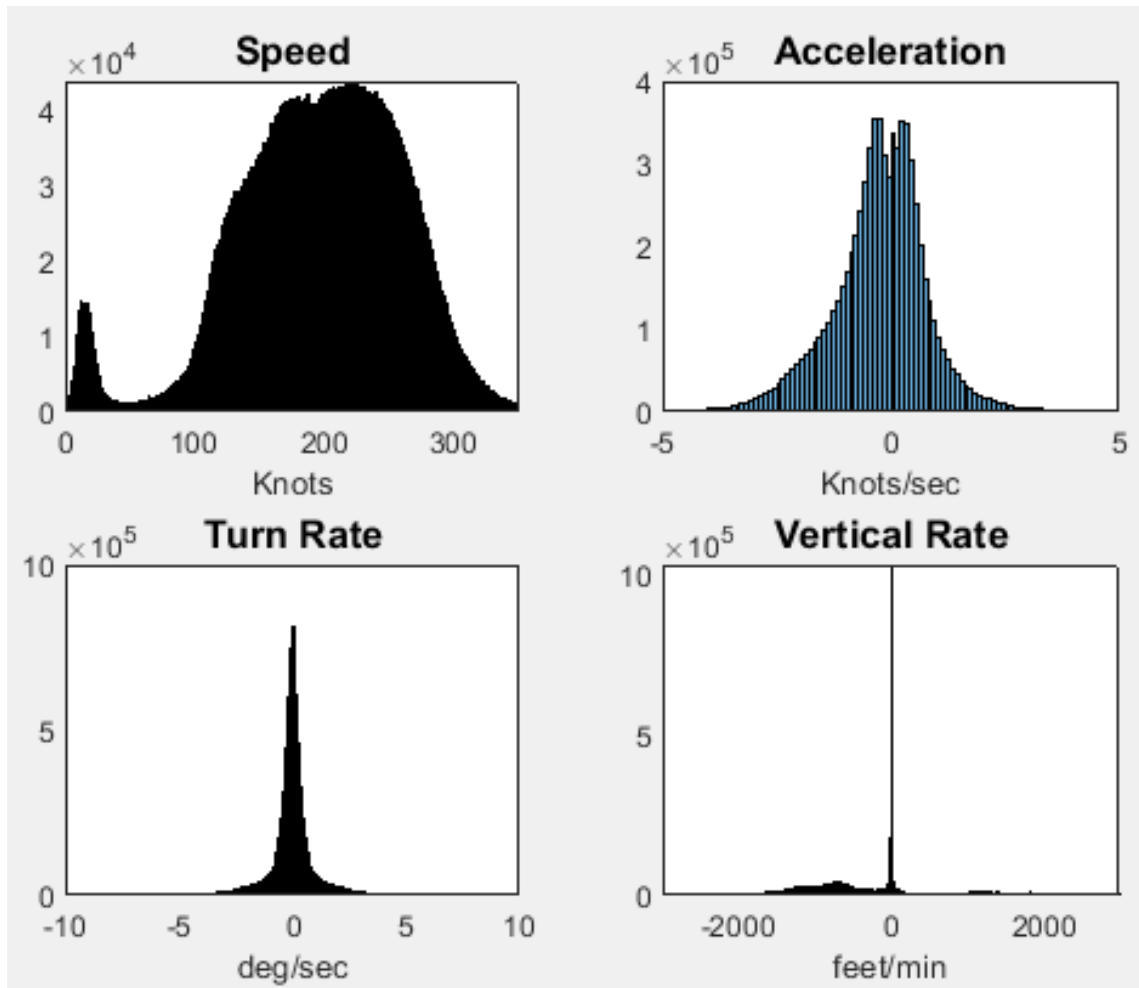


Figure 50: Transition Distributions for Light aircraft model above 25,000 ft ASL

#### B.4 Medium aircraft below 10,000 ft ASL

**Table 28:** Medium aircraft model cut point for tracks below 10,000 ft ASL

Medium Aircraft Model from 0-10,000 ft ASL	
Variable	Cut-Points
Altitude	1200, 3000, 5000
Speed	25, 75, 125, 175, 226, 276, 326, 376
Acceleration	-6.3, -3.8, -1.3, 1.3, 3.8, 6.3
Vertical Rate	-6510, -4580, -2640, -700, 1230, 3170, 5110, 7040
Turn Rate	-6.7, -4.0, -1.3, 1.3, 4.0, 6.7



**Figure 51:** Medium aircraft model histograms below 10,000 ft ASL

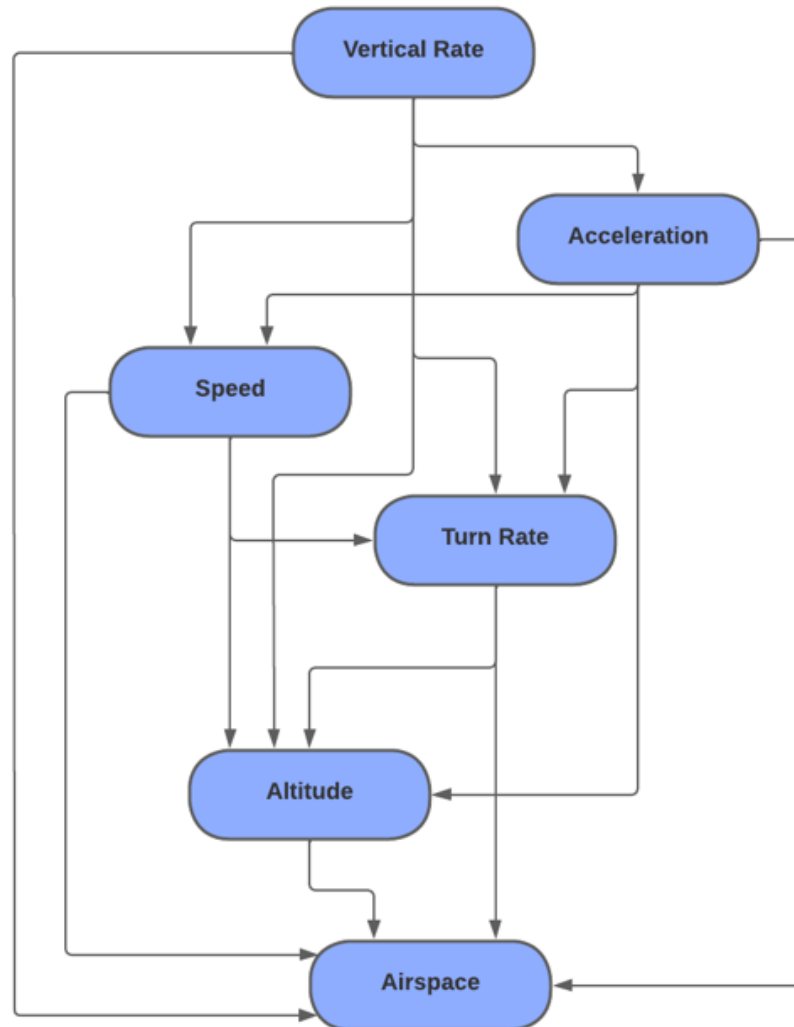


Figure 52: Initial Distributions for Medium aircraft model below 10,000 ft ASL

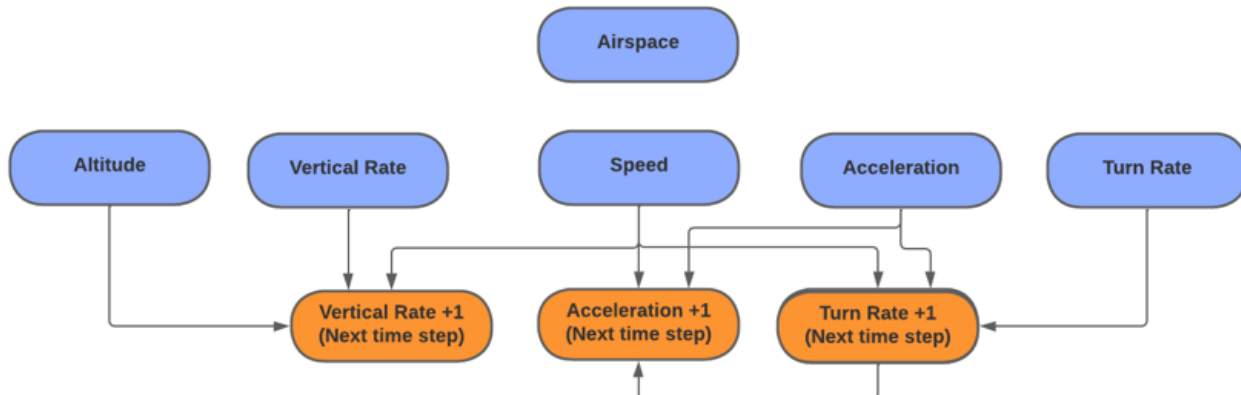
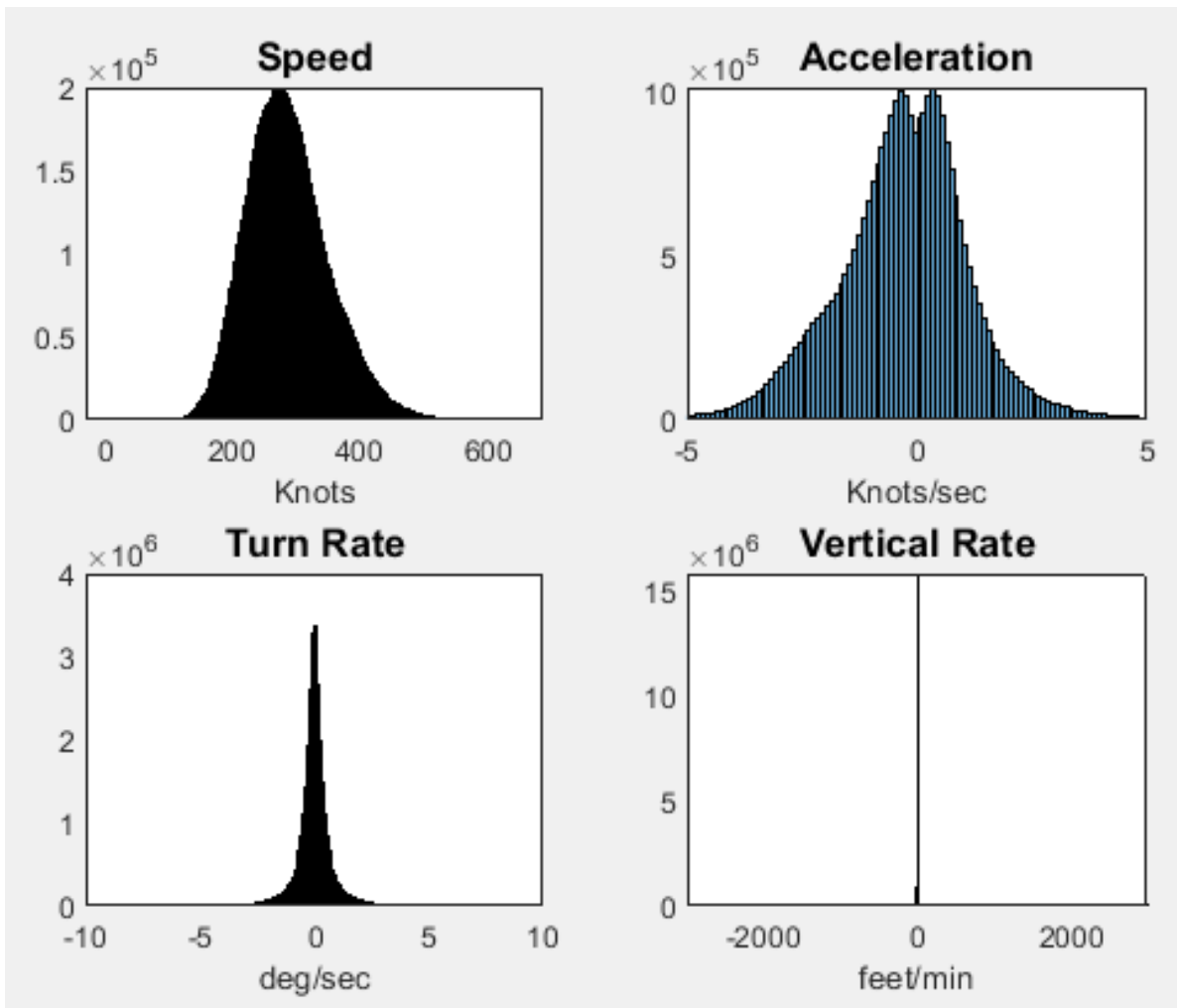


Figure 53: Transition Distributions for Medium aircraft model below 10,000 ft ASL

## B.5 Medium aircraft between 10,000 and 25,000 ft ASL

**Table 29:** Medium aircraft model cut point for tracks between 10,000-25,000 ft ASL

Medium Aircraft Model from 10,000-25,000 ft ASL	
Variable	Cut-Points
Altitude	12500, 18000
Speed	41, 118, 183, 249, 323, 395, 504, 539, 568
Acceleration	-6.3, -3.8, -1.3, 1.3, 3.8, 6.3
Vertical Rate	-6970, -4950, -2930, -910, 1120, 3140, 5160, 7180
Turn Rate	-6.7, -4.0, -1.3, 1.3, 4.0, 6.7



**Figure 54:** Medium aircraft model histograms between 10,000-25,000 ft ASL

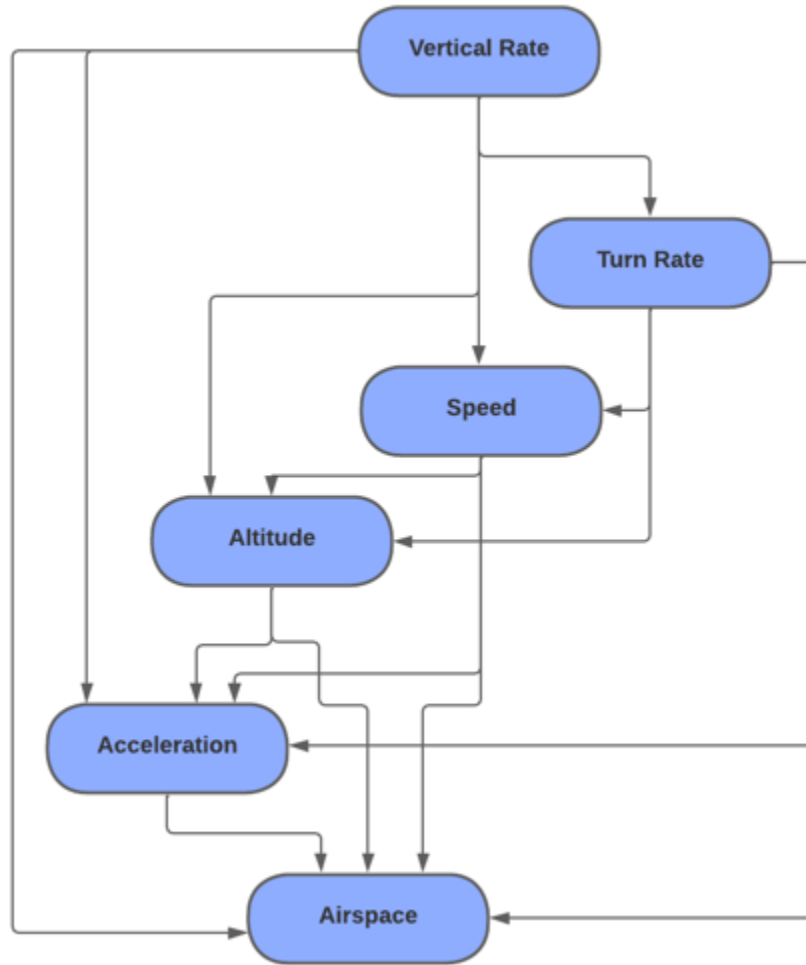


Figure 55: Initial Distributions for Medium aircraft model between 10,000-25,000 ft ASL

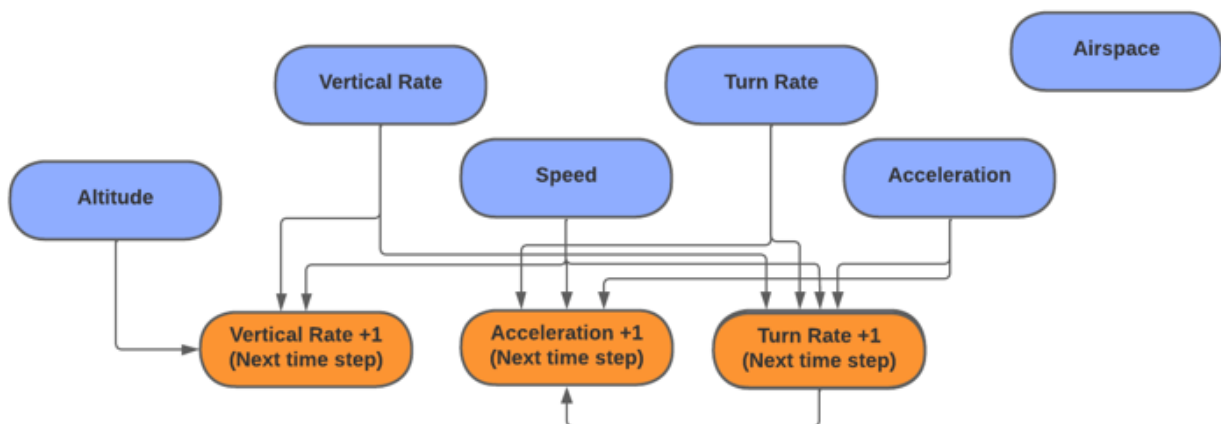
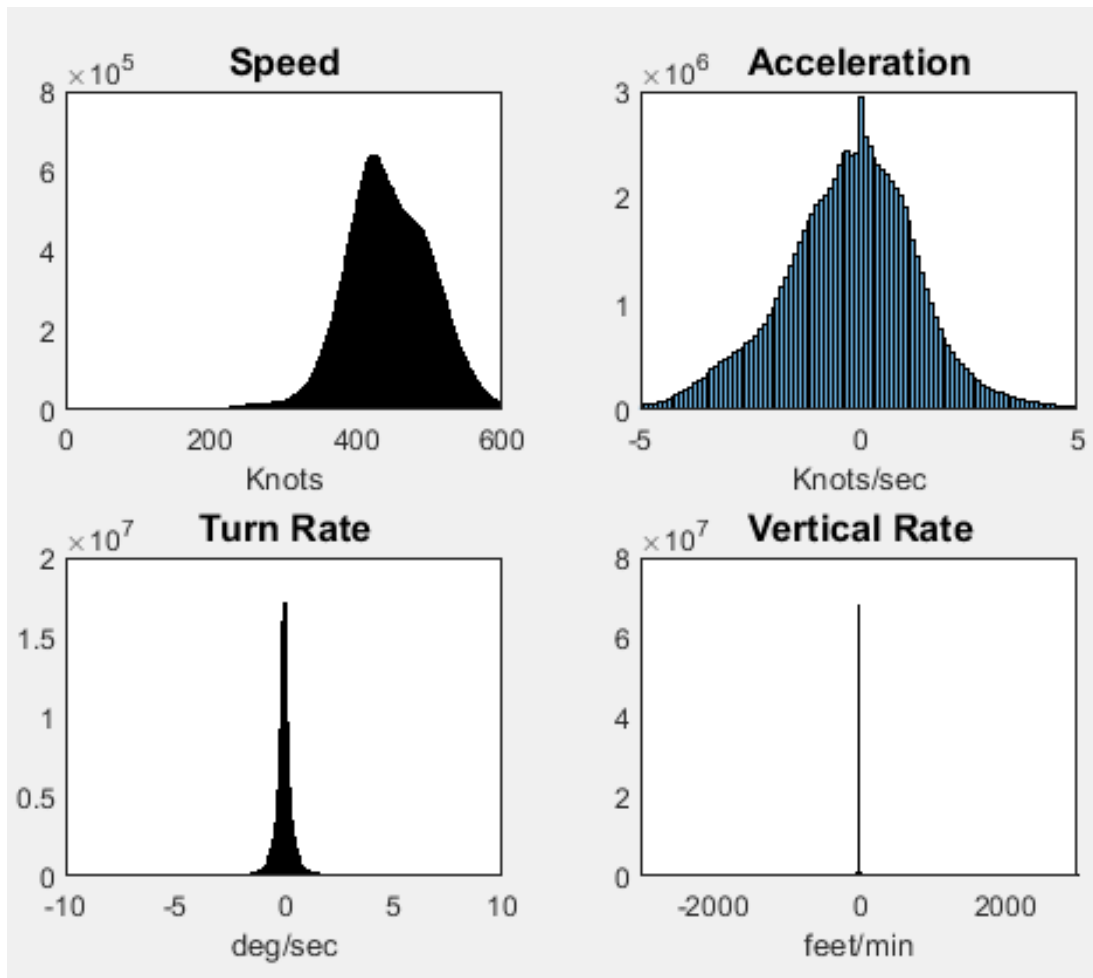


Figure 56: Transition Distributions for Medium aircraft model between 10,000-25,000 ft ASL

## B.6 Medium aircraft above 25,000 ft ASL

**Table 30:** Medium aircraft model cut point for tracks above 25,000 ft ASL

Medium Aircraft Model above 25,000 ft ASL	
Variable	Cut-Points
Altitude	35000, 40000, 60000
Speed	66, 143, 210, 289, 356, 437, 508, 561, 626
Acceleration	-6.3, -3.8, -1.3, 1.3, 3.8, 6.3
Vertical Rate	-7270, -5170, -3080, -980, 1120, 3220, 5310, 7410
Turn Rate	-6.7, -4.0, -1.3, 1.3, 4.0, 6.7



**Figure 57:** Medium aircraft model histograms above 25,000 ft ASL

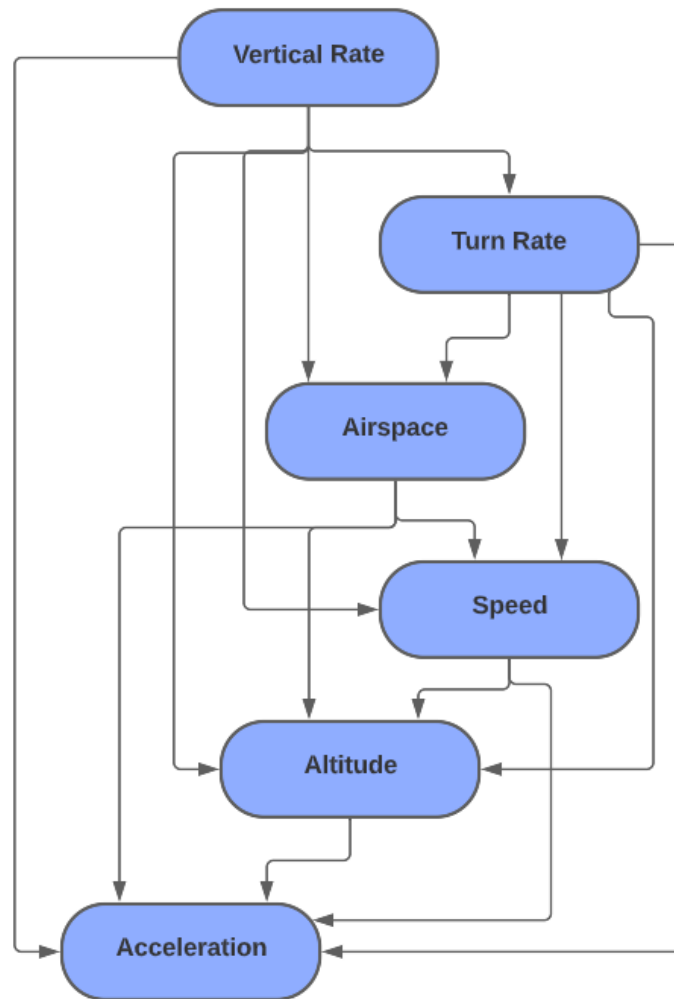


Figure 58: Initial Distributions for Medium aircraft model above 25,000 ft ASL

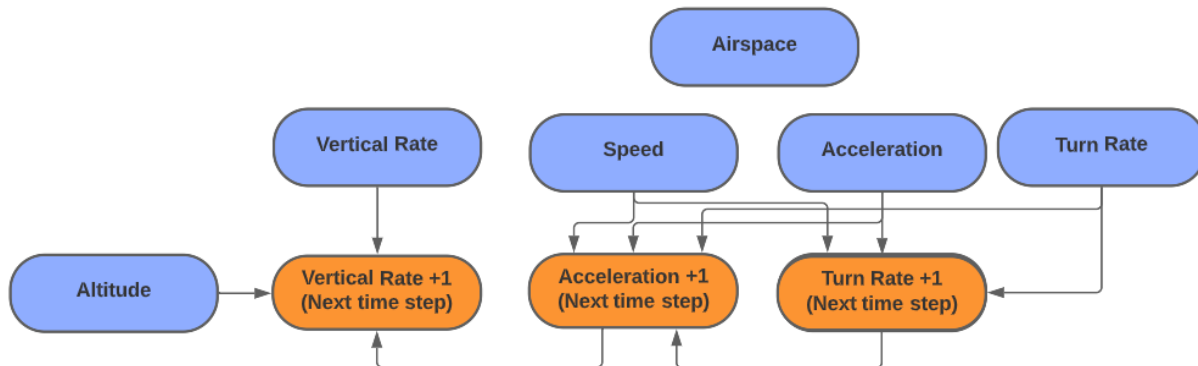
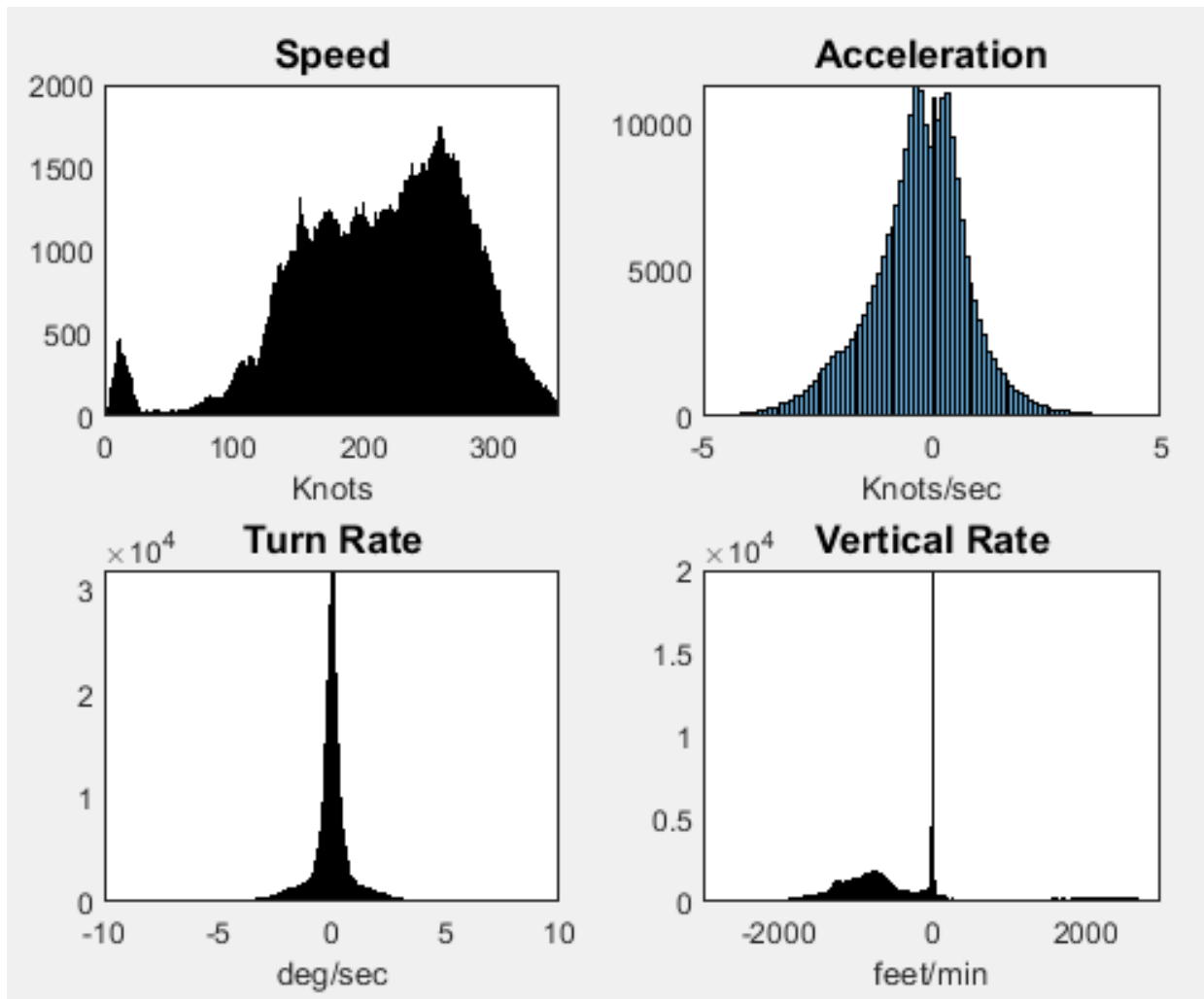


Figure 59: Transition Distributions for Medium aircraft model above 25,000 ft ASL

## B.7 Heavy aircraft below 10,000 ft ASL

**Table 31: Heavy aircraft model cut point for tracks below 10,000 ft ASL**

Heavy Aircraft Model from 0-10,000 ft	
Variable	Cut-Points
Altitude	1200, 3000, 5000
Speed	26, 74, 119, 171, 214, 273, 314, 341
Acceleration	-6.3, -3.8, -1.3, 1.3, 3.8, 6.3
Vertical Rate	-6690, -5020, -3360, -1700, -30, 1630, 3290, 4960
Turn Rate	-6.7, -4.0, -1.3, 1.3, 4.0, 6.7



**Figure 60: Heavy aircraft model histograms below 10,000 ft ASL**

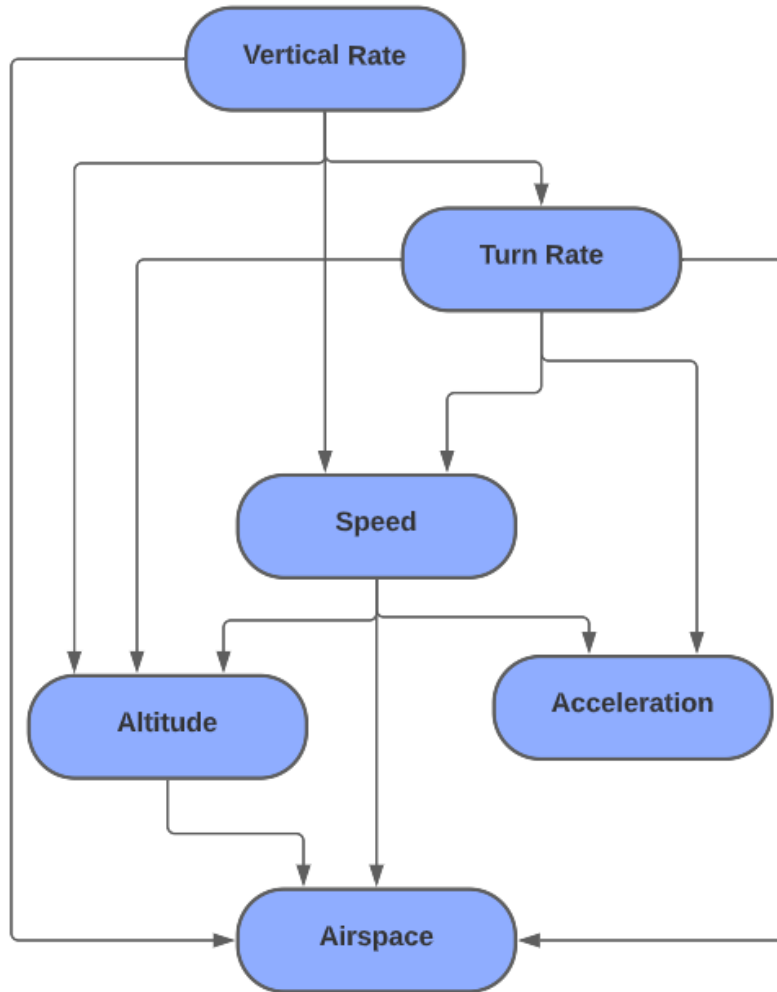


Figure 61: Initial Distributions for Heavy aircraft model below 10,000 ft ASL

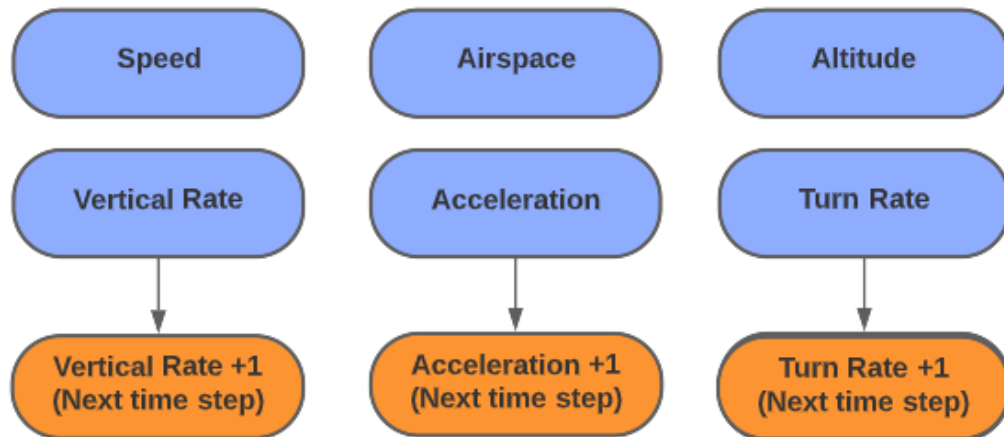


Figure 62: Transition Distributions for Heavy aircraft model below 10,000 ft ASL

## B.8 Heavy aircraft between 10,000 and 25,000 ft ASL

Table 32: Heavy aircraft model cut point for tracks between 10,000-25,000 ft ASL

Heavy Aircraft Model from 10,000-25,000 ft ASL	
Variable	Cut-Points
Altitude	12500, 18000
Speed	164, 219, 247, 282, 336, 379, 519, 613, 637
Acceleration	-6.3, -3.8, -1.3, 1.3, 3.8, 6.3
Vertical Rate	-5950, -4300, -2660, -1010, 630, 2280, 3920, 5570
Turn Rate	-6.7, -4.0, -1.3, 1.3, 4.0, 6.7

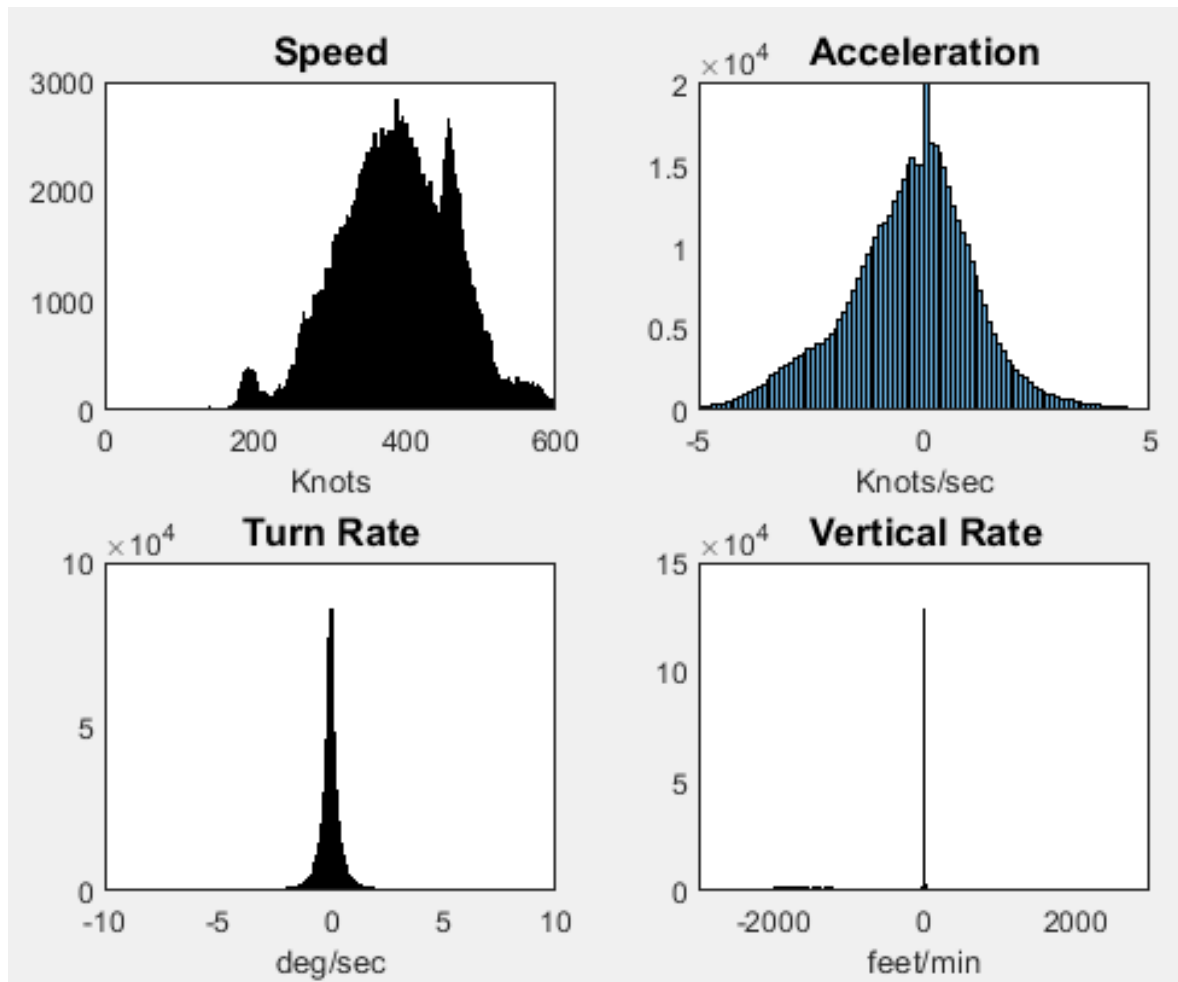


Figure 63: Heavy aircraft model histograms between 10,000-25,000 ft ASL

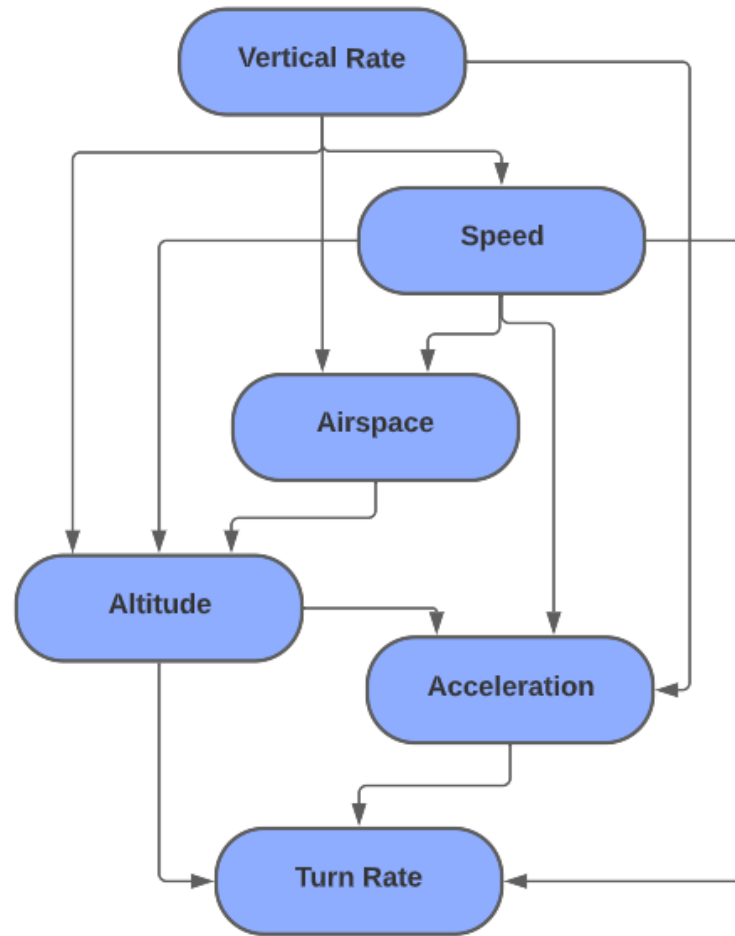


Figure 64: Initial Distributions for Heavy aircraft model between 10,000-25,000 ft ASL

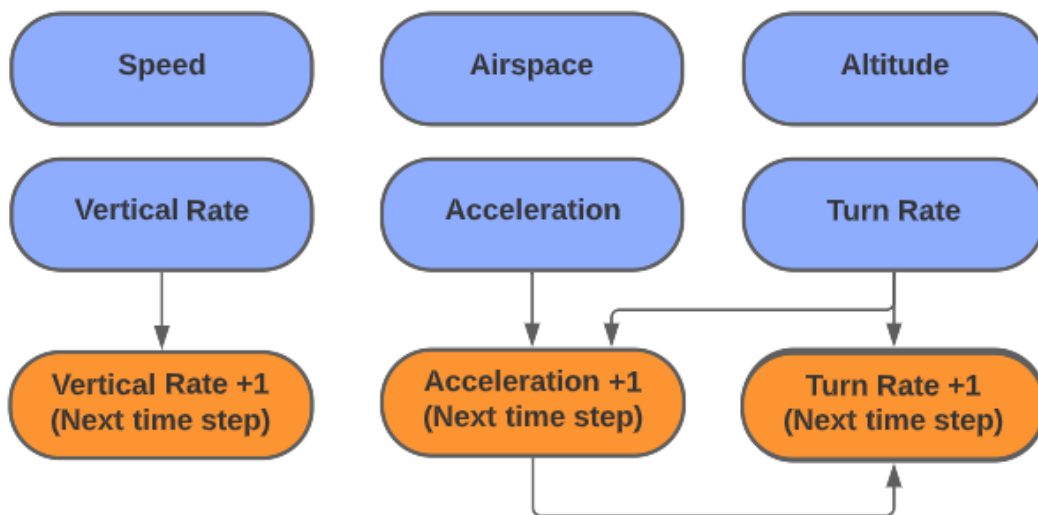


Figure 65: Transition Distributions for Heavy aircraft model between 10,000-25,000 ft ASL

## B.9 Heavy aircraft above 25,000 ft ASL

Table 33: Heavy aircraft model cut point for tracks above 25,000 ft ASL

Heavy Aircraft Model above 25,000 ft ASL	
Variable	Cut-Points
Altitude	35000, 40000, 60000
Speed	175, 239, 289, 369, 434, 490, 535, 598, 649
Acceleration	-6.3, -3.8, -1.3, 1.3, 3.8, 6.3
Vertical Rate	-7170, -5110, -3050, -990, 1080, 3140, 5200, 7260
Turn Rate	-6.7, -4.0, -1.3, 1.3, 4.0, 6.7

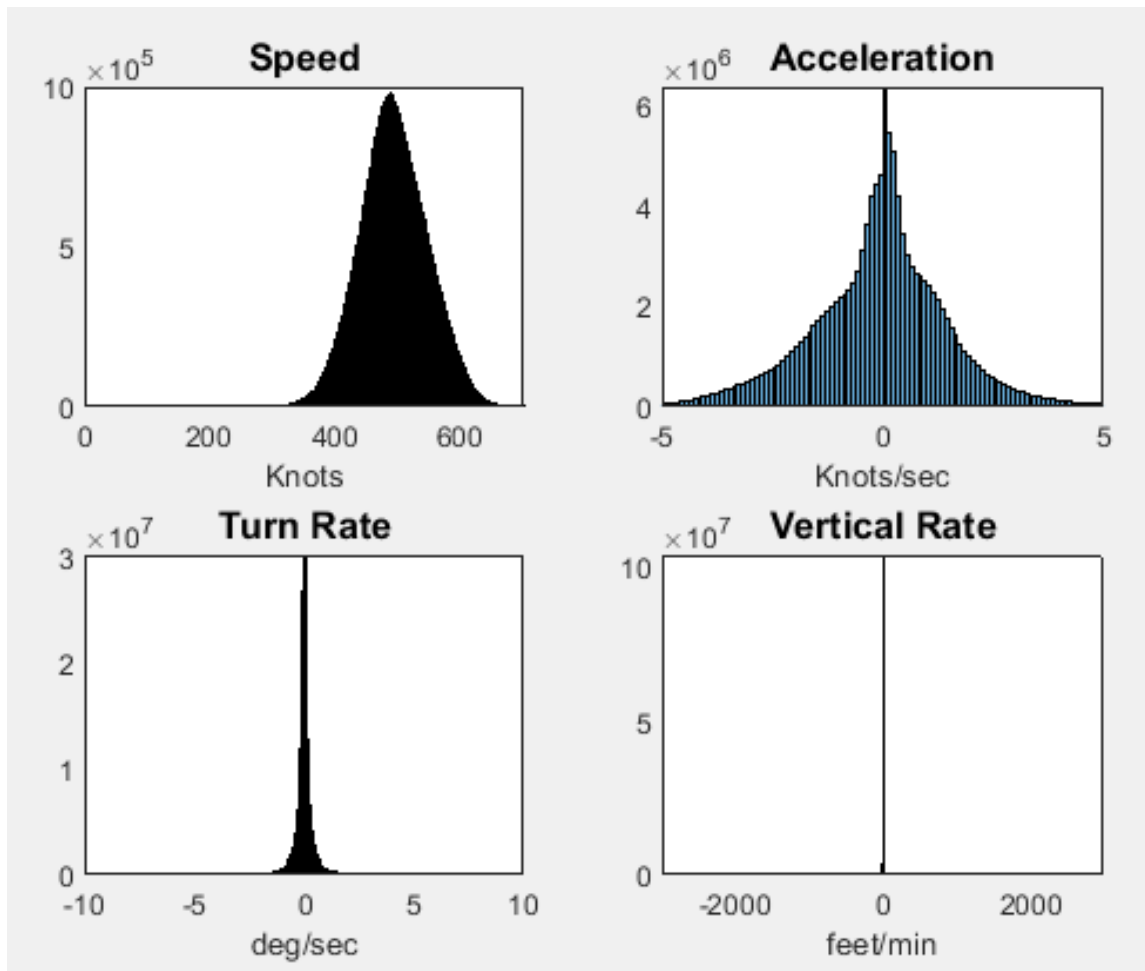


Figure 66: Heavy aircraft model histograms above 25,000 ft ASL

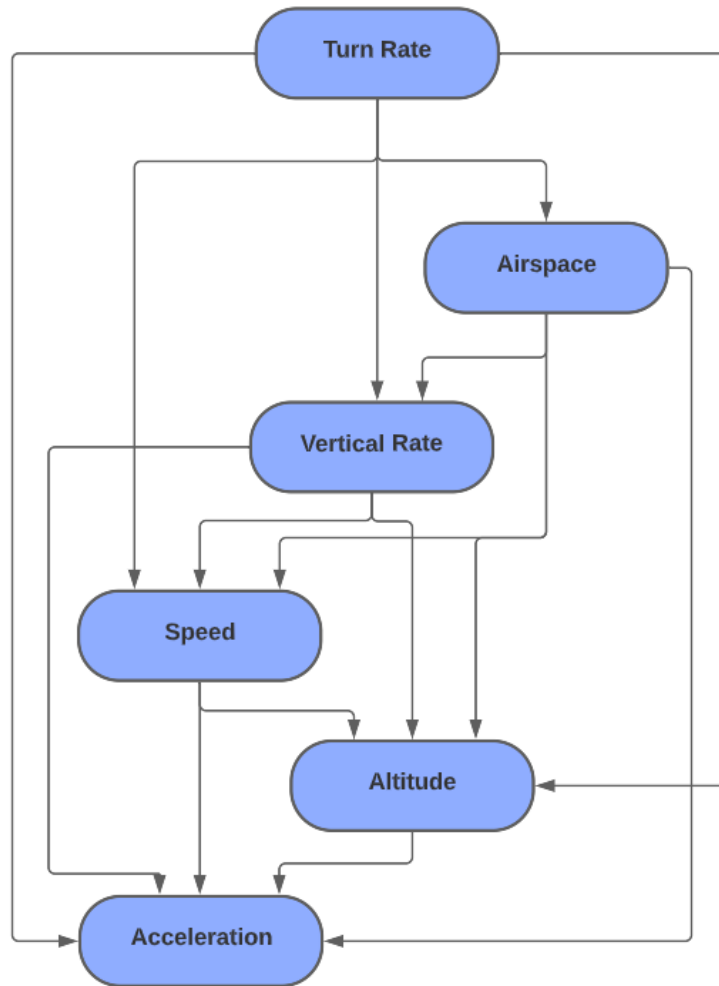


Figure 67: Initial Distributions for Heavy aircraft model above 25,000 ft ASL

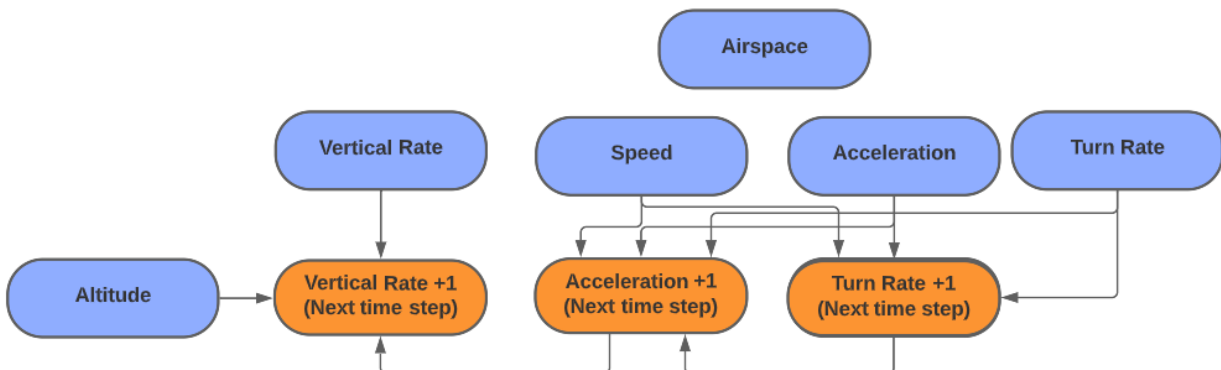
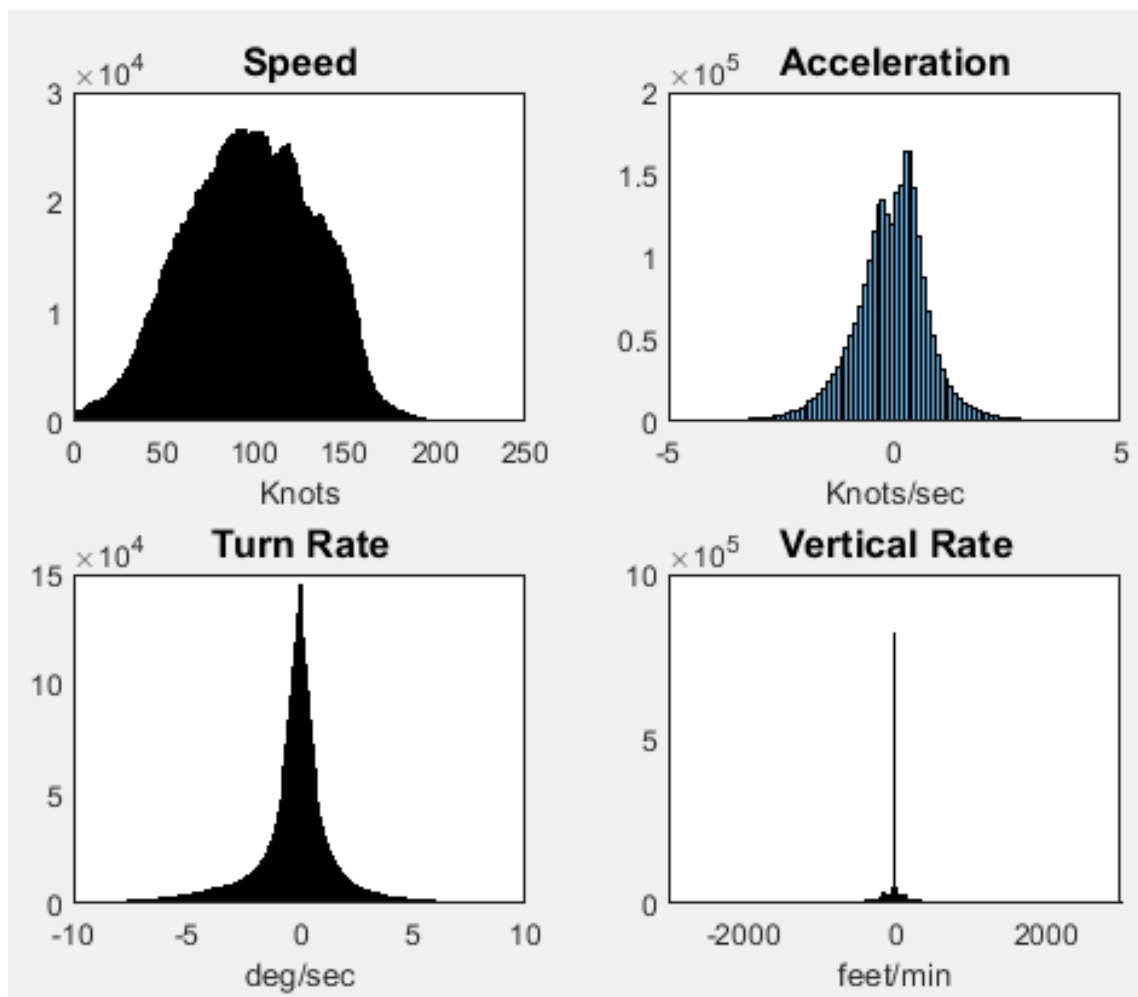


Figure 68: Transition Distributions for Heavy aircraft model above 25,000 ft ASL

### B.10 Helicopter aircraft below 10,000 ft ASL

**Table 34: Helicopter aircraft model cut point for tracks below 10,000 ft ASL**

Helicopter Aircraft Model from 0-10,000 ft	
Variable	Cut-Points
Altitude	1200, 3000, 5000
Speed	16, 49, 81, 113, 145, 178, 210, 242, 275
Acceleration	-6.3, -3.8, -1.3, 1.3, 3.8, 6.3
Vertical Rate	-6550, -4910, -3270, -1630, 20, 1660, 3300, 4940
Turn Rate	-6.7, -4.0, -1.3, 1.3, 4.0, 6.7



**Figure 69: Helicopter aircraft model histograms below 10,000 ft ASL**

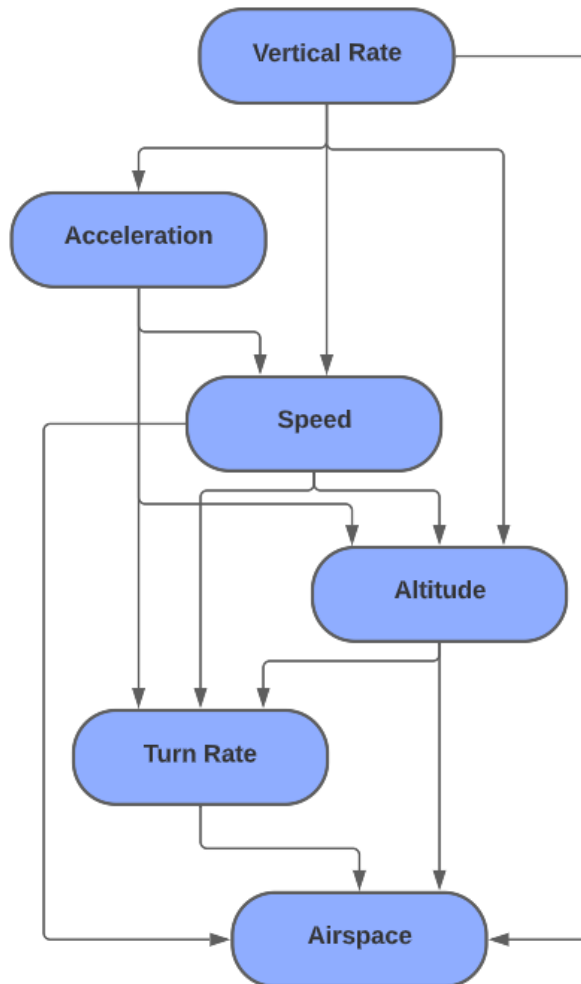


Figure 70: Initial Distributions for Helicopter aircraft model below 10,000 ft ASL

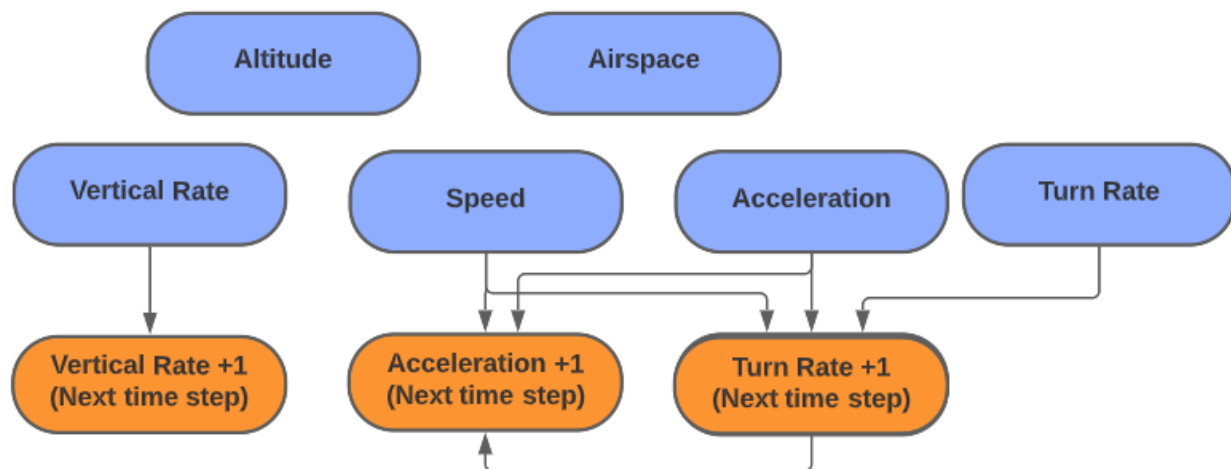


Figure 71: Transition Distributions for Helicopter aircraft model below 10,000 ft ASL